# A study of dispersed Ru + alkaline oxides in dual function materials (DFM) for direct air capture of carbon dioxide and from natural gas power plants with subsequent methanation using renewable hydrogen

Chae Woon Jeong-Potter

Submitted in partial fulfillment of the
requirements for the degree of
Doctor of Philosophy
under the Executive Committee
of the Graduate School of Arts and Sciences

COLUMBIA UNIVERSITY

2022

# Abstract

A study of dispersed Ru + alkaline oxides in dual function materials (DFM) for direct air capture of carbon dioxide and from natural gas power plants with subsequent methanation using renewable hydrogen

Chae Woon Jeong-Potter

The rise of anthropogenic $CO_2$ emissions and the associated increasing levels of $CO_2$ in the atmosphere are expected to bring uninhabitable conditions on earth due to global climate change and numerous associated environmental crises. To reduce these impacts, warming must be kept to 1.5°C above pre-industrial levels. With the slow transition to more favorable energy generation methods with lower carbon emissions, it is clear that power plants utilizing fossil fuel combustion for electricity will not be reduced to an acceptable level. Thus, the deployment of negative emission and carbon capture, utilization, and storage (CCUS) technologies will be crucial to meet the 1.5°C target.

The current state-of-the-art carbon capture technology is point source amine scrubbing, in which diluted aqueous amine solutions are used to absorb $CO_2$ from power plant flue gases. The $CO_2$ is captured at ~40°C by the formation of an amine/$H_2O$—$CO_2$ complexes. The absorbent solution, now containing $CO_2$, must be heated to release the $CO_2$ for further processing and to regenerate the amine for recycling. Though this technology is well-engineered and commercially available, there are some major drawbacks such as energy intensity mainly due to vaporization of the water during $CO_2$ separation from the amine, corrosivity of the amine material, and the need to transport the released $CO_2$ for further utilization or sequestration. To this end, dual function materials (DFM) were developed to address these issues.

DFMs eliminate the need for the energy intensive regeneration of liquid amine solutions and transportation of $CO_2$. Comprised of both a capture and catalytic component co-dispersed on the same high surface area carrier, the DFM is able to selectively capture $CO_2$ from the effluent flue gas and catalytically convert it to methane (or renewable natural gas) with the introduction of preferably renewable $H_2$ in the same reactor. The DFM can operate isothermally at around 320°C by harnessing the sensible heat of typical power plant effluent flue gases. 5% Ru, 6.1% "$Na_2O$"/$Al_2O_3$ was shown to be a very robust, demonstrating stable performance after 50 cycles of capture and catalytic conversion with simulated flue gas.

In addition to point-source capture, negative emission technologies like direct air capture (DAC) are required to mitigate climate change. Thus, we investigate the use of DFM for a new application – the direct air capture of $CO_2$ and subsequent catalytic methanation. Furthermore, for such applications, the loading of Ru was dramatically decreased to alleviate the economic burden for commercialization and wide-scale deployment.

This thesis demonstrates the flexibility of the DFM as a carbon capture technology for direct air capture of $CO_2$ at ambient air temperatures and subsequent methanation (DAC-M) at temperatures in excess of 200°C. Recognizing the energy intensity of isothermal DAC-M operation, the capture and conversion cycles were modified for temperature-swing operation, with adsorption occurring at 25°C, followed by heating up to 300°C in $H_2$ for methanation. Short-term aging was conducted on 1% Ru, 10% $Na_2O/Al_2O_3$ in a packed bed configuration for 10 cycles of adsorption in dry air conditions (400ppm $CO_2$ in air) and methanation. The sample was also tested in humid adsorption conditions (400ppm $CO_2$, ~2% $H_2O$/air) to better simulate ambient environments. These tests showed that the DFM is able to operate in a temperature swing mode and exhibits a higher, stable $CO_2$ adsorption capacity in humid conditions unlike other capture

technologies using amines and physical adsorption methods, which show a significant decline in capture capacity. We were able to establish that the DFM has great potential for DAC-M. Consequently, these materials are moving towards advanced process development with our engineering partners under the sponsorship of DOE. Critical parameters such as pressure drop, heating rate, and methanation temperature are primary parameters that must be optimized.

New low Ru loading DFMs, 0.5% Ru and 1% Ru DFM, were aged with simulated power plant flue gas (7.5% $CO_2$, 4.5% $O_2$, 15% steam, balance $N_2$) for over 50 cycles of capture and catalytic conversion to $CH_4$ (and water) in a packed bed configuration. These conditions of continuous operation at 320°C with 15% steam and 4.5% $O_2$ are far more severe than for DAC which adsorbs low levels of $CO_2$ from air at ambient air conditions (0-40°C with 2-5% moisture). Therefore, these power plant effluent test conditions can be considered accelerated aging for DAC-M. A reduced level of 0.5-1% Ru DFM was tested under simulated power plant effluent conditions on several $Al_2O_3$ structures, particularly tablets and ring tablets for scale-up of the technology. These tests showed a subtle but gradual deactivation of the material. Characterization with CO chemisorption and in-situ FT-IR indicated that the Ru component is deactivated – most likely by sintering – due to the presence of $O_2$ and $H_2O$ in the flue gas. Microreactor studies show that in the presence of $O_2$ and $H_2O$, adsorption capacity is reduced and the rate of methanation is decreased. Upon removing $O_2$ and $H_2O$ from the adsorption step, the adsorption capacity is restored but the rate and selectivity of methanation declines steadily, indicating that the deactivation is irreversible. Interestingly, the DFM with higher Ru loading showed more stable performance suggesting that higher catalytic content is required for more improved stability. Fortunately, Ru can be leased and recycled, reducing the capital economic burden of higher Ru loadings. Additionally, we expect that given the milder conditions for capture in DAC scenarios,

low Ru loaded DFMs will be more stable. Initial DAC-M data substantiates this stability, but longer aging times are required for confirmation. Furthermore, stability may be favored with the use of higher concentration $H_2$.

Finally, this thesis also investigates the use of other Ru+sorbent/carrier combinations for DAC and the apparent enhancement of adsorption arising from the use of a reactive sorbent (e.g., addition of Ru). After screening $Al_2O_3$-supported $Na_2O$, CaO, MgO, and BaO in combination with 1% Ru, we are able to show that Ru+$Na_2O$/$Al_2O_3$ has the best adsorption capacity. This material, relative to the other alkaline oxides studied, shows a unique enhancement in the $CO_2$ adsorption capacity compared to the bare supported sorbent ($Na_2O$/$Al_2O_3$). The enhancement effect is shown to be an asymptotic function of an increasing Ru loading, plateauing after 3% Ru. $ZrO_2$-supported Ru+$Na_2O$ is also tested but does not show favorable adsorption capacity, indicating that $Al_2O_3$ is also a crucial component of the DFM formulation. This technology is the subject of a provisional patent application.

# Table of Contents

# List of Figures

# List of Tables

# Acknowledgments

I would like to, first and foremost, express my deepest gratitude and appreciation to my PhD advisor, Prof. Robert Farrauto. Bob has provided me with the best opportunity of my life and has showered me with endless encouragement, support, and guidance. He has been my shining example of what a diligent researcher, practical educator, compassionate mentor, confident leader, and – more generally – good person looks like. I have been inspired by Bob's expertise in and passion for catalysis and his love for the planet; I will carry these pillars with me for the rest of my scientific career. I have been so fortunate to have had him as my advisor and have gained a mentor and friend for life.

I would like to thank my committee members for their time and guidance on my research: Prof. Ngai Yin Yip, Prof. Athanasios Bourtsalas, Prof. Jingguang Chen, and Dr. Raghubir Gupta. I would also like to thank Prof. Ben Davis for his continued mentorship and guidance for 10 years. It was through him that I learned and got excited about chemical engineering. Additionally, I thank Prof. Amanda Simson for introducing me to Bob's research group as well as her continued involvement in my scientific and professional progress.

I also sincerely thank Viveka "Vicky" Cohn Gould for her generous donations to our research through the Cohn Endowment, in honor Dr. J. Cohn. I also thank AngloAmerican Platinum and the United State Department of Energy for their financial support.

Throughout my graduate studies, I have had the honor to work with several incredible scientists. I thank the Susteon team, especially Cory Sanderson and Dr. Raghubir Gupta, for their partnership in our endeavors to bring the DFM closer to commercialization. I also thank Dr. Alessandro Porta and Prof. Luca Lietti from Polytechnic University of Milan for their partnership

and guidance as well as Prof. Melis Duyar, Prof. Tomas Ramirez Reina, and Angie Merkouri from the University of Surrey.

My PhD journey stands on the foundations set by previous group members. I particularly thank Dr. Martha Arellano-Treviño for her mentorship and friendship. It is through her that I got acclimated to Columbia, the lab, and DFM research. I also thank Prof. Melis Duyar, Dr. Ashley Wang, and Dr. Angela Zheng. Additionally, I thank all former and present Columbia students that I've worked with: Aylin Kulur, Minghui Cai, Xiaoxuan Tang, Jonathan Moallem, and Mark Goldman. I especially thank my good friend, Monica Abdallah, who has been my friend since before my time at Columbia and joined our group during COVID. She kept me company in the lab during the abnormal days of social distancing and online campus life. She has shared my passion and dedication for this work and has shown me so much patience and understanding.

I leave Columbia having made many lifelong friendships. I especially thank Sara Hamilton, who has been my closest friend and colleague since we entered the program together. Adam Massman, Kinnari Shah, Hanqing Fan, Xi Chen and Shripad Patil have also all made my time at Columbia enjoyable through their loving friendships. I also thank my friends Allison Xiao, Sharon Choi, and Vicky Gong, who have become my sisters since our friendship began over 15 years ago. They have always been my cheerleaders and shoulders to lean on.

Finally, I dedicate this thesis to my family. My husband, Jake, who has been my greatest day-to-day support and has always been kind and caring. My brother, Chris, for whom I always seek to be an example. My aunts, Joanne and Cindy, who are my surrogate mothers and my everlasting friends. My dad, Dong-Kyun, who is always the proudest of me, and my mom, Young-Ja, who has worked so hard for me to get to where I am today. Everything I do is for them, and I am blessed to be their wife, sister, niece, and daughter.

*To my family. My husband Jake, my brother Chris, my aunts Joanne and Cindy, my parents Dong-Kyun and Young-Ja.*

# Chapter 1 : Introduction

## 1.1 Motivation

The average concentration of $CO_2$ in the atmosphere exceeded 410 ppm in 2019, confirming the steadily increasing levels since the industrial revolution [1]. The detrimental effect of a high concentration of $CO_2$ in the atmosphere are well known, and international agreements have been put in place to limit anthropic $CO_2$ emissions. Together with a decrease in the carbon emissions, which can be achieved thanks to the increase in the efficiency of the emitting processes and the shift towards renewable energies, carbon capture technologies will play an important role in reducing $CO_2$ atmospheric concentrations [2]. $CO_2$ can be captured at point sources (e.g., power production facilities, industrial sites) using liquid or solid adsorbent [3]. In both cases the main drawback of the technology is the high amount of energy required to regenerate the adsorbent material. Furthermore, when the adsorbent is regenerated captured $CO_2$ is released and needs to be effectively stored or – even better – recycled to useful products.

In this context, dual function materials (DFM) were developed in our lab in 2015 to effectively couple the two steps of carbon capture and utilization [4]. These materials act both as solid adsorbents for capture $CO_2$ and as catalysts for production of fuel from the captured carbon upon $H_2$ exposure. For this reason, these materials require a carbon capture function (usually an alkaline or alkaline earth metal) and a hydrogenating function (usually Ru) supported on a high surface area carrier [5,6]. In particular, these materials have been developed for selective $CO_2$ capture and catalytic methanation, envisaging a possible application in cleaning and recycling the carbon content from flue gases of natural gas-fired power plants [7,8]. These materials operate in cyclic conditions: first, the material is exposed to the flue gases (7.5% $CO_2$, 4.5% $O_2$, 15% steam

and balance $N_2$) and saturated with $CO_2$. The DFM, with adsorbed $CO_2$, is then exposed to a (renewable) $H_2$ stream to catalytically convert it to methane (renewable natural gas, RNG). The energy required for the adsorbent regeneration and methanation reaction is supplied by the sensible heat of the flue gases, avoiding the need for external energy inputs. Thus, capture and utilization can be achieved with a single material isothermally.

To date, the most successful DFM consists of Ru dispersed on $\gamma$-$Al_2O_3$ and doped with "$Na_2O$" arising from the reduction of $Na_2CO_3$ [6,7,9–12]. This combination of catalyst and sorbent has good $CO_2$ adsorption capacity and fast methanation kinetics [6]. Prior studies have also shown that 5% Ru, 6.1% "$Na_2O$"/$Al_2O_3$ DFM tablets were stable for over 50 cycles of capture of $CO_2$ from flue gas compositions (i.e., 7.5% $CO_2$ and 4.5% $O_2$, 15% $H_2O$, balance $N_2$) and subsequent catalytic conversion to methane [3,11]. Improved performances were observed on the aged material (~ 100 hours of cyclic operation), linked to slight re-dispersion of the Ru and "$Na_2O$" [11].

As point-source $CO_2$ emissions are already being addressed with push towards the utilization of renewable sources such as solar and wind for power generation, it is logical to consider other future decarbonizing applications for DFM. One such application is direct air capture (DAC) technologies for reducing the increasing levels of $CO_2$ in the atmosphere [13–16]. DFM for DAC has the additional advantage of geographic freedom and, thus, it can be placed aptly near a $H_2$ source to reduce logistical issues regarding $H_2$ transportation and storage. Successful demonstration of DFM for DAC and subsequent methanation (DAC-M) would further improve the attractiveness of this technology for commercialization. Additionally, for wide deployment of this technology, it is beneficial to reduce the cost of materials, mainly by reducing Ru content, which is priced at $22.35/g as of September 2021.

Herein, the objective of this thesis is to investigate low Ru content in the DFM, demonstrate the feasibility of DAC-M with this material, and evaluate its stability for selective $CO_2$ capture followed by catalytic methanation of $CO_2$ using simulated natural gas power plant effluent and conditions for direct air capture of ~ 400 ppm $CO_2$ in ambient air.

## 1.2 Thesis Structure

This thesis presents the evaluation of <1% Ru loading DFM for commercial viability and its potential for wide-scale deployment. First, the feasibility of applying DFMs for combined DAC and methanation is evaluated. Then, low Ru loading DFMs (0.5% and 1% Ru) are evaluated and aged under simulated flue gas conditions, containing $O_2$ and steam, to establish their stability.

In Chapter 2, we provide an overview of the existing literature and relevant background information to motivate the need for new work. This chapter highlights the effects of rising anthropogenic $CO_2$ emissions and the need for carbon capture and utilization technologies. A thorough background of the DFM technology originating from our lab as well as adaptations found in literature is also provided.

The detailed experimental methodology is found in Chapter 3. In this chapter, specifics of sample preparation, employed instrumentation, and testing parameters are provided. All the relevant experimental details outlined in Chapter 3 are thoroughly referenced in the corresponding chapters.

A feasibility study of translating DFM technology to DAC-M is detailed in Chapter 4. First the DFM is directly translated to DAC and is shown to operate isothermally, successfully selectively adsorbing $CO_2$ from simulated ambient air (400 ppm $CO_2$ in dry air) and subsequently methanating it with the introduction of $H_2$. Recognizing the energy intensity of operating DAC-M

we investigate its performance in a temperature-swing operation. The DFM is cycled to adsorb $CO_2$ in ambient conditions (25°C) and then heated in $H_2$ up to 300°C for catalytic methanation. It is also cycled in the presence of humidity, during with performance is greatly enhanced. This chapter shows that the DFM has excellent potential to be used widely for DAC-M.

In Chapter 5, long term aging with simulated flue gas is performed on DFMs with 0.5% and 1% Ru. Several configurations of the DFM are tested (granules, tablets, ring tablets) and the DFM is also aged with a clean stream of $CO_2$ (no $O_2$ and steam) for reference. After aging, the DFMs are characterized using chemisorption and in-situ FT-IR to better describe the changes experienced by the DFM. We determined that due to the presence of $O_2$ and steam in the flue gas, the low Ru loading DFMs experience subtle but gradual deactivation, most likely due to sintering of the catalyst component. Deactivation is shown to be less severe for the higher Ru loading DFM (1%), indicating a path to achieve long term stability.

In Chapter 6, we establish that the combination of oxidized $Ru+Na_2O/Al_2O_3$ shows an unexpected enhancement of $CO_2$ adsorption compared to the bare supported sorbent ($Na_2O/Al_2O_3$). Uniquely, the enhancement is observed with adsorption in the presence of $O_2$ during which Ru is oxidized. The resulting species, $RuO_x$, is unable to adsorb any $CO_2$ itself. A provisional patent application has been submitted for this phenomenon. Additional work in progress to understand the mechanism more fully.

Finally, in Chapter 9, we provide conclusions and suggest some future work to advance the DFM closer towards commercialization and deployment.

# Chapter 2 : Background and Literature Review

## 2.1 The effects of rising anthropogenic $CO_2$ emissions and the increasing atmospheric $CO_2$ concentration

Global $CO_2$ emissions continue to rise with global energy demand, with energy-related emissions reaching a historical high of 33.1 Gt $CO_2$ in 2018 [17] and 2019 [18]. As a result, atmospheric $CO_2$ concentrations have increased at an alarming average rate of 2.4ppm/year in the past decade [19], surpassing 414 ppm in May 2019 [20]. High levels of atmospheric $CO_2$ are associated with global climate change and a myriad of other environmental crises [21]. At this current rise of emissions and atmospheric $CO_2$ concentrations, it is predicted that the average global temperature will increase by 4°C by 2100 [22]. In this 4°C scenario ("business-as-usual"), the Intergovernmental Panel on Climate Change (IPCC) predicts that the average atmospheric concentration of $CO_2$ will hit 650 ppm by 2100 and result in 9m of sea level rises, impacting up to 760 million people; frequent and severe droughts; high levels of food insecurity; and extinction of 50% of all plant and animal species.

Pending these severe ramifications of global climate change, nearly 200 countries pledged to limit warming to 2°C by 2100 via the Paris Agreement (2015) [23,24]. However, in 2018, the IPCC released a special report on limiting warming to 1.5°C, citing that there is significant risk of long-lasting and irreversible changes with 2°C of warming.

## 2.2 Curtailing past, present, and future $CO_2$ emissions: carbon capture technology

With strong evidence linking $CO_2$ emissions to the increased in global surface temperatures, strategies for limiting warming to 1.5°C rely heavily on $CO_2$ emission abatement. In 2013, the

IPCC called for a commitment to address "past, present, and future" $CO_2$ emissions [25]. Efforts to reduce *future* $CO_2$ emissions include fuel switching. In particular, there is societal push to move away from carbon-heavy fuels such as coal – in fact, during the most recent United Nations Climate Change Conference (COP26), 40 countries pledged to stop using coal by 2050 [26]. Replacing coal use with more carbon-lean fuels, like natural gas, does much to reducing energy-related $CO_2$ emissions. For example, natural gas emits about 50% less $CO_2$ than coal per unit of energy produced (95.74 vs 52.91 kg-$CO_2$/MMBTU) [27]. However, the most significant change will be brought on by the wide-spread use of non-fossil-derived energy (i.e., nuclear, solar, wind), which are associated with little to no $CO_2$ emissions per unit energy generated. Additionally, the use of more energy efficient technologies should be adopted.

The IPCC predicts that to keep warming to 1.5°C, coal will need to be eliminated from the global electricity mix by 2050 [28]. Additionally, renewables will need to supply up to 48% by 2030 and at least 63% by 2050. **Figure 2.1** shows the breakdown of the world's electricity mix between 1971 and 2019. Unfortunately, over this period of almost 50 years, there has not been any significant reduction in the use of fossil fuels. The major difference is the decline of oil usage to the rise of natural gas usage; however, in 2019, fossil fuels still make up most of the electricity mix (~63%) and renewables only make up about a quarter of the mix (26.5%). This is far removed from the target mix required to mitigate the effects of climate change, requiring rapid and extensive investment in infrastructure changes in the coming decade.

Given the persistent use of fossil fuels, the *present* emissions must be addressed, requiring technologies to reduce $CO_2$ emissions associated with current operations. In this context, carbon capture, utilization, and storage (CCUS) technologies are important. $CO_2$ not only needs to be

captured at the source of emission (i.e., point-source) but also upgraded, recycled, or sequestered to approach net zero emissions.

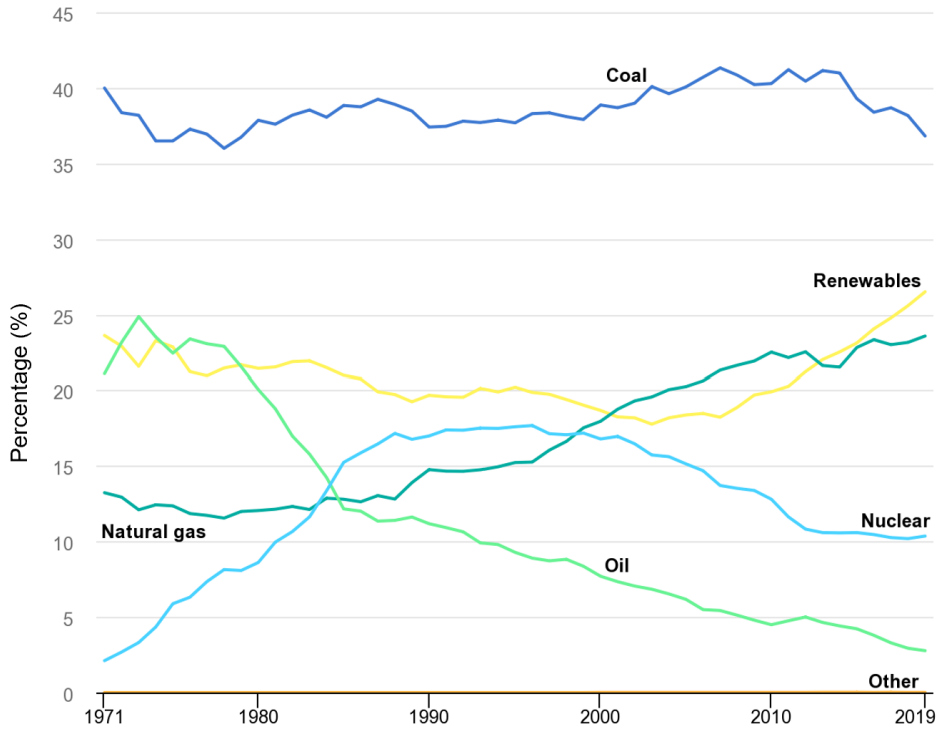


**Figure 2.1:** Breakdown (as percentages) of world's electricity mix by source between 1971 to 2019 [29].

For utilization or sequestration, $CO_2$-containing gas feeds must be purified and/or concentrated. Concentrated $CO_2$ emission streams can be achieved with "clean combustion", in which fuels are combusted for energy generation with production of little to no byproducts and a stream of simply $CO_2$ and water; condensation is then the only separation required to obtain pure $CO_2$. Oxy-fuel combustion and chemical looping are two main technologies in achieving this, both of which deliver pure $O_2$ for efficient and complete combustion of C-containing fuels to $CO_2$+$H_2O$ [30]. Given some economic concerns and immaturity of these technologies, post-combustion $CO_2$ capture is more commonly used to envision CCUS schemes.

Amine scrubbing is the most widely used post-combustion capture technology. It involves the use of liquid amine absorbents such as monoethanolamine (MEA) [31]. Due to the amine's high viscosity and corrosivity, a diluted aqueous solution is used (15-30% MEA, balance $H_2O$). The $CO_2$ emission stream (e.g., power plant flue gases) is cooled to about 40-45°C and introduced into an absorption column to react with the MEA solution. The $CO_2$ selectively binds to the MEA, creating a stable MEA—$CO_2$ complex (carbamate, R-NH-COO) and all other gas components are released. The $CO_2$-rich MEA solution is then heated in a stripper column to break the MEA—$CO_2$ bond, releasing the $CO_2$ and regenerating the MEA absorbent material. This produces a concentrated stream of $CO_2$ (>99%) which needs to be compressed for transportation. Though this is a commercially available technology, it has a few major disadvantages. It is energy intensive, requiring a large amount of heat for sorbent regeneration and vaporization of the water present as well as energy for compression and transportation of the purified $CO_2$. The sorbent has a short lifetime and is lost in the process due to vaporization during heating and degradation in the presence of $O_2$ and $SO_x$. The sorbent is also corrosive, requiring high capital cost equipment [31].

The Intergovernmental Panel on Climate Change (IPCC) predicts that to limit warming to 1.5°C above pre-industrial levels, $CO_2$ emissions will need to reach net zero by 2050 [28]. It is, however, not possible to remove all $CO_2$ emissions; some sectors are more difficult to decarbonize, not all emissions sources can be fit with $CO_2$ capture technology and these do not capture 100% of emissions [32–34]. Negative emission technologies, such as direct air capture (DAC) of $CO_2$, will be necessary to achieve net zero emissions and should be considered for climate change mitigation (**Figure 2.2**) [13–16]. These set of technologies address the *past* emissions.

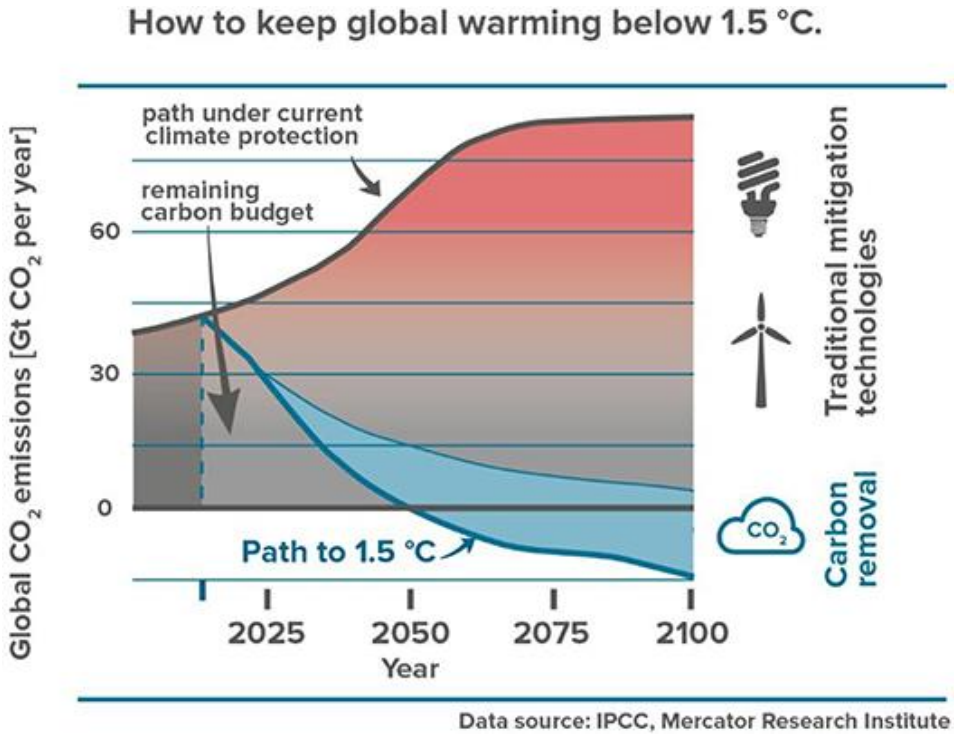


**Figure 2.2:** Technologies required to keep global warming below 1.5°C by 2100 [35].

DAC is a process in which $CO_2$ is separated from the other components of ambient air and concentrated for further storage or utilization [13,15]. Two major separation media have gained notable traction: aqueous alkaline solutions and solid sorbents [34,36]. Aqueous alkaline solutions (i.e. $Ca(OH)_2$, NaOH) absorb $CO_2$ from air upon contact at ambient conditions. Release of $CO_2$ from aqueous alkaline solutions involves decomposition or calcination of alkaline carbonates (e.g., $CaCO_3$) at high temperatures (above 800°C [14,37]). Solid sorbents (e.g., metal organic frameworks (MOFs), alkali/alkaline earth metal oxides/carbonates, zeolites) operate through an adsorption process in which the $CO_2$ is physi- or chemisorbed onto the sorbent surface. Desorption of physi- or weakly chemisorbed $CO_2$ from solid sorbents can be achieved at lower temperatures (around 150-250°C [34,38,39]). Once desorbed from either medium, the $CO_2$ is available for

storage or utilization. Most of these materials are known to lose effectiveness in the presence of moisture in the air [38]– this is a critical issue to be addressed with DAC technologies as moisture can be present in a variety of ambient environments.

## 2.3 Methanation: Coupling of $CO_2$ utilization and Power-to-X technologies

The transition to renewable sources of energy is understood to occur slowly over future decades so fossil fuel combustion will continue for decades. Accepting this reality, it is understood that $CO_2$ issues must be addressed. Although sequestration and storage of emitted $CO_2$ would be preferred to achieve negative emissions, utilization to a saleable and useful product is an economic incentive to further develop carbon capture and DAC technologies and can be a viable short-term option as storage technologies are further investigated [36].

Utilization of $CO_2$ in the synthesis of fuels by reacting with $H_2$ from water electrolysis appears to be especially prevalent as a "Power-to-X" and hydrogen storage scheme [40–42]. Given that DAC technologies have freedom of geography, they can be aptly placed near $H_2$ generation or waste facilities. This would remove the economic and energy burdens related to compression and long-distance transportation of the purified $CO_2$ [34]. Several companies exist that have coupled DAC with fuel synthesis. Climeworks (Switzerland), which uses a solid sorbent, has partnered with other companies to establish production of synthetic fuels using $CO_2$ captured from the air [43]. Carbon Engineering (Canada) uses an alkaline aqueous solution and aims to achieve synthetic liquid fuel production by way of their DAC technology [44,45].

Of the hydrocarbon fuels that can be produced, methane, or renewable natural gas (RNG), is quite attractive. In the presence of well-established catalysts, the Sabatier reaction (1) can occur at moderate temperatures ($T \leq 300°C$) and atmospheric pressure [46,47]. High conversions of $CO_2$

with 100% $CH_4$ selectivity can be achieved with the right choice of catalysts and process conditions [47], generating a product stream that can be dried to achieve methane at high purities. The resulting RNG can be transported easily using the existing natural gas infrastructure.

$$CO_2 + 4H_2 \xrightarrow{\text{catalyst}} CH_4 + 2H_2O \qquad \Delta H^o_r = -165 \text{ kJ/mol} \qquad (1)$$

For such reasons, combining $CO_2$ capture and methanation has gained interest in the literature [3,48]. Of particular note, Veselovskaya et al. have proposed a novel way of combining DAC with $CO_2$ methanation (DAC-M) using a single reactor [49]. Their process employs a supported sorbent ($K_2CO_3/Al_2O_3$), which adsorbs $CO_2$ at room temperature. In the same reactor, $Ru/Al_2O_3$ is used as the methanation catalyst but is present as a separate catalytic bed. Upon heating to 300-350°C and addition of $H_2$, the $CO_2$ is desorbed from the sorbent bed and consequently methanated over the catalytic bed. More recently, these authors have shown the use of two separate reactors for adsorption/desorption and subsequent methanation to improve the conversion of $CO_2$ to $CH_4$ [50,51]. In this thesis, we explore the feasibility of using DFM for DAC-M, using a single active bed in a single reactor while achieving similar conversion. The use of a single reactor (rather than two separate reactors) can greatly reduce the energy requirement of the process as only a single bed will need to be heated. This will also allow for more continuous operation as multiple reactors can be utilized in parallel.

## 2.4 Dual function materials (DFM)

The DFM was initially developed in our laboratory to capture $CO_2$ from point-sources (i.e., natural gas power plant flue gas) and produce RNG using a single material under isothermal conditions [7,8]. The DFM is composed of an alkaline adsorbent and catalytic metal nano-dispersed on the same, high-surface area carrier. After screening multiple alkaline chemisorbents and catalytic metals, the combination of "$Na_2O$" and Ru supported on $\gamma$-$Al_2O_3$ allowed for the best adsorption as well as complete and rapid methanation kinetics [6].

DFM, as stated in the literature, refers to a class of reactive materials that adsorb $CO_2$ and, with the introduction of a reactive gas (like $H_2$ or $C_2H_6$), generates a useful product [3,52]. The sorbents most commonly studied include alkaline metal oxides such as CaO, $Na_2O$, and BaO [5–7,53,54]. Ni, Ru, and Rh have been extensively studied as the catalytic component for methanation pathways [5–7,10–12]; other catalysts (such as Fe and Cu) have been suggested for alternative reaction pathways [3,52].

The DFM allows for cyclic power plant operation of selective $CO_2$ capture (step 1) and catalytic conversion (step 2) to $CH_4$ (and 2 $H_2O$) at a single temperature of about 320°C. Upon introduction of a flue gas stream, $CO_2$ is captured at the interface of "$Na_2O$" and $\gamma$-$Al_2O_3$ (i.e., Al—O—$Na^+$ sites) as surface bicarbonate and bidentate carbonate species (2) [55,56]. Because most feed streams will include oxygen, the Ru will oxidize (3) [57] to a catalytically inactive $RuO_x$ or $RuO_2$ species [58,59]. Upon the introduction of hydrogen in step 2, $RuO_2$ will be rapidly reduced to catalytically active metal due to its unique redox properties (4) [6]. The close proximity of the adsorbent and catalyst allows for migration of the $CO_2$ from "$Na_2O$" sites to Ru sites (5) where it is subsequently converted (6). $\gamma$-$Al_2O_3$ is not included in (2)-(6) for simplicity.

| | | |
|---|---|---|
| **Step 1 ($CO_2$ Adsorption in the presence of $O_2$):** | "$Na_2O$" + $CO_2$ → "$Na_2O$"—$CO_2$ | (2) |
| | $Ru + O_2 \rightarrow RuO_2$ | (3) |
| **Step 2 (Conversion with $H_2$ addition):** | $RuO_2 + 2H_2 \rightarrow Ru + 2H_2O$ | (4) |
| | "$Na_2O$"—$CO_2$ + Ru → "$Na_2O$" + Ru—$CO_2$ | (5) |
| | Ru—$CO_2 + 4H_2 \rightarrow CH_4 + 2H_2O$ + Ru | (6) |

An extended 50-cycle (100 hour) aging study on 5% Ru, 6.1% "$Na_2O$"/$Al_2O_3$ DFM tablets (5mm x 5 mm) showed that the material is stable for both $CO_2$ capture in simulated flue gas conditions (7.5% $CO_2$, 4.5% $O_2$, 15% $H_2O$, balance $N_2$) and subsequent catalytic conversion exclusively to $CH_4$ [11]. Most recent studies have shown that DFMs with even lower Ru loadings can sufficiently capture and convert $CO_2$ with 100% $CH_4$ selectivity [12].

# Chapter 3 : Experimental Methodology

## 3.1 DFM for DAC-M

### 3.1.1 Material Synthesis

The materials tested for DAC-M application can be found in **Table 3.1**. These materials were all prepared on γ-$Al_2O_3$ (Sasol TH100) 300µm spherical granules using incipient wetness impregnation.

**Table 3.1:** DFM compositions used for DAC-M studies and the corresponding sorbent precursor salts.

| Ru Loading | Sorbent Loading | Sorbent Precursor Salt |
|---|---|---|
| 0.5% Ru | 6.1% "$Na_2O$" | $Na_2CO_3$ (Sigma Aldrich) |
| 1% Ru | 10% "$Na_2O$" | $Na_2CO_3$ (Sigma Aldrich) |
| 1% Ru | 10% CaO | $Ca(NO_3)_2 \cdot 4H_2O$ (Sigma Aldrich) |

First, an aqueous solution of the sorbent precursor salts (see **Table 3.1**) is impregnated onto the alumina granules to reach the desired sorbent loadings. Multiple impregnation steps were occasionally needed to reach the target sorbent loading due to the limits of precursor salt solubility. The partially loaded sample was dried overnight (>12 hours) in static air at 100°C between incipient wetness impregnations. A slight excess of solution, with respect to the total pore volume of the granules, was used to favor the uniformity of the DFM batch. Once the target loading was achieved, the sample was calcined for 3 hours at 400°C to decompose the precursor salt and achieve the final sorbent form.

Subsequently, Ru was impregnated onto the calcined sample using an aqueous solution of ruthenium (III) nitrosyl nitrate ($Ru(NO)(NO_3)_3$) precursor salt (Alfa Aesar, Ru 32%). Again, a

slight excess of solution, with respect to total pore volume of the granules, was used during impregnation to favor uniform impregnation of Ru. The Ru-loaded sample was dried for 2 hours in static air at 120°C and subsequently calcined for 3 hours at 250°C to decompose the precursor salt. The final active form of the sample is achieved after $H_2$ pre-treatment before TGA and packed bed experimentation as are described in the subsequent sections.

### 3.1.2 Thermal gravimetric analysis (TGA)

The following thermal gravimetric studies were performed in a NETZSCH TG 209 F1 Libra unit. For all studies, samples (20-30 mg) were loaded into an alumina crucible and dried in $N_2$ at 120°C for 3 hours. All steps were carried out with a total gas flow of 80 ml/min (NTP: normal temperature and pressure; 1atm and 20°C) at 1 atm. All heating steps were carried out at 5 K/min and all cooling steps at 10 K/min. Any deviations from these specifications are detailed in the appropriate sections.

#### 3.1.2.1 Adsorption capacity of Ru+$Na_2O$ DFM at 25°C and 320°C

$CO_2$ adsorption capacity of 1% Ru, 10% $Na_2O/Al_2O_3$ DFM was studied at two different temperatures. Following drying, samples were pre-reduced in 15% $H_2/N_2$ at 300°C for 6 hours. After pre-reduction, the temperature was increased to 320°C and the sample was exposed to a stream of 375 ppm $CO_2$, 19% $O_2$, and balance $N_2$ for 6 hours. After a 30-minute purge with $N_2$ to evacuate $O_2$ from the instrument chamber, 15% $H_2/N_2$ (at 320°C) was introduced for 6 hours to reduce the sample and clear the surface of adsorbed $CO_2$. The sample was then cooled to 25°C in $N_2$ and subsequently exposed to the same adsorption stream (375 ppm $CO_2$, 19% $O_2$, and balance $N_2$) for 6 hours. This generated isotherms at 320 and 25$^o$C.

#### 3.1.2.2 Temperature programmed reduction (TPR) of DFM oxidized at 25°C

Reduction of $RuO_x$ species was tested on $Ru+Na_2O/Al_2O_3$ DFM (1% Ru, 10% $Na_2O/Al_2O_3$). After pre-reduction the temperature was reduced to 25°C and the sample was exposed to a stream of 7.5% $O_2/N_2$ for 6 hours. After a 20-minute inert $N_2$ purge, the sample was heated in a stream of 15% $H_2/N_2$ at 10 K/min to 300°C (TPR).

### 3.1.3 Packed bed studies

In the following studies, 0.5 g of DFM granules were loaded in a quartz tube reactor (O.D. = 12.75 mm, I.D. = 10.5 mm, L = 500 mm) and secured with glass wool (Supelco Inc, USA). The remaining space in the reactor was packed with 3mm diameter glass beads (McKesson, USA) to decrease dead volume. The reactor tube was fitted in a microthermal furnace (MTSC12.5R x 18-1Z, Mellen, USA) and a K-type thermocouple (Omega, USA) at the middle of the DFM bed for temperature feedback control. Mass flowmeters were used to feed and mix compressed gases at designated flowrates. A saturator ambient temperature and pressure was placed after the flowmeters to introduce moisture to the system during humid adsorption. The saturator was bypassed during dry adsorption cycles. An ice bath was placed at the exit of the reactor to condense any moisture present in the system. Dry exit gas compositions were analyzed at NTP using a LI-830 $CO_2$ gas analyzer (LI-COR, USA) for ppm-level detection of $CO_2$ (± 2 ppm accuracy) and an Enerac 700 (Enerac, USA) for ppm-level detection of $CH_4$ and percentages of CO and $O_2$. A set up of the reactor is shown in **Figure 3.1**.

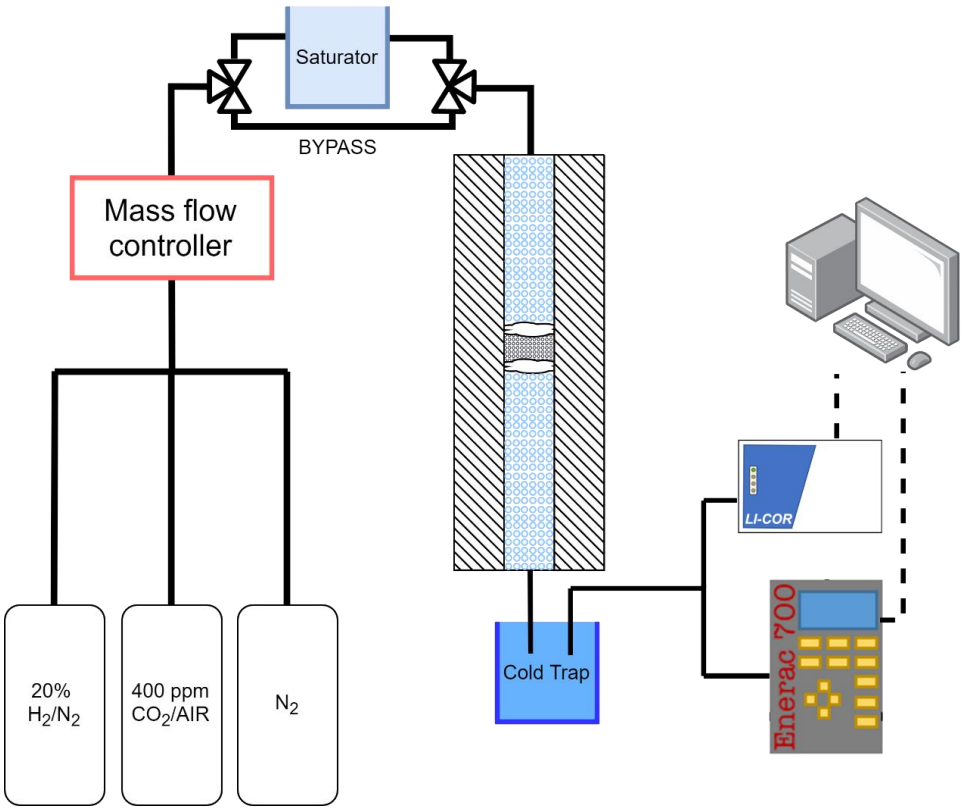


**Figure 3.1:** Reactor set up with a saturator for DAC adsorption + methanation/desorption studies.

#### 3.1.3.1 DAC isothermal adsorption and methanation cycles

Four isothermal cycles of adsorption/methanation were conducted on the DFM (0.5% Ru, 6.1% "$Na_2O$"/$Al_2O_3$) in a fixed bed configuration using simulated ambient air (400 ppm $CO_2$, 21% $O_2$, balance $N_2$) at 320°C.

The DFM sample was pre-reduced in situ at 350°C (heating rate: 2°C/min) for 3 hours with 20% $H_2/N_2$ with a total flow rate of 33 ml/min (GHSV: 4 L(NTP)/h/g, 2286 $h^{-1}$) to reduce the $RuO_x$ species to catalytically active $Ru^o$ and to hydrogenate the γ-$Al_2O_3$ supported $Na_2CO_3$ precursor to "$Na_2O$". The temperature was reduced to 320°C and isothermal cycles were then performed to include:

1. $CO_2$ capture step with simulated ambient air (400 ppm $CO_2$/dry air) for 45 minutes
2. Hydrogenation step with 15% $H_2/N_2$ for 45 minutes

It should be mentioned that the very first adsorption step was 1.5 hours long to ensure saturation of the material. An inert $N_2$ purge was required between the two steps to avoid contact of $O_2$ present in the simulated ambient air with $H_2$. All steps were performed at 320°C and 1 atm with a total flow rate of 200 ml/min (GHSV: 24 L(NTP)/h/g, 13900 $h^{-1}$).

#### 3.1.3.2 Isothermal DAC $CO_2$ adsorption and desorption cycles

Immediately following the last adsorption/methanation cycle as outlined in Section 3.1.3.1, isothermal adsorption/desorption cycles were performed on the same 0.5 g sample of DFM at 320°C. The cycles included:

1. $CO_2$ capture step with simulated ambient air (400 ppm $CO_2$/air) for 45 minutes
2. Desorption with inert purge (100% $N_2$) for 45 minutes

Both steps were performed at 320°C and 1 atm with a total flow rate of 200 ml/min (GHSV: 24 L(STP)/h/g, 13900 $h^{-1}$).

#### 3.1.3.3 Temperature-swing DAC-M

Samples of 0.5g of DFM granules (1% Ru, 10% "$Na_2O$"/$Al_2O_3$ and 1% Ru, 10% $CaO/Al_2O_3$) were loaded and pre-treated at 300°C (heating rate: 5°C/min) for 3 hours with 20% $H_2/N_2$ at a total flowrate of 16.7 ml/min (GHSV: 2L(NTP)/h/$g_{DFM}$, 1160$h^{-1}$) to ensure complete reduction of $RuO_x$ to catalytically active $Ru^0$ and to hydrogenate any carbonates that had formed on the surface.

The following steps were taken for subsequent adsorption/methanation cycles:

1. $CO_2$ capture step at 25°C with simulated ambient air (400 ppm $CO_2$/air) at 400 ml/min (NTP) until saturation (>2 hours for dry conditions; >4 hours for humid conditions)
2. 15-min purge with $N_2$ at 100 ml/min (NTP)
3. Heating to 300°C in 30 minutes (9-10°C/min) in 15% $H_2/N_2$ at 100 ml/min (NTP)
4. Hold at 300°C for 2 hours in 15% $H_2/N_2$ at 100 ml/min (NTP).

Humid adsorption and methanation cycles were also performed, during which simulated ambient air (400 ppm $CO_2$/air) was passed through a water saturator at ambient temperature to achieve ~2% $H_2O$ content in the adsorption feed (equivalent to ~90% humidity at 25°C). The subsequent conditions for heating and 300°C temperature hold was identical to that described above.

#### 3.1.3.4 Adsorption flowrate test

A 0.5g sample of DFM granules (1% Ru, 10% $Na_2O/Al_2O_3$) was loaded into the reactor in a packed bed configuration (**Figure 3.1**) and pre-treated at 300°C (heating rate: 5°C/min) for 3 hours with 20% $H_2/N_2$ at a total flowrate of 16.7 ml/min (GHSV: 2L(NTP) $h^{-1}$ $g_{DFM}^{-1}$, 1160$h^{-1}$) to the clean surface and ensure the complete reduction of $RuO_x$ to catalytically active $Ru^0$ as well as hydrogenation of any remaining $Na_2CO_3$ to "$Na_2O$." Subsequently, adsorption behavior of Ru+$Na_2O/Al_2O_3$ DFM was tested by exposing the sample to an adsorption feed of 400 ppm $CO_2$/air at 25°C until saturation (i.e., $CO_2$ concentration at outlet reads ~400ppm). Four flowrates were tested: 100, 200, 300, and 400 ml/min (NTP). Between each adsorption test, the sample was heated to 300°C in 30 minutes in 15% $H_2/N_2$ (100ml/min). The sample was held at 300°C for 4 hours in 15% $H_2/N_2$ to clear the DFM of adsorbed $CO_2$ by conversion to $CH_4$.

### 3.1.4 Materials characterization with $H_2$ chemisorption

$H_2$ chemisorption tests were performed on fresh and aged samples of the DFM (1% Ru, 10% "$Na_2O$"/$Al_2O_3$ granules before and after humid adsorption cycling) using a ChemBET Pulsar TPR/TPD unit (Quantachrome). $H_2$ adsorbed per gram of DFM was obtained at 100°C after in-situ reduction in 10% $H_2/N_2$ (30 ml/min, NTP) at 320°C for 24 hours. Dispersion was obtained by assuming that stoichiometry for chemisorption is one H atom per Ru site.

## 3.2 Aging of 0.5% Ru and 1% Ru DFMs in simulated natural gas power plant effluent flue gas

### 3.2.1 Materials synthesis

0.5% Ru, 6.1% "$Na_2O$"/$Al_2O_3$ and 1% Ru, 6.1% "$Na_2O$"/$Al_2O_3$ DFMs were prepared on γ-$Al_2O_3$ cylindrical tablets (5mm x 5mm, Sasol TH100). 0.5% Ru, 6.1% "$Na_2O$"/$Al_2O_3$was also prepared on γ-$Al_2O_3$ cylindrical ring tablets (5mm x 5mm, 2mm axial opening, Sasol TH100). The supports were calcined to 500°C for 5h prior to the introduction of the active phases by impregnation. At first, Ru was impregnated using an aqueous solution of ruthenium (III) nitrosyl nitrate ($Ru(NO)(NO_3)_3$) precursor salt (Alfa Aesar, Ru 32%) to obtain a nominal metal loading of 0.5 wt.% and 1 wt.%. A 10% excess volume with respect to the total pore volume of the support was used during the impregnation in order to favor the uniformity of each catalyst batch. The addition of $HNO_3$ was required in this step when tablets and ring tablets were used as supports, to achieve homogenous penetration of Ru, according to a previously reported preparation method [60]. Following a similar approach, the amount of $HNO_3$ (WVR BDH Chemicals, 68%) in the solution was set to a molar ratio of $HNO_3$/Ru = 70 for the 0.5 wt% Ru loading and $HNO_3$/Ru=40 for the 1 wt% Ru loading. $HNO_3$ was not added to the Ru impregnating step when DFM were

prepared using the granules as the support. All Ru impregnated samples were dried overnight (15 hours) in static air at 120°C.

The dried Ru-impregnated samples were subsequently reduced in $H_2$ (5% $H_2/N_2$, 2 L(NTP)/h/$g_{DFM}$) at 350°C for 3h (heating rate: 2°C/min) to fully decompose the precursor salt and residual $HNO_3$ possibly remaining on the catalyst after the preparation. The reduced samples were cooled in pure $N_2$ and passivated at room temperature in a diluted $O_2$ stream (2% $O_2/N_2$, 1 L(NTP)/h/$g_{DFM}$). NTP refers to normal temperature and pressure conditions; 20°C and 1 atm.

An aqueous precursor solution of $Na_2CO_3$ (Sigma Aldrich, >99%) was impregnated onto the passivated sample in order to obtain a nominal metal loading of 10% $Na_2CO_3$ (corresponding 6.1% "$Na_2O$" on the finished DFM weight). A 10% excess of solution with respect to the initial support pore volume was used. The samples were dried using the same procedure as the first impregnation step.

0.5% Ru, 6.1% "$Na_2O$"/$Al_2O_3$ was also prepared on 300μm granules (γ-$Al_2O_3$, Sasol TH100) with the same procedure but without $HNO_3$.

### 3.2.2 Packed bed studies

#### 3.2.2.1 Aging studies with simulated flue gas on 0.5% Ru and 1% Ru DFM

The 0.5% Ru, 6.1% "$Na_2O$"/$Al_2O_3$ and 1% Ru, 6.1% "$Na_2O$"/$Al_2O_3$ tablet, ring tablet, and granule samples were aged for at least 50 cycles. In aging tablet and ring tablets, 10 g of sample was placed in a quartz packed bed reactor (O.D. = 25.8 mm, I.D. = 22 mm, L = 600 mm). The reactor tube was placed in a microthermal furnace (MTSC12.5R x 18-1Z, Mellen, USA) with temperature feedback control from a K-type thermocouple (Omega, USA) at the middle of the DFM bed. Compressed gases were mixed at designated flow rates with mass flow controllers.

Steam was delivered using a reactor feed tube pre-heated to 200°C, which vaporized water injected by a syringe pump (Cole-Parmer, USA). An ice bath was placed at the exit of the reactor to condense the steam from the feed as well as that produced during the methanation reaction. The dry gas composition was analyzed in an Enerac 700 at NTP. A set up of the reactor system is found in **Figure 3.2**.

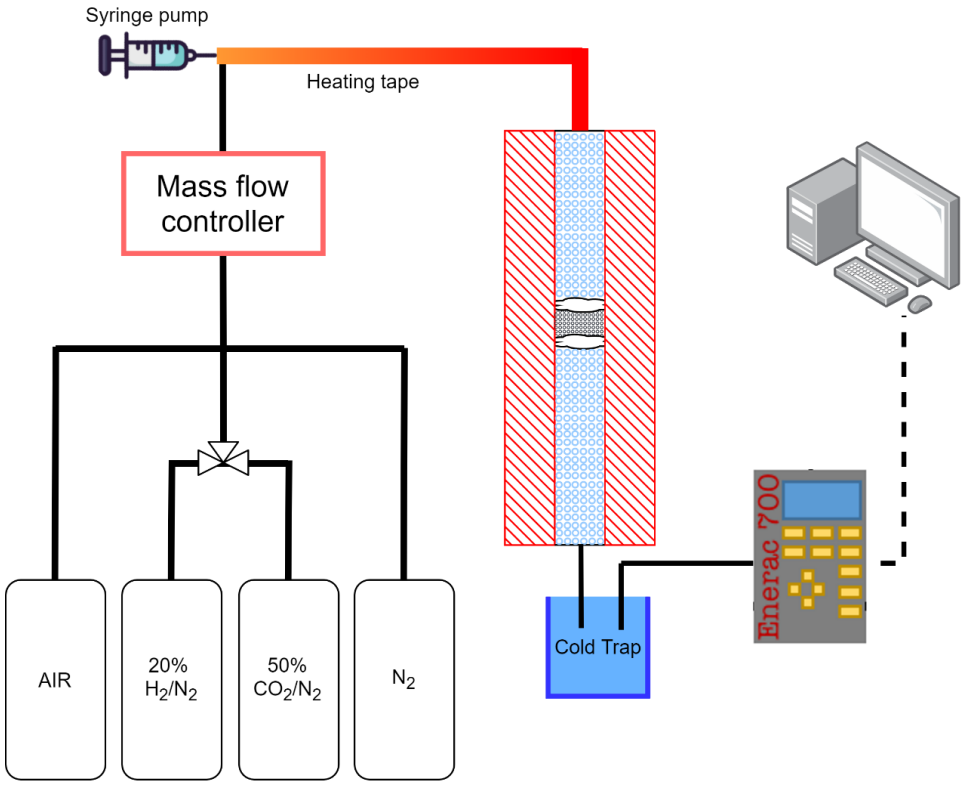


**Figure 3.2:** Set up of reactor for simulated power plant flue gas cyclic studies.

Tablet and ring tablet samples were pre-reduced in-situ at 350°C (at a heating rate of 2°C/min) for 3 hours with 20% $H_2/N_2$ with a total flow rate of 2 L(NTP)/h/$g_{DFM}$ to form catalytically active $Ru^0$ and to hydrogenate the $Na_2CO_3$ precursor to "$Na_2O$". After pre-reduction, the reactor was cooled to 320°C for isothermal cycles. Details of each of the cycle steps are found in **Table 3.2**; each step was carried out at 320°C with a total flowrate of 400 ml/min (Gas Hourly

Space Velocity (GHSV): 1300 $h^{-1}$). Steps 2 and 4 ($N_2$ purge) were required to avoid contact of $O_2$, always present in the simulated flue gas, and $H_2$. At least 50 consecutive $CO_2$ adsorption/methanation cycles were performed.

**Table 3.2:** Steps for cycles of adsorption and methanation in simulated power plant flue gas conditions.

| Step # | Description | Duration | Gas composition |
|---|---|---|---|
| 1 | Adsorption | 10 min | 7.5% $CO_2$, 4.5% $O_2$, 15% $H_2O$, balance $N_2$ |
| 2 | Purge | 4 min | $N_2$ |
| 3 | Hydrogenation | 10 min | 15% $H_2/N_2$ |
| 4 | Purge | 4 min | $N_2$ |

Similarly, 1 g of 0.5%Ru, 6.1% "$Na_2O$"/$Al_2O_3$ DFM granules was loaded in a smaller quartz tube reactor (O.D. = 12.75 mm, I.D. = 10.5 mm, L = 500 mm) and aged in the set up described above **Figure 3.2**. The granules were also pre-reduced in-situ following the same procedure; after pre-reduction, the reactor was cooled to 320°C for isothermal cycles under the same conditions detailed above (**Table 3.2**) but using a total flowrate of 200 ml/min (GHSV: 7700 $h^{-1}$).

Following the cycles, all samples were left to cool to room temperature in $N_2$ and passivated using a dilute stream of $O_2$ (2% $O_2/N_2$) at a flow rate of 1 L(NTP)/h/$g_{DFM}$ before discharging the reactor to protect against over oxidation.

For comparison, a 50-cycle aging study was performed on 0.5% DFM granules using a clean stream of $CO_2$ during adsorption (i.e., 7.5% $CO_2/N_2$, no $O_2$ or $H_2O$). All other conditions and cyclic durations are as detailed above.

#### 3.2.2.2 Fixed bed microreactor transient studies to evaluate the effect of $O_2$ and $H_2O$ (performed at Polytechnic University of Milan)

Transient analysis of the flue gas $CO_2$ adsorption/reduction cycles were also performed. These experiments were performed on 120 mg of 0.5% Ru, 6.1% "$Na_2O$"/$Al_2O_3$ DFM granules loaded in a quartz microreactor (internal diameter = 8 mm) connected to a gas manifold for step changes in the inlet gas concentration. The gases leaving the reactor were continuously analyzed by means of a Pfeiffer QMS200 mass spectrometer and a MKS Multigas 2030FT-IR spectrometer. An Agilent micro gas chromatograph was also used for periodic analysis of $CH_4$, CO and $CO_2$.

Before the test, the sample was pre-treated in 4% $H_2$/He at 500°C with a heating rate of 10°C/min to decompose the carbonate precursor. Cyclic experiments were performed at the constant temperature of 350°C and with a constant flowrate of 200 ml (NTP)/min (GHSV: 60000 $h^{-1}$). A $CO_2$ capture and methanation cycle is composed by a 10-minute adsorption step and a 10-minute reduction step, each followed by a 5-minute inert purge.

A total of 9 cycles were performed on the same sample, divided in 3 sets composed of 3 cycles each. After each set the temperature was increased in 4% $H_2$/He to 500°C to sweep the DFM surface. The reduction phase atmosphere was maintained equal to 4% $H_2$/He for each cycle. On the other hand, two different adsorption atmospheres have been tested: 1% $CO_2$/He, defined as "ideal" conditions, and 1% $CO_2$/3% $O_2$/2.5% $H_2O$/He, defined as "air + steam" conditions. The first set (3 cycles) was carried out with an "ideal" adsorption atmosphere; the second set (3 cycles) with a "air + steam" adsorption atmosphere; the third set (3 cycles) with an "ideal" adsorption atmosphere.

### 3.2.3 Characterization of fresh and aged power plant samples

#### 3.2.3.1 In-situ FT-IR (performed at Polytechnic University of Milan)

FT-IR spectra were obtained using a Nicolet Nexus Fourier Transform instrument equipped with a DTGS detector with a resolution of 4 $cm^{-1}$ (number of scans = 20). The analysis was carried out on 15 mg of sample, crushed and compressed in a self-supporting disc of 13 mm diameter, and placed in a stainless-steel cell (ISRI Infrared Reactor, Granger, IN, USA) that allows in-situ thermal treatments under vacuum or controlled atmosphere. FT-IR tests were carried out on the fresh and aged 0.5%Ru, 6.1% "$Na_2O$"/$Al_2O_3$ DFM granules in order to characterize the adsorbed species at reaction conditions. Three $CO_2$ capture and methanation cycles were performed at 320°C by alternating $CO_2$ capture (5 mbar $CO_2$, 10 min) and reduction (40 mbar $H_2$, 10 min). After each phase, the sample was vacuumed for 5 min to evacuate unreacted gases. All shown spectra refer to the third cycle of capture and methanation.

In order to characterize the fresh and spent material, CO adsorption (5 mbar) was performed at 25°C. Before all measurements, the samples were pretreated at 375 °C in $H_2$ (300 mbar) for 30 minutes.

#### 3.2.3.2 CO chemisorption (performed at Polytechnic University of Milan)

CO pulse chemisorption tests were performed on fresh and aged 0.5% Ru, 6.1% "$Na_2O$"/$Al_2O_3$ granule samples using a Thermoquest TPDRO1100 equipped with a thermal conductivity detector. CO pulses were introduced at room temperature on 100 mg of sample, after in-situ pre-reduction (5% $H_2$/Ar, 1 h at 500°C, heating rate: 10°C/min) and inert purge (30 min at 500°C then cooled to room temperature). In all cases, 1:1.5 Ru:CO stoichiometry was assumed for

the evaluation of the dispersion [61] and a hcp (hexagonal close-packed) Ru particle was assumed for the calculation of the average particle diameter, using the correlation reported in [61].

## 3.3 The role of $RuO_x$ in enhancement of $CO_2$ adsorption

### 3.3.1 Materials synthesis

#### 3.3.1.1 Supported alkali and alkaline earth metal sorbents

Four alkaline sorbents ($Na_2O$, CaO, MgO, and BaO) were prepared on $\gamma$-$Al_2O_3$ at 10% loading. Aqueous solutions of $Na_2CO_3$ (Sigma Aldrich), $Ca(NO_3)_2 \cdot 4H_2O$ (Sigma Aldrich), $Mg(NO_3)_2 \cdot 6H_2O$ (Sigma Aldrich), and $Ba(NO_3)_2$ (Sigma Aldrich) were impregnated into the alumina granules using the incipient wetness method. Multiple impregnation steps were occasionally needed to reach the target sorbent loading due to the limits of precursor salt solubility. The partially loaded sample was dried overnight (>12 hours) in static air at 100°C between incipient wetness impregnations. A slight excess of solution, with respect to the total pore volume of the granules, was used to favor the uniformity of the DFM batch. Once the target loading was achieved, the sample was calcined for 3 hours at 400°C to decompose the precursor salt and achieve the final sorbent form. 6.1% $Na_2O$ was also impregnated onto the granules and zirconium (IV) oxide-yttria stabilized ($ZrO_2$-Y) (Sigma Aldrich, submicron powder) following the above procedure.

#### 3.3.1.2 Supported alkali and alkaline earth metal sorbents with Ru

All of the samples in Section 3.3.1.1 were also prepared with 1% Ru. First, the sorbents were impregnated onto the carriers as described. After calcination, the adsorbent samples were impregnated with Ru using an aqueous solution of ruthenium (III) nitrosyl nitrate ($Ru(NO)(NO_3)_3$)

precursor salt (Alfa Aesar, Ru 32%). Again, a slight excess of solution, with respect to total pore volume of the granules, was used during impregnation to favor uniform impregnation of Ru. The Ru-loaded samples were dried for 2 hours in static air at 120°C and subsequently calcined for 3 hours at 250°C to decompose the precursor salt.

Samples of x% Ru, 10% $Na_2O/Al_2O_3$ (x = 0.1, 0.5, 1, 3, 5) and 1% $Ru/Al_2O_3$ (no sorbent) were also prepared with the above procedure.

### 3.3.2 Thermal gravimetric analysis (TGA)

The following thermal gravimetric studies were performed in a NETZSCH TG 209 F1 Libra unit. For all studies, samples (20-30 mg) were loaded into an alumina crucible and dried in $N_2$ at 120°C for 3 hours. All steps were carried out with a total gas flow of 80 ml/min (STP) at 1 atm. All heating steps were carried out at 5 K/min and all cooling steps at 10 K/min unless otherwise specified.

#### 3.3.2.1 Adsorption capacity of supported alkali and alkaline earth metal sorbents at ambient air conditions

Room temperature (25°C) $CO_2$ adsorption capacity of the supported alkaline sorbents was studied. After drying as described above, samples were calcined in a mixture of 7:1 air/$N_2$ at 400°C for 6 hours. Samples were then cooled to 25°C in $N_2$ and subsequently exposed to a stream of 375 ppm $CO_2$, 19% $O_2$, and balance $N_2$ for 6 hours.

#### 3.3.2.2 Adsorption capacity of supported alkali and alkaline earth metal sorbents with Ru at ambient air conditions

$CO_2$ adsorption capacity of the supported Ru + sorbent/$Al_2O_3$ samples was studied at 25°C. After drying, samples were reduced under a 15% $H_2/N_2$ stream at 300°C for 6 hours. Once cooled to 25°, samples were exposed to a stream of 375 ppm $CO_2$, 19% $O_2$, and balance $N_2$ for 6 hours.

#### 3.3.2.3 Adsorption capacity of 10% $Na_2O/Al_2O_3$ with varying levels of Ru

x% Ru, 10% $Na_2O/Al_2O_3$ (x= 0.1, 0.5, 1, 3, 5) samples were studied for their room temperature $CO_2$ adsorption capacities. After drying, samples were reduced under a 15% $H_2/N_2$ stream at 300°C for 6 hours. Once cooled to 25°C, samples were exposed to a stream of 375 ppm $CO_2$, 7.5% $O_2$, and balance $N_2$ for 6 hours.

#### 3.3.2.4 Extent of Ru oxidation

The extent of Ru oxidation on alumina-supported 1% Ru, 10% sorbent samples was studied at 25°C, the condition for direct air capture of $CO_2$. After drying, samples were reduced under a 15% $H_2/N_2$ stream at 300°C for 6 hours. Once cooled to 25°C, samples were exposed to a stream of 19% $O_2$ in $N_2$ for 6 hours.

x% Ru, 10% $Na_2O/Al_2O_3$ (x= 0.1, 0.5, 1, 3, 5) samples were also tested for extent of Ru oxidation at room temperature. After drying, samples were reduced under a 15% $H_2/N_2$ stream at 300°C for 6 hours. Once cooled to 25°C, samples were exposed to a stream of 7.5% $O_2$ in $N_2$ for 6 hours.

#### 3.3.2.5 Adsorption capacity of 1% $Ru/Al_2O_3$ at ambient air conditions

The $CO_2$ adsorption of a Ru-only sample (1% $Ru/Al_2O_3$) was tested at 25°C. After drying, the sample was reduced under a 15% $H_2/N_2$ stream at 300°C for 6 hours. Once cooled to 25°C, the sample was exposed to a stream of 375 ppm $CO_2$, 19% $O_2$, and balance $N_2$ for 6 hours.

### 3.3.3 Packed bed studies

Using the set up described in Section 3.1.3 and **Figure 3.1**, adsorption and methanation cycles as described in Section 3.1.3.1 were conducted on 0.1% Ru, 10% $Na_2O/Al_2O_3$ and 1% Ru, 10% $Na_2O/Al_2O_3$ samples using 400ppm $CO_2$/dry air as the adsorption gas.

Adsorption and desorption cycles were performed on 10% $Na_2O/Al_2O_3$. The sample was pre-treated at 400°C (heating rate: 5°C/min) for 2 hours with $N_2$ at a total flow rate of 100 ml/min to decompose any $Na_2CO_3$ to "$Na_2O$". The following steps were taken for subsequent adsorption/desorption cycles:

1. $CO_2$ capture step at 25°C with simulated ambient air (400 ppm $CO_2$/air) overnight to ensure saturation of material
2. Heating to 400°C in 40 minutes (9-10°C/min) in $N_2$
3. Hold at 400°C for 80 minutes in $N_2$

All steps were performed at 1 atm with a total flow rate of 100 ml/min (GHSV: 12 L(STP)/h/g, 6950 $h^{-1}$).

### 3.3.4 Materials characterization with $H_2$ chemisorption

0.1% Ru, 10% $Na_2O/Al_2O_3$, 1% Ru, 10% $Na_2O/Al_2O_3$ and 3% Ru, 10% $Na_2O/Al_2O_3$ were characterized for Ru dispersion using $H_2$ chemisorption. The same procedure outlined in Section 3.1.4 was used on these samples.

# Chapter 4 : Feasibility Study of dual function materials ($Ru+Na_2O/Al_2O_3$) for direct air capture of $CO_2$ and *in-situ* catalytic methanation: the impact of realistic ambient conditions

*The results presented in this chapter have been published in C. Jeong-Potter, R.J. Farrauto, Feasibility Study of Combining Direct Air Capture of $CO_2$ and Methanation at Isothermal Conditions with Dual Function Materials, APCATB: Environmental, 282 (2021) 119416 (Available online August 2020) and submitted for publication in C. Jeong-Potter, M.J. Abdallah, C. Sanderson, M. Goldman, R. Gupta, and R.J. Farrauto, Dual function materials ($Ru+Na_2O/Al_2O_3$) for direct air capture of $CO_2$ and in-situ catalytic methanation: the impact of realistic ambient conditions.*

This chapter explores the feasibility of translating DFM technology to direct air capture (DAC) applications. Cost of DAC is a large issue and thus, low Ru loadings were used (0.5%, 1%) for this application. Successful cyclic capture of 400 ppm $CO_2$ followed by methanation of the adsorbed $CO_2$ at isothermal conditions (320°C) is demonstrated as a first step in translating the existing DFM technology to DAC. Then, recognizing that isothermal operation for DAC is too energy intensive, we have adopted a temperature-swing operation. We examine the ability of this material to capture $CO_2$ at ambient temperature (25°C) and produce methane upon $H_2$ introduction and heating. Cyclic performance of the material is established through some extended cyclic studies in both dry adsorption and humid adsorption conditions. We discuss the effect of temperature on adsorption capacity and establish flowrate-dependent rates of adsorption to assist in reactor design and sizing. Lastly, a comparative study is performed with a Ru + $CaO/Al_2O_3$ DFM. The work presented is a material study in which DFMs are evaluated for activity and stability. The DFM is evaluated for activity and stability with the goal of depositing it as an active

washcoat on a monolith structure to minimize pressure drop, as is common for the catalytic converter in vehicles.

## 4.1 Contextualizing DFM for DAC

The proposed process of using DFM for combined DAC and methanation is conceptualized in **Figure 4.1**. In the first step, $CO_2$/air is filtered of particulates before it enters the DFM at ambient conditions (25°C) upon which the $CO_2$ is selectively adsorbed, expelling $CO_2$-free air. Upon saturation of the DFM, the material is heated in the presence of $H_2$ to catalytically methanate the adsorbed $CO_2$. The product stream ($CH_4 + 2H_2O$) can be dried and compressed for re-introduction to the existing natural gas infrastructure. It is expected that multiple reactors will operate in parallel for a continuous operation.

Multiple DAC studies have suggested that an array of renewable energy sources can be used to provide temperatures required for methanation ($T < 300°C$) [34] (i.e., renewable electricity [39,62], concentrated solar power [37]). To ensure a low carbon footprint for the proposed technology, we recommend the use of renewable (or waste) energy sources to provide the necessary heat and additional energy for equipment such as fans and compressors. Since renewable $H_2$ is expected to be available on site for methane, using a $H_2$ powered fuel cell is suggested.

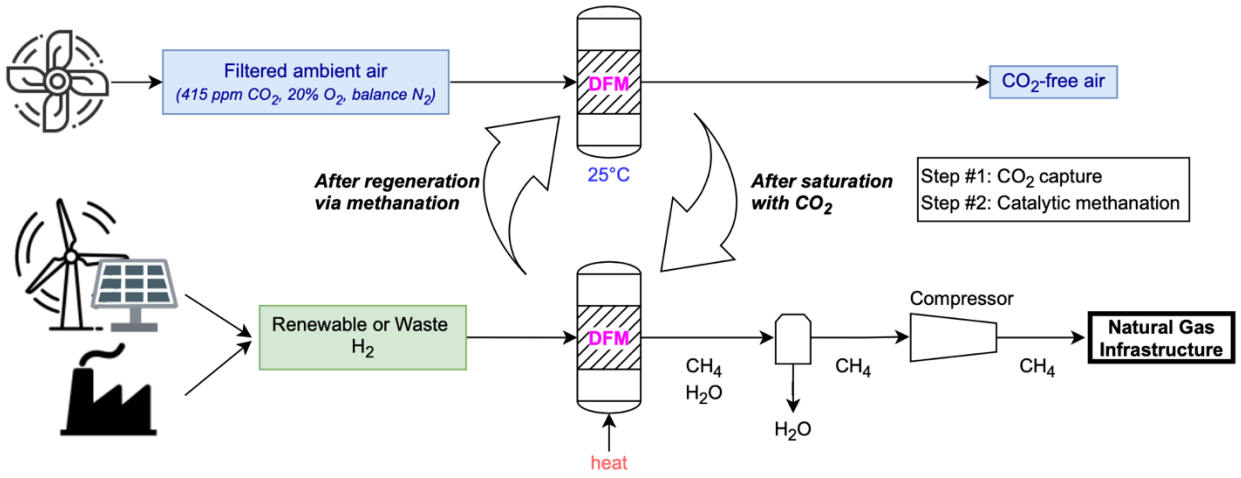


**Figure 4.1**: Proposed temperature-swing process of combining DAC and methanation using DFM. Adsorption occurs at ambient temperatures (0-40°C) and methanation occurs at T > 200°C for DAC-M; in isothermal conditions (i.e., power plant application), the adsorption temperature may be ~300°C. Multiple parallel reactors are anticipated for continuous capture and conversion.

## 4.2 Cyclic operation of DFM for DAC in isothermal conditions (320°C)

Packed bed reactor studies of isothermal adsorption/methanation cycles (**Figure 4.2**a) and adsorption/desorption cycles (**Figure 4.2**b) were conducted on the DFM (0.5% Ru, 6.1% "$Na_2O$"/$Al_2O_3$) using 400 ppm $CO_2$ in air (21% $O_2$, balance $N_2$) in the adsorption step. Four cycles are shown for each set of tests.

**Figure 4.2**a shows that the DFM is indeed able to adsorb $CO_2$ (gray dots) from a dilute source (400ppm $CO_2$ in dry air) and produce methane (purple bars). Hydrogenation not only produces methane but also regenerates the DFM fully in the 45-minutes to adsorb a similar amount of $CO_2$ in subsequent cycles. Desorption was also investigated in this case due to the geographic flexibility of DAC. One can imagine that a DAC unit would have the freedom to be located strategically at the point of utilization to avoid the $CO_2$ transportation issues common with the effluent capture case. In the DAC case, methane production may not be required and instead, the $CO_2$ can be captured and desorbed for another utilization pathway. However, simple desorption

(green bars in **Figure 4.2**b) via an inert purge does not regenerate the same amount of DFM capacity as hydrogenation. In fact, during the 45-minute purge, only 20% of the DFM is regenerated for subsequent cycles. This indicates that methanation of the adsorbed $CO_2$ is the more efficient method of cyclic DFM operation.

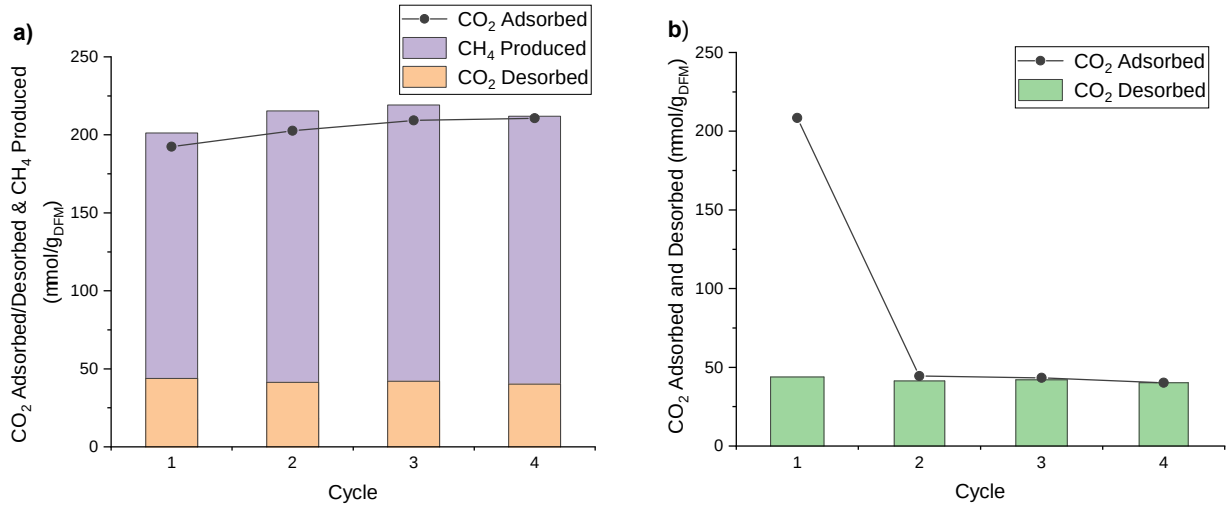


**Figure 4.2**: Results of isothermal (320°C) **(a)** adsorption-methanation cycles and **(b)** adsorption-desorption cycles on 0.5% Ru, 6.1% "$Na_2O$"/$Al_2O_3$ granules (300µm) in a packed bed reactor. Details of cycle steps and operating conditions can be found in Section 3.1.3.1 and 3.1.3.2.

## 4.3 Short-term packed bed aging of Ru+$Na_2O$/$Al_2O_3$ DFM in temperature-swing operation with ambient temperature adsorption

The viability of 1% Ru, 10% $Na_2O/Al_2O_3$ (Ru+$Na_2O/Al_2O_3$ DFM) for combined DAC and methanation in a temperature swing operation was tested through a short-term packed bed aging study. The results of 10 cycles of adsorption (dry air) and methanation are shown in **Figure 4.3**.

The DFM adsorbs an average of 550 $\mu mol_{CO2}/g_{DFM}$ at 25°C. The adsorption performance (black dots) is consistent from cycle to cycle, showing stability. The amount of methane produced from cycle to cycle (purple bars) after heating and with a hold at 300°C is also consistent, averaging

about 300 $\mu mol_{CH4}/g_{DFM.}$ As a result, 54.5% of the total $CO_2$ adsorbed was converted to $CH_4$. Selectivity towards $CH_4$ is 100% in all cycles and no other products (including CO) were detected.

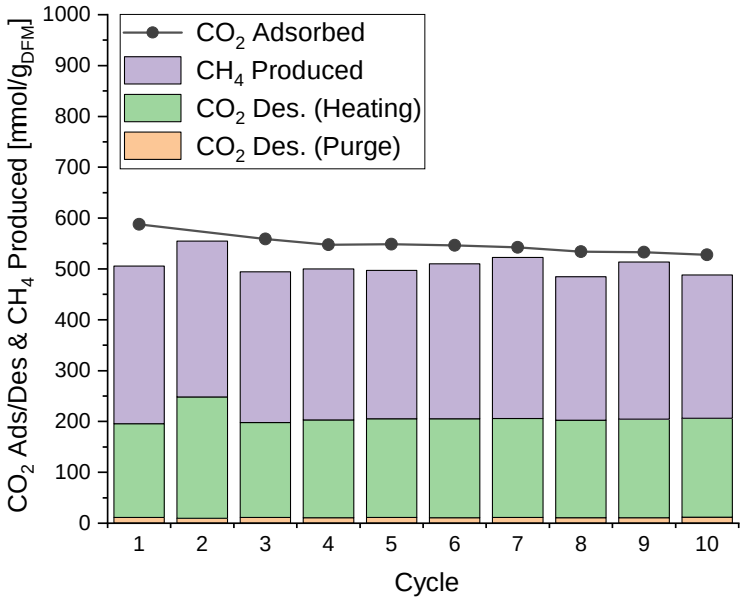


**Figure 4.3:** $CO_2$ adsorption (black dots), $CO_2$ desorption (orange bars and green bars), and $CH_4$ production (purple bars) for 10 cycles of adsorption/methanation on Ru+$Na_2O$ DFM as follows: i) adsorption at 25°C in the presence of 400 ppm $CO_2$/air (dry), ii) heating to 300°C in 15% $H_2/N_2$, and iii) 2-hour hold at 300°C in 15% $H_2/N_2$. The reactor was purged after adsorption to avoid mixing $O_2$ and $H_2$. Experimental details can be found in Section 3.1.3.3.

A major contribution to the observed low $CH_4$ production is the amount of $CO_2$ that is desorbed (about 35% of the adsorbed quantity) unreacted during heating. This is an artifact of how $H_2$ is introduced and how the bed is heated.

**Figure 4.4** shows the profiles of $CO_2$ desorbed (green solid line) and $CH_4$ produced (purple solid line) during heating from 25°C to 300°C in cycle 10.

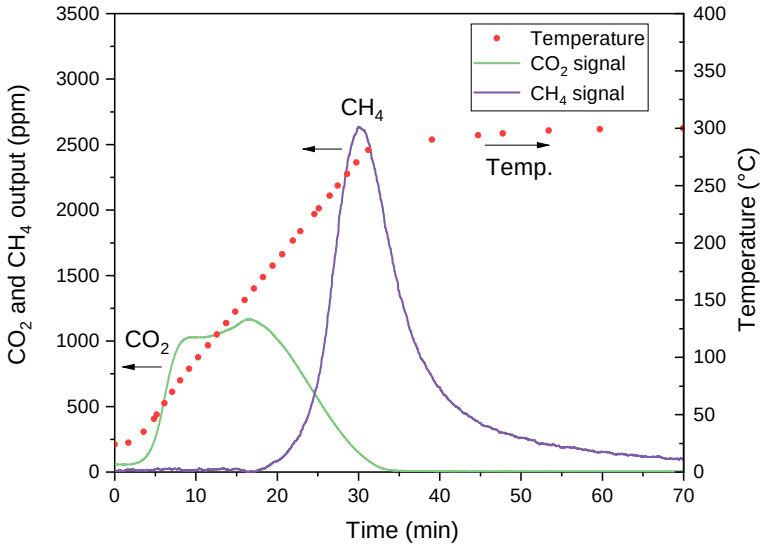


**Figure 4.4:** $CO_2$ (green solid line) desorbed and $CH_4$ (purple solid line) generated with temperature readings (red dots) from 25°C to 300°C with 15% $H_2/N_2$ in packed bed configuration. Profiles correspond to cycle 10 of adsorption/methanation (**Figure 4.3**); experimental conditions can be found in Section 3.1.3.3.

During heat up, $CO_2$ is detected at the reactor outlet starting as low as 50°C and broad peak between 100°C and 175°C is exhibited. After 175°C, the $CO_2$ output decreases and $CH_4$ is detected. Duyar et al. observed that methanation over $Ru/Al_2O_3$ catalyst also began at 175°C [5], corroborating the results shown here. $CH_4$ output peaks between 250°C and 275°C, indicating that the highest kinetic rate is achieved beyond 250°C. The catalytic component of the DFM (i.e., Ru) is oxidized during adsorption due to the presence of $O_2$; subsequently, the material must be heated to a sufficient temperature to allow the $RuO_x$ species to be reduced to catalytically active $Ru^0$ before methanation can occur. In addition, the kinetics for methanation must be more favorable than desorption, which can also only be achieved at sufficiently high temperature. As such, desorption of unreacted $CO_2$ is favored until a sufficiently high temperature is achieved for methanation light-off. This theory was verified with a temperature programmed reduction (TPR) of oxidized $Ru+Na_2O/Al_2O_3$ DFM to determine the temperature at which reduction of the $RuO_x$ species begins. The resulting TG mass change profile found in **Figure 4.5**.

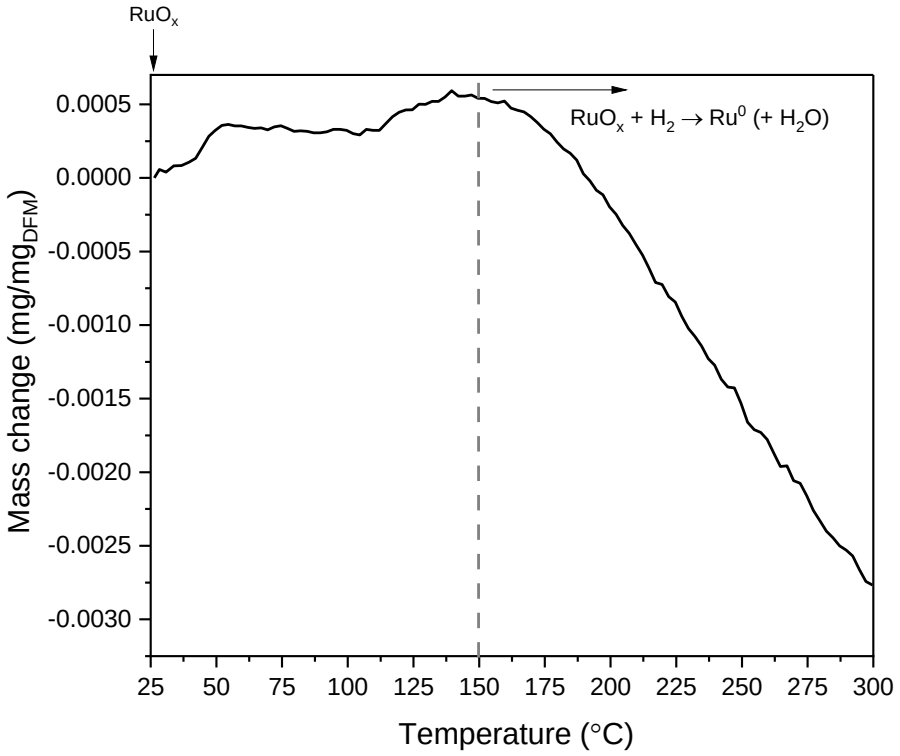


**Figure 4.5:** TG mass profile for TPR of oxidized Ru+$Na_2O/Al_2O_3$ DFM with 15% $H_2/N_2$ sweep gas. Temperature at which mass loss is first detected (150°C) is demarked by a gray dashed line. Experimental conditions can be found in Section 3.1.2.2.

It can be seen that the sample starts losing mass at around 150°C (gray dashed line) and a fast linear rate of mass loss is achieved after 175°C, signaling active reduction of the $RuO_x$ species to catalytically active $Ru^0$. This correlates well with the light-off of methanation seen in **Figure 4.4** indicating that there is sufficient reduction of the $RuO_x$ to then initiate methanation at 175°C.

Identifying techniques to reduce the amount of $CO_2$ that desorbs during heating will be crucial for increasing $CH_4$ production (relative to the total $CO_2$ adsorbed). Strategies for selectively heating the washcoat on the monolith will be addressed in future scale up work. In actual application of the DFM, we expect the $H_2$ source will be in higher concentration (>50% if from waste streams, or better yet pure green $H_2$ from renewable electrolysis). As a result, it is likely that

methane light-off may occur at lower temperatures, thus reducing the amount of $CO_2$ that is unreacted. It is also possible that the $H_2$ will be delivered to the system at higher pressure, which would also reduce the methane light-off temperature. In fact, Kosaka et al. have observed positive results by elevating reaction pressures on Ni-Na/$Al_2O_3$. Through their cycles of adsorption (5% $CO_2/N_2$) and reduction at 450°C, they showed that methane production increased with reduction pressures (between 0.1 and 0.9 MPa) [63]. Additionally, a TPR of $CO_2$-loaded Ni-Na/$Al_2O_3$ showed that as pressure increased, the onset methanation temperature decreased [63]. We expect that similar trends would be observed with our DFM, improving the cyclic conversion of adsorbed $CO_2$ to $CH_4$.

## 4.4 Effect of ambient air humidity (moisture) during adsorption on cyclic performance of Ru+$Na_2O/Al_2O_3$ DFM

Realistic ambient environments for DAC will operate with varying levels of moisture (i.e., humidity). Therefore, it is necessary to test the Ru+$Na_2O/Al_2O_3$ DFM for stable cyclic performance after exposure to humid air during adsorption.

**Figure 4.6** shows the results of 5 cycles of humid adsorption (~2% $H_2O$, 90% relative humidity at 25°C) and subsequent methanation. Average results from 10 cycles of dry adsorption and methanation (**Figure 4.3**) are included and labelled "DRY AVG." for comparison to the humid adsorption and methanation cycles (1-5).

Cycles performed with humid air showed overall superior adsorption and methanation with stable performance. In these cycles, the average total $CO_2$ adsorbed (black dots) was about 1300 $\mu mol_{CO2}/g_{DFM}$, which is a 2.36-fold increase in capture capacity compared to dry cycles. This is most likely due to the formation of $NaHCO_3$ induced by the presence of $H_2O$ [5,64]. Duyar et al.

speculated the formation of $NaHCO_3$ on the DFM after exposure to moisture [5] but it has yet to be confirmed. Wang et al. has shown that it is difficult to detect the Na-species that are present on the DFM, particularly by x-ray diffraction, due to their amorphous nature [11].

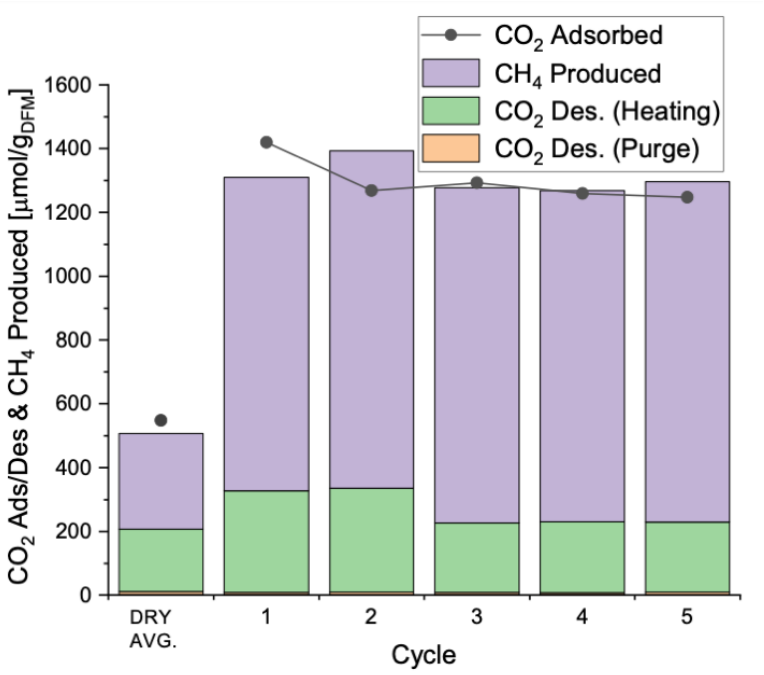


**Figure 4.6:** $CO_2$ adsorption (black dots), $CO_2$ desorption (orange bars and green bars), and $CH_4$ production (purple bars) for 5 cycles of adsorption/methanation on $Ru+Na_2O/Al_2O_3$ DFM as follows: i) adsorption at 25°C in the presence of 400 ppm $CO_2$, ~2% $H_2O$/air (~90% humidity), ii) heating to 300°C in 15% $H_2/N_2$, and iii) 2-hour hold at 300°C in 15% $H_2/N_2$. Average results from 10 cycles of dry adsorption and methanation (labelled "DRY AVG.") are shown. Experimental details can be found in Section 3.1.3.3.

As a consequence of greater adsorption, average methane production (purple bars) also increased to about 1040 $\mu mol_{CH4}/g_{DFM}$ (3.47 times an average production in dry conditions). Interestingly, the amount of unreacted $CO_2$ that desorbed during heating (green bars) was only 260 $\mu mol_{CO2}/g_{DFM}$ (~21% compared to 35% for the dry system shown in **Figure 4.3**). This translates to an increase in $CH_4$ production and an increase in the amount of adsorbed $CO_2$ that is converted to $CH_4$ (80% compared to 54.5% for dry adsorption conditions). Once again, we see that product selectivity is 100% towards $CH_4$. These results show promise in using the $Ru+Na_2O/Al_2O_3$ DFM

in a variety of ambient conditions. A series of adsorption temperatures and humidity levels will need to be tested to clearly define the range of adsorption and methanation capacities of this material.

The stability of the Ru+$Na_2O$ DFM after cycling was verified with stable methanation performance and no changes in dispersion as measured by $H_2$ chemisorption. As seen in **Table 4.1**, the cycled material (Ru+$Na_2O$ DFM after 5 cycles of humid (relative humidity of 90%) adsorption and methanation) maintains similar $H_2$ adsorption and Ru dispersion values as the fresh material. This indicates that the Ru sites are stable after exposure to high levels of $O_2$ and moisture during the adsorption followed by methanation up to 300°C. This is consistent with characterization of our DFMs by TEM and EDS mapping after long term aging in simulated flue gas conditions [11].

**Table 4.1:** $H_2$ chemisorption and Ru dispersion on fresh and cycled Ru+$Na_2O$ DFM (1% Ru, 10% $Na_2O/Al_2O_3$). The "cycled" material was tested for 5 cycles of humid adsorption at ambient conditions and methanation to 300°C (**Figure 4.6**). Experimental conditions of chemisorption can be found in Section 3.1.4.

| Sample Condition | $H_2$ adsorbed [µL/g] | Dispersion |
|---|---|---|
| Fresh | 48.16 | 4.34% |
| Cycled | 50.72 | 4.57% |

## 4.5 Comparison of Ru+$Na_2O/Al_2O_3$ DFM and Ru+$CaO/Al_2O_3$ DFM: importance of simulating realistic humidity testing conditions

CaO is an alternative sorbent previously investigated in DFMs [5,7,8]; however, $Na_2O$ (in concert with Ru) has been shown to have more favorable kinetics to methanation [6]. Arellano-Treviño et al. reported that CaO-containing DFM required a much longer time for complete

methanation of the adsorbed $CO_2$ and attributed this to the presence of strong carbonates [6]. The presence of strongly bound carbonates is favorable for temperature swing operation where retention of adsorbed $CO_2$ during heat up needs to be maximized. This is supported by comparing the $CO_2$ and $CH_4$ reactor output profiles as a function of temperature as found in **Figure 4.7**.

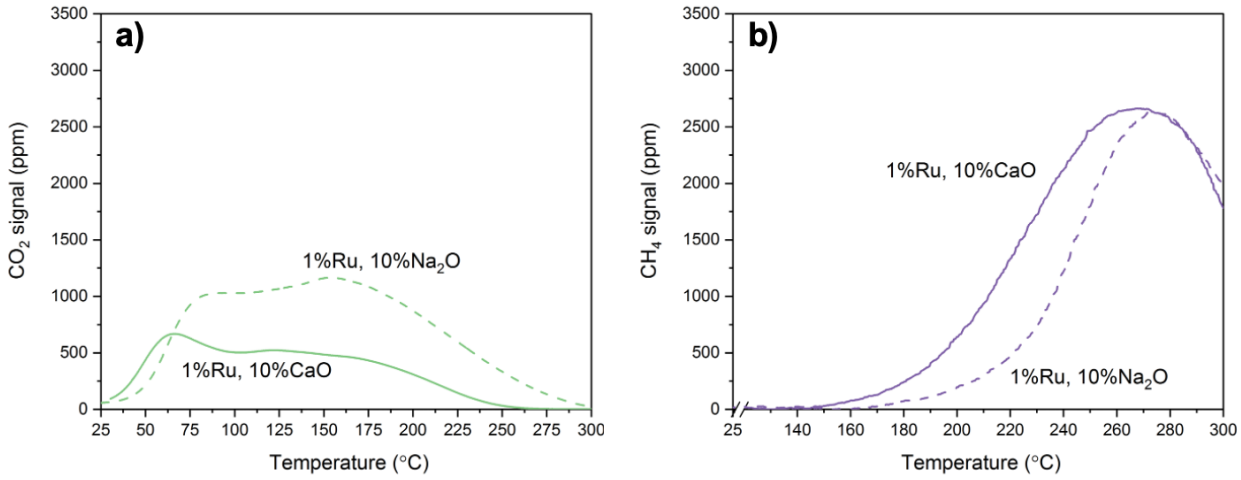


**Figure 4.7:** Output profiles of (**a**) $CO_2$ (green) and (**b**) $CH_4$ (purple) as a function of temperature during heating from 25°C to 300°C with 15% $H_2/N_2$ in packed bed configuration. Profiles for $Ru+Na_2O/Al_2O_3$ DFM (dashed curves) correspond to cycle 10 of dry adsorption/methanation and profiles for $Ru+CaO/Al_2O_3$ DFM (solid curves) correspond to cycle 3 of dry adsorption/methanation; experimental conditions can be found in Section 3.1.3.3.

When comparing the $CO_2$ desorption profiles of Ru+CaO (solid line) and $Ru+Na_2O$ (dashed line) DFM in **Figure 4.7**a, we see that the initial rate of $CO_2$ desorption (occurring until about 50°C) is higher with Ru+CaO. However, the rate of $CO_2$ desorption from the $Ru+Na_2O$ DFM quickly surpasses this rate; as discussed in Section 4.3, the $CO_2$ desorption is maintained in peak values between 75 and 175°C. These values are much higher than the second, broader peak seen on the desorption profile of the Ru+CaO DFM, which spans between 100°C and 175°C before tailing off. In general, the Ru+CaO DFM desorption profile is less broad and intense than that of the $Ru+Na_2O$ DFM, equating to less $CO_2$ desorption upon heating. In the cycles shown, the amount

of $CO_2$ desorbed was 96 $\mu mol_{CO2}/g_{DFM}$ for the Ru+CaO DFM and 195 $\mu mol_{CO2}/g_{DFM}$ for the Ru+$Na_2O$ DFM, indeed showing that Ru+CaO retains more $CO_2$ during heat up.

In **Figure 4.7**b, we also see that the Ru+CaO DFM (solid line) methane light-off occurs at ~150°C while for Ru+$Na_2O$ DFM (dashed line) light-off is about 175°C. Peak $CH_4$ production with the Ru+CaO DFM at around 260°C, but at around 270°C with the Ru+$Na_2O$ DFM. Overall, Ru+CaO DFM shows a higher methane production at 350 $\mu mol_{CH4}/g_{DFM}$ (compared to 280 $\mu mol_{CH4}/g_{DFM}$ with the Ru+$Na_2O$ DFM) due to higher $CO_2$ retention as exhibited by less desorption. These results were all in the dry adsorption conditions; it is important to determine the effects of humidity on the Ru+CaO DFM since DAC will contain various amounts of moisture. The results of cycling the Ru+CaO for adsorption and methanation in dry and humid adsorption conditions are found in **Figure 4.8**.

As shown in cycles 1-3, performance of the Ru+CaO DFM in dry adsorption conditions is promising. Though total $CO_2$ adsorption (averaging 470 $\mu mol_{CO2}/g_{DFM}$) is lower than that of the Ru+$Na_2O$ DFM, methane production averages 360 $\mu mol_{CH4}/g_{DFM}$ (purple bars) with less $CO_2$ desorbed during heating (green bars, averaging 96 $\mu mol_{CO2}/g_{DFM}$). Methane production is about 77% of the adsorbed $CO_2$.

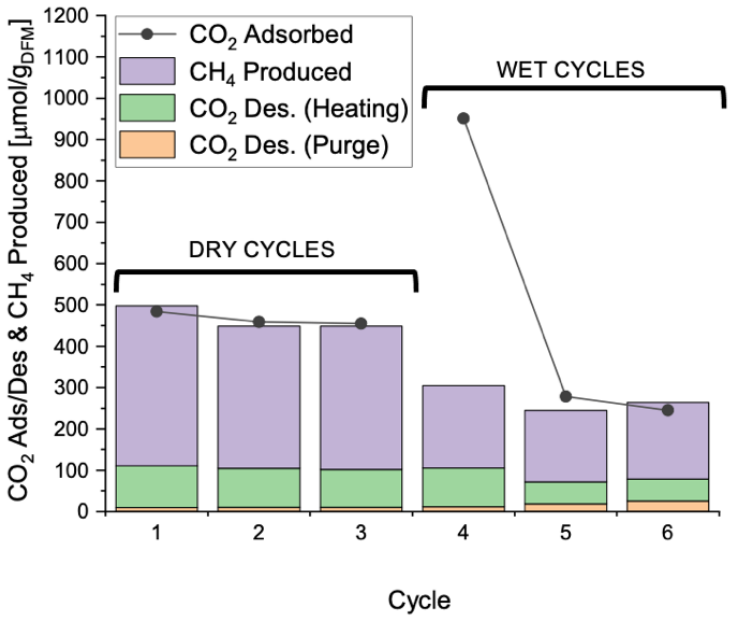


**Figure 4.8:** $CO_2$ adsorption (gray dots), $CO_2$ desorption (orange bars and green bars), and $CH_4$ production (purple bars) for 6 total cycles of adsorption/methanation on Ru+CaO/$Al_2O_3$ DFM. Cycles 1-3 (labeled "Dry Cycles") were done with dry adsorption gas (400 ppm $CO_2$/air) and cycles 4-6 (labeled "Wet Cycles") were done with humid adsorption gas (400 ppm $CO_2$, ~2% $H_2O$/air). The cycle steps are as follows: i) adsorption at 25°C, ii) heating to 300°C in 15% $H_2/N_2$, and iii) 2-hour hold at 300°C in 15% $H_2/N_2$. Experimental details can be found in Section 3.1.3.3.

Significant reduction in methane production is observed in humid adsorption conditions (cycles 4-6). In cycle 4, the total $CO_2$ adsorption is greatly increased to about 950 $\mu mol_{CO2}/g_{DFM}$, following the same trend seen with the Ru+$Na_2O$ DFM; however, only a small fraction of this $CO_2$ is either desorbed or methanated (32%), greatly reducing the $CO_2$ adsorption capacity in the subsequent cycles. In cycles 5 and 6, the adsorption capacity averages to about 260 $\mu mol_{CO2}/g_{DFM}$ and methane production averages to about 180 $\mu mol_{CO2}/g_{DFM}$. This indicates that the Ru+CaO DFM is not a suitable replacement for the Ru+$Na_2O$ DFM under realistic ambient air conditions when attempting to mitigate the desorption of unreacted $CO_2$.

## 4.6 Optimization of the rate of adsorption on $Ru+Na_2O/Al_2O_3$ DFM for reactor design

Optimizing the rate of adsorption is critical for reactor sizing and design. First, the effect of temperature was studied through thermal gravimetric analysis (TGA). Adsorption isotherms generated at 25°C and 320°C are shown in **Figure 4.9**. The high temperature (320°C) was chosen to represent an isothermal operation case (much like our earlier work in power plant DFM [5–7,11,12]).

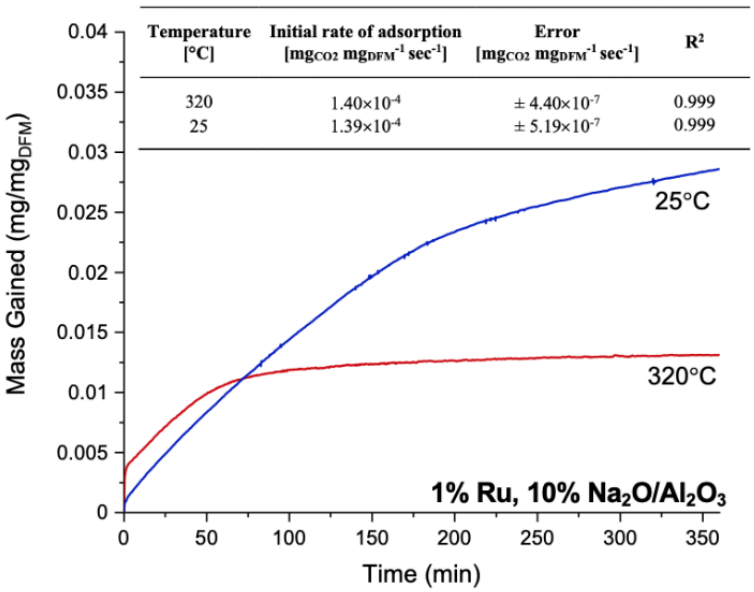


**Figure 4.9:** TG mass gain profiles of $Ru+Na_2O/Al_2O_3$ DFM upon exposure to 375 ppm $CO_2$, 19% $O_2$, and balance $N_2$ at 320°C (red solid line) and 25°C (blue solid line). Initial rates of $CO_2$ adsorption as determined by linear fit of mass change profiles between 0.005 and 0.0075 $mg/mg_{DFM}$ of mass gain can be found in embedded table. Experimental conditions can be found in Section 3.1.2.1.

The initial rates of adsorption are about the same ($1.4\times10^{-4}$ $mg_{CO2}$ $mg_{DFM}^{-1}$ $sec^{-1}$), suggesting a mass tranfer effect. Clearly, adsorption is thermodynamically favored at 25°C (blue) compared to 320°C (red solid line). This is aligned with the fact that $CO_2$ adsorption onto the DFM is an exothermic process [6]. **Figure 4.9** also shows that the rate of adsorption at 25°C remains in the

fast, linear region until well over 100 minutes of $CO_2$/air exposure. This indicates that we can maintain fast kinetics while achieving high adsorption capacities.

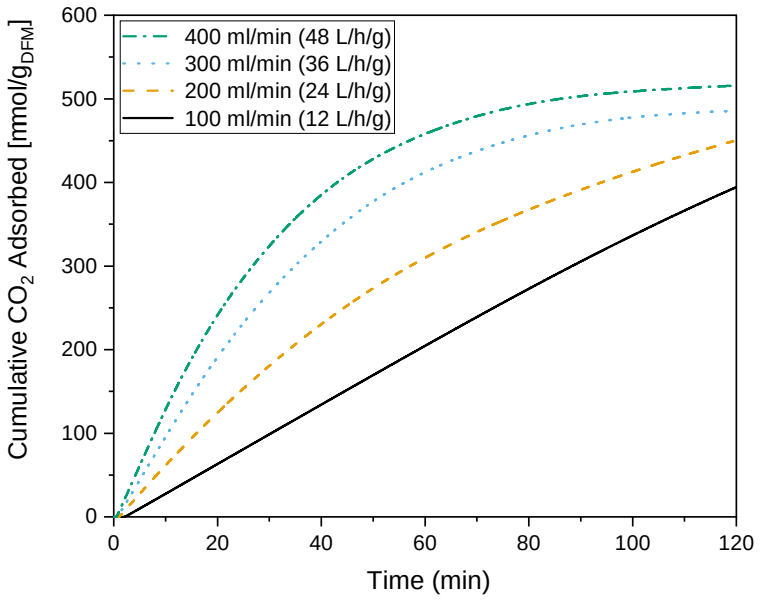


**Figure 4.10:** Cumulative $CO_2$ adsorbed over time on Ru+$Na_2O$ DFM at four different flowrates of 400ppm $CO_2$/air: 100 ml/min (black solid line), 200 ml/min (yellow dashed line), 300 ml/min (blue dotted line), and 400 ml/min (green dash-dot line). Experimental details for these packed bed tests can be found in Section 3.1.3.4.

Four flowrates were tested in a packed bed configuration (**Figure 4.10**) to observe the effect on adsorption behavior. The cumulative amount of $CO_2$ adsorbed over 2 hours shows higher flowrates indeed result in higher initial rates of adsorption. This further confirms that the rate of adsorption in this system is limited by mass transfer of $CO_2$ (in both transfer through the bulk air and in supply of $CO_2$ into the system as induced by the low $CO_2$ concentration). The observed rates of adsorption were quantified by the slopes of the cumulative $CO_2$ adsorption curves in **Figure 4.10** as determined by linear fits. These values can be found in **Table 4.2**.

**Table 4.2:** Initial rates of $CO_2$ adsorption at 25°C on Ru+$Na_2O$ DFM as determined by linear fit of cumulative $CO_2$ adsorption curves found in **Figure 4.10**. The regression was fit for the first 10 minutes of the $CO_2$ adsorption curves. Space velocity is expressed as flowrate per gram of DFM.

| **Flowrate [ml/min]** | **Space Velocity [L(NTP) $h^{-1}$ $g_{DFM}^{-1}$]** | **Initial rate of adsorption [µmol $g_{DFM}^{-1}$ $sec^{-1}$]** | **Error [µmol $g_{DFM}^{-1}$ $sec^{-1}$]** | **$R^2$** |
|---|---|---|---|---|
| 100 | 12 | 0.059 | $\pm 2.93\times10^{-7}$ | 1 |
| 200 | 24 | 0.108 | $\pm 5.36\times10^{-5}$ | 0.999 |
| 300 | 36 | 0.173 | $\pm 2.06\times10^{-5}$ | 1 |
| 400 | 48 | 0.229 | $\pm 3.92\times10^{-5}$ | 1 |

As seen in **Table 4.2**, a four-fold increase in flowrate results in a 3.88-fold increase in rate (0.229 µmol $g_{DFM}^{-1}$ $sec^{-1}$ with an increase to 400 ml/min). This trend is critical when considering the trade-offs between rate, pressure drop, and power requirements. As flowrate is increased, pressure drop will increase, which will in turn increase power requirements of the fans driving air into the system. In future embodiments of the process, DFM – the active material – will be washcoated onto monoliths in order to reduce pressure drop. The monolith will also reduce energy requirements as just the thin washcoat will need to be heated. Such artifacts have made the monolith a primary choice for applications such as the automotive catalytic converter, which requires low pressure drop and rapid heating.

# Chapter 5 : Aging study of low Ru loading Dual Function Materials (DFM) in simulated natural gas power plant flue gas

*The results presented in this chapter have been submitted for publication in C. Jeong-Potter, A. Porta, R. Matarrese, C.G. Visconti, L. Lietti, R.J. Farrauto, Aging study of low Ru loading Dual Function Materials (DFM) for combined power plant effluent $CO_2$ capture and methanation.*

The prior generation of DFM contained 5% Ru and showed excellent stability after aging in simulated flue gas. However, economics of 5% Ru ($22.35/g as of Sept 2021) can be quite burdensome for wide deployment of this technology, and it is beneficial to reduce the cost of materials. This chapter addresses the stability of different Ru-based dual function materials (DFM, x% Ru, 6.1% "$Na_2O$"/$Al_2O_3$, x = 0.5, 1) during cycles of $CO_2$ capture from simulated power plant effluent (320°C; 7.5% $CO_2$, 15% steam, 4.5% $O_2$, balance $N_2$ (v/v)) and subsequent catalytic methanation. Aging studies were carried out to simulate natural gas combustion flue gas. Stability increases with Ru loading; however, 0.5% Ru DFMs demonstrate a small but steady loss of $CH_4$ produced per cycle consistent with deactivation of the Ru component due to exposure to high levels of $O_2$ and steam in the flue gas. CO chemisorption, in-situ FT-IR, and transient microreactor studies all verify that there is loss in Ru active surface area, possibly due to sintering, which consequently results in lower methanating ability. This study, conducted at 320°C for both adsorption and methanation, serves as a baseline performance indicator for future embodiments of the DFM in both DAC and power plant applications. Due to more mild adsorption conditions (ambient temperatures), the DFM is expected to experience less severe deactivation in DAC-M cases. Additionally, deactivation may not be as prominent with the use of higher concentration $H_2$.

## 5.1 Fixed bed reactor aging study of low Ru loading DFM

Fixed bed, cyclic aging studies were performed on low Ru loading DFM supported on γ-$Al_2O_3$ granules, tablets, and ring tablets in simulated power plant flue gas conditions (7.5% $CO_2$, 4.5% $O_2$, 15% steam, balance $N_2$) to assess their stability. Cyclic quantification of $CO_2$ adsorption and $CH_4$ production of 0.5% DFM and 1% DFM tablets are shown in **Figure 5.1**.

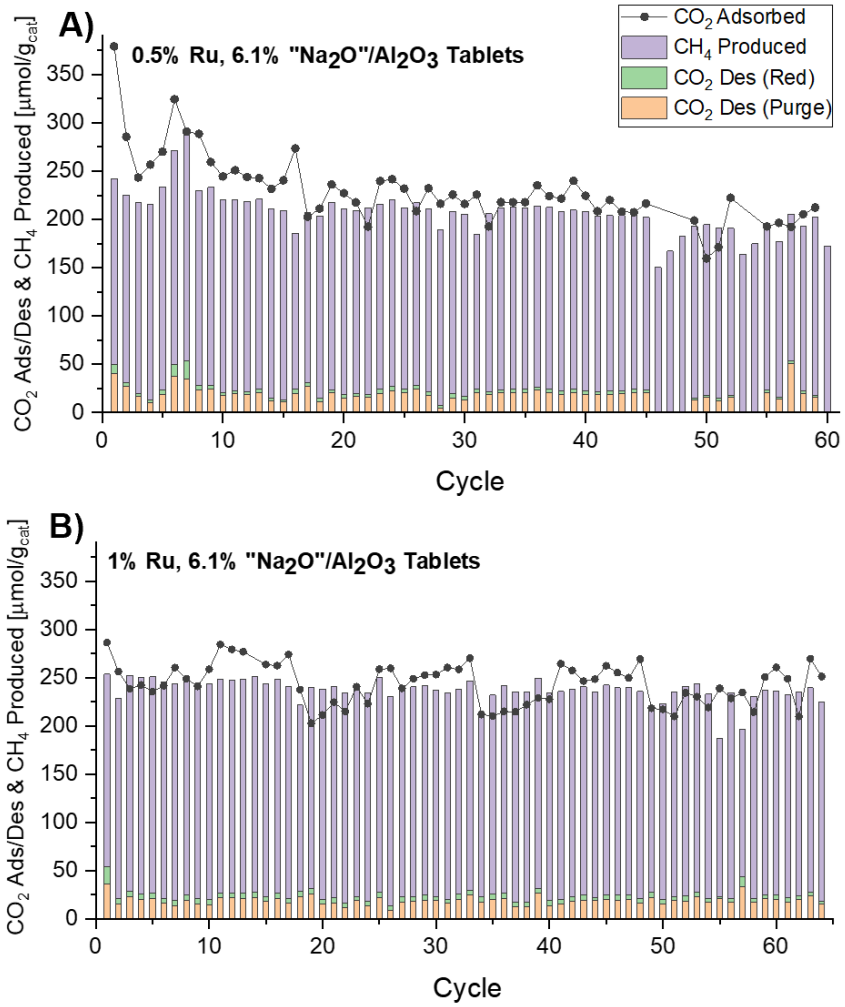


**Figure 5.1:** $CO_2$ adsorption (black dots) and $CH_4$ production (purple bars) for 60+ cycles of adsorption/methanation on (**a**) 0.5% DFM tablets and (**b**) 1% DFM tablets. All cycles were performed at 320°C and 1atm; adsorption was conducted under simulated flue gas composition (7.5% $CO_2$, 4.5% $O_2$, 15% steam, balance $N_2$) and methanation under 15% $H_2/N_2$. Experimental details can be found in Section 3.2.2.1.

It is also evident in **Figure 5.1** that for both materials, there is consistency between the $CO_2$ adsorbed and the amount of $CH_4$ produced; however, the $CH_4$ production data is more consistent and reliable. Methane production during aging of all samples is shown in **Figure 5.2.**

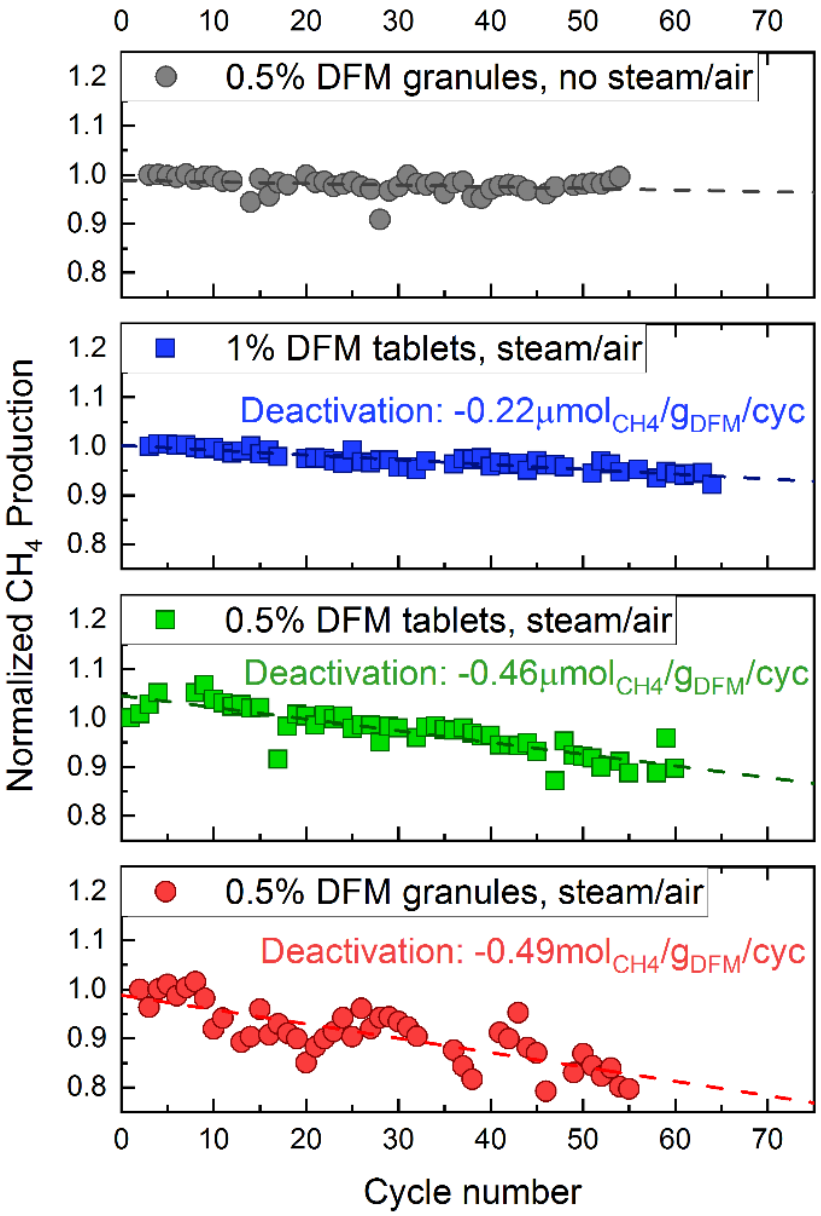


**Figure 5.2:** Methane production results from aging on 0.5 and 1% DFMs. The reported apparent deactivation rates were evaluated by linear regression. Adsorption conditions: 7.5% $CO_2$, 4.5% $O_2$, 15% $H_2O$, balance $N_2$, 10 minutes. Reduction conditions: 15% $H_2/N_2$, 10 minutes. Aging was also performed without $O_2$ and $H_2O$ (gray dots). All tests are performed at 320°C and 1 atm, 1300 $h^{-1}$ GHSV for tablets and ring tablets, and 7700 $h^{-1}$ GHSV for granules.

Without $O_2$ or $H_2O$ (top, gray profile) present in the adsorption step, the 0.5% DFM γ-$Al_2O_3$ granules show stable and consistent methane production. The results of aging 0.5% Ru in simulated flue gas (with $O_2$ and steam; green and red profiles), however, show a clear trend of $CH_4$ production loss with increasing cycles. This, compared to the $O_2$ and steam free profile, demonstrates that the combination of $O_2$ and $H_2O$ in the feed contribute to the deactivation of the material. In particular, it is suspected that $O_2$ causes sintering of the catalyst species as previously shown by Bermejo-López et al. By aging Ru-NiNa and NiNa DFMs over 20 cycles with and without $O_2$, the authors showed that both DFMs only deactivated in the cycles with $O_2$ [29]. Sintering of the Ru has also been observed in the current study, as will be shown in Sections 5.2 and 0.

The 1% DFM (blue squares) exhibits a deactivation rate of 0.22 $\mu mol_{CH4}/g_{DFM}$/cycle when aged with adsorption in steam and air. This is half the cyclic deactivation rate of the 0.5% DFMs, indicating that a higher Ru loading adds stability to the performance. This is consistent with the previous study that demonstrated stability for 5% Ru, 6.1% "$Na_2O$"/$Al_2O_3$ tableted materials in the same simulated flue gas condition [11]. Furthermore, the tested 1% DFM and 5% Ru, 6.1% "$Na_2O$"/$Al_2O_3$ DFM have the same $Na_2O$ loading; the fact that the 5% Ru DFM showed no deactivation over 50 cycles of capture/methanation in the same simulated flue gas indicates that the main deactivating component is Ru and not $Na_2O$.

Three DFM configurations were investigated for the 0.5% DFM and all exhibited a similar deactivation rate. The γ-$Al_2O_3$ tablets (green squares) deactivate at a rate of 0.46 $\mu mol/g_{DFM}$/cycle and the 300-μm γ-$Al_2O_3$ granules (red circles) at 0.49 $\mu mol/g_{DFM}$/cycle. Ring γ-$Al_2O_3$ tablets were also tested and these deactivate at a rate of 0.43 $\mu mol/g_{DFM}$/cycle. As all the 0.5% DFMs deactivate at essentially the same rate, it can be concluded that the different geometries, preparation methods,

and type of alumina do not contribute to deactivation. Specifically, the large amounts of $HNO_3$ introduced in the preparation of the tablets and ring tablets do not seem to alter the catalytic activity of the material. This was also previously observed during cofeeding tests of $CO_2$ and $H_2$ [60].

## 5.2 FT-IR characterization of fresh and aged samples

FT-IR was used to better understand the mechanism of DFM deactivation. 0.5% Ru DFM was studied in detail due its more severe deactivation. **Figure 5.3** shows spectra on fresh (A) and aged (B) DFM after exposure to adsorptive and reducing environments.

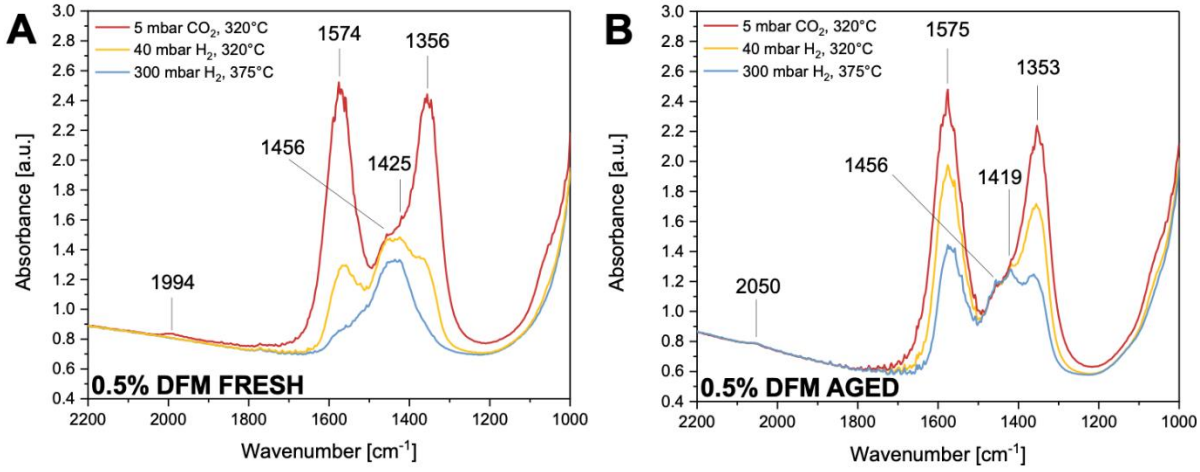


**Figure 5.3:** FT-IR spectra recorded after 10 min of 5 mbar of $CO_2$ at 320°C (red), subsequent exposure to 40 mbar $H_2$ at 320°C (yellow), and subsequent exposure to 300 mbar $H_2$ at 375°C (blue) on the fresh (**a**) and aged (**b**) 0.5%Ru DFM granules. Experimental details can be found in Section 3.2.3.1.

The red spectra in **Figure 5.3** reflects species that are present on the fresh (a) and aged (b) 0.5% Ru, 6.1% "$Na_2O$"/$Al_2O_3$ DFM granules after 10 min of $CO_2$ adsorption at 320°C. In both fresh and aged samples, two intense features at 1575 and 1355 $cm^{-1}$ arise after $CO_2$ exposure, corresponding to bidentate carbonates forming on Na [54,57]. The broad shoulder visible at 1420-1460 $cm^{-1}$ is associated to the asymmetric stretch of carbonate ions indicating the presence of

monodentates and/or bulk carbonates on Na [54,65]. This is likely indicative of residual bulk $Na_2CO_3$ species from the preparation step. A contribution of bicarbonates species cannot be ruled out [56,66] but is not detected in this study. Interestingly, the total amount of bidentate carbonate formation upon $CO_2$ exposure is very similar between the fresh and aged sample (red spectra in **Figure 5.3**a and b), indicating that the overall storage capacity of $CO_2$ is not affected by the aging process and therefore the $Na_2O$ component is unaffected.

Upon introduction of 40 mbar of $H_2$ for 10 min at the same temperature of 320°C, a substantial amount of bidentate carbonates is reduced in the fresh sample (**Figure 5.3**a, yellow spectrum). The aged sample, however, shows only a slight reduction in the amount of bidentate carbonate species (**Figure 5.3**b, yellow spectrum). This indicates that the aged sample is not able to reduce the surface bidentate carbonates to the same degree of the fresh sample, indicating that some deactivation of the Ru may be occurring. It is suspected that upon aging, stronger carbonates are resistant to hydrogenation due to lower methanating ability of the Ru.

Subsequently, both samples were also treated with 300 mbar of $H_2$ for 1 h at 375°C (blue spectra). On the fresh sample, the bands corresponding to bidentate carbonates are essentially undetectable while the band of monodentate/bulk sodium carbonates remains evident. This indicates that these carbonates species are more difficult to hydrogenate, in agreement with previous observations in similar conditions reported in the case of carbonates formed on Ba upon $CO_2$ exposure [54]. On the aged sample the bands of bidentate carbonates are still clearly present even after conditioning in a more favorable reducing environment (high $H_2$ partial pressure and high temperature). In addition, the band corresponding to monodentate/bulk carbonates remains almost unchanged. This clearly points at a lower hydrogenating ability of the aged sample,

considering that no significant differences in the nature of the adsorbed species was evidenced by FT-IR observations. This is also consistent with a reduced activity of aged Ru.

**Figure 5.4** shows the results of the FT-IR characterization during $CO_2$ capture and reduction in $H_2$ at 320°C on the fresh and aged 0.5% Ru, 6.1% "$Na_2O$"/$Al_2O_3$ DFM granules. All spectra are the result of a subtraction, using as subtrahend the corresponding spectrum obtained at the end of the hydrogenation phase (i.e., the yellow spectra reported in **Figure 5.3**), in order to compare the net amount of carbonates adsorbed and reduced in each cycle. The spectra reported in **Figure 5.4** refer to the third capture/hydrogenation cycle to ensure representative results.

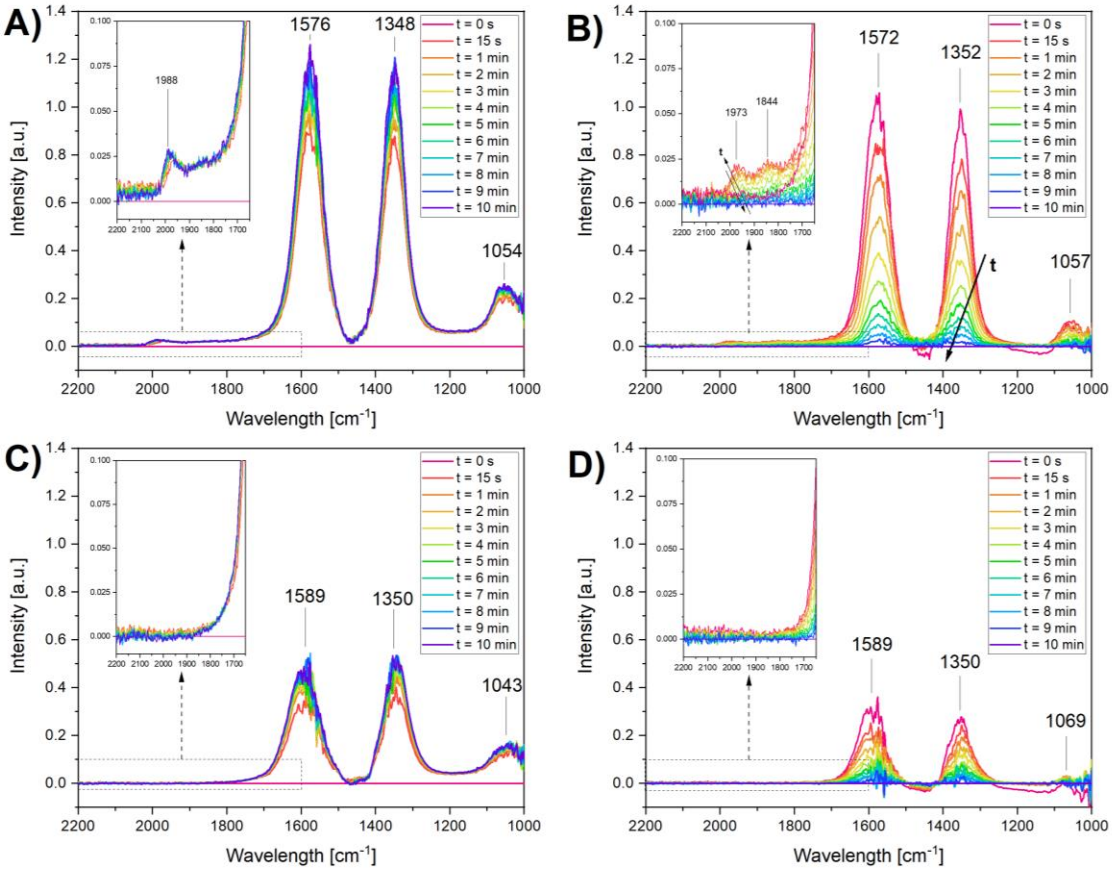


**Figure 5.4:** FT-IR spectra during the third cycle of $CO_2$ capture (**a**) and subsequent hydrogenation (**b**) at 320 °C on the fresh 0.5%Ru, 6.1% "$Na_2O$"/$Al_2O_3$ DFM granules. The corresponding spectra obtained during capture and hydrogenation on the aged 0.5%Ru, 6.1% "$Na_2O$"/$Al_2O_3$ DFM granules are reported in panels (**c**) and (**d**),

respectively. $CO_2$ capture conditions: 5 mbar $CO_2$, 10 min; hydrogenation conditions: 40 mbar $H_2$, 10 min. Experimental details can be found in Section 3.2.3.1.

When the fresh sample is exposed to $CO_2$, three intense bands at 1576, 1348 and 1054 $cm^{-1}$ grow rapidly in the first 15 s of exposure (**Figure 5.4**a). These features are associated with surface carbonates formed on Na. In addition, a small and broad spectral feature appears in the range 2050-1800 $cm^{-1}$, with a maximum at ~1990 $cm^{-1}$. This is associated with the presence of carbonyl species in multiple configurations on Ru sites in multiple oxidation states [67], likely as a result of the reaction of $CO_2$ with residual $H_2$ from the hydrogenation phase of the previous cycle [53,68].

During the vacuum purge (not shown) between the adsorption and the hydrogenation step, only minor amounts of Na-carbonates are removed from the catalyst surface, while Ru-carbonyls are completely removed (compare the spectra at t = 10 min in **Figure 5.4**a with the spectra at t = 0 s in **Figure 5.4**b).

The bands associated with carbonates on Na decrease upon $H_2$ admission at 320°C, with a 60% reduction of band intensity in the first 2 min of $H_2$ exposure. While the carbonates monotonically decrease with time, carbonyls on Ru rapidly increase to reach their maximum intensity after 1 min of $H_2$ exposure. This band progressively decreases until t = 5 min, after which it is no longer detected. This is well in line with the role of adsorbed CO as intermediate product in the $CO_2$ methanation reaction [69,70].

**Figure 5.4**c and d show the results of the FT-IR characterization during $CO_2$ capture and subsequent reduction in $H_2$ at 320°C on the aged 0.5% DFM granules. When the aged sample is exposed to $CO_2$ (**Figure 5.4**c), bidentate carbonate bands are formed with the same dynamic discussed in the case of the fresh sample, but with much lower intensity. This indicates that the total amount of carbonate species on the aged DFM is comparable to the fresh sample (as discussed

with **Figure 5.3**), but the amount of carbonates formed per cycle (i.e. the amount of $CO_2$ adsorbed per cycle) is much lower in the case of the aged DFM. Interestingly, those bands of carbonyls species on Ru are not detected during the adsorption step, and during the reduction step. This agrees well with the lower hydrogenation activity of the aged sample.

## 5.3 CO chemisorption on fresh and aged samples

CO pulse chemisorption was carried out on fresh and aged DFMs to characterize the active Ru sites. The results are reported in **Figure 5.5** in terms of CO uptake and average Ru crystallite size. The average particle diameter was calculated for each sample from the total CO chemisorbed and by assuming the nominal Ru loading for each sample.

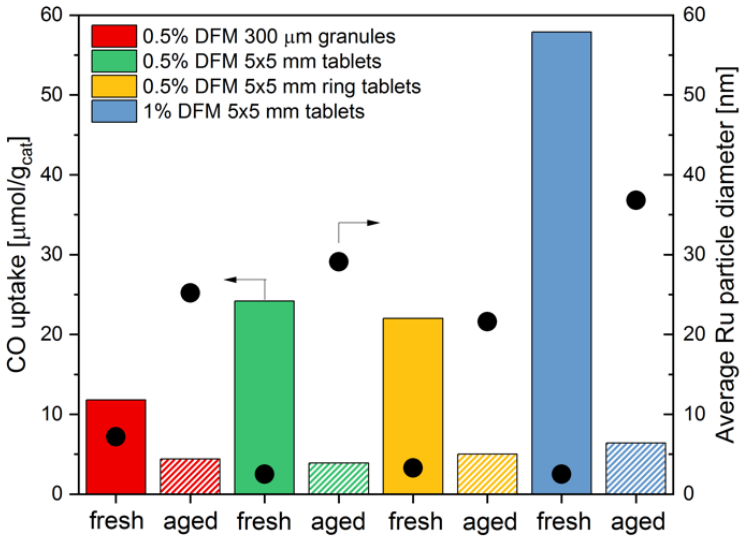


**Figure 5.5:** CO uptake (bars) and corresponding average Ru particle size (dots) evaluated from pulse chemisorption at room temperature on fresh DFMs (solid) and aged DFM (hatched). Experimental details can be found in Section 3.2.3.2.

The amount of CO chemisorbed is consistently lower for the aged samples compared to the corresponding fresh samples (compare solid bars with hatched bars). This indicates that there

is less active Ru surface area available for CO adsorption, which is consistent with the decrease in $CH_4$ formation caused by aging (**Figure 5.2**). This points to two possible modes of deactivation when the material is aged in the presence of steam and $O_2$ in the capture step: Ru sintering or $RuO_x$ volatilization.

While it is possible that some fraction of the available Ru can be oxidized to bulk $RuO_x$ (particularly $RuO_2$) at DFM operating temperatures (320°C – 350°C), volatilization of the oxidized species is not feasible [58,73]. When studying Ru/Na-Y as a catalyst for CO oxidation, Villani et al. found that even after treating their catalyst in dry air at 500°C, there was no loss in total Ru content. In addition, TGA studies showed that loss of Ru by volatilization only occurred at temperatures above 900°C [71]. This leaves sintering of the Ru to be main suspected mode of deactivation.

All aged samples exhibit much CO uptake values (consistently below 10 μmol/$g_{DFM}$), resulting in larger average particle sizes (in all cases larger than 20 nm) with respect to their corresponding fresh samples, indicating that there is loss in Ru active sites most likely due to sintering. Further evidence of Ru sintering is shown by FT-IR analysis during CO adsorption in **Figure 5.6**.

The fresh sample (green) shows a complex envelope, with three main bands at 2032,1963 and 1909 $cm^{-1}$. The band at 2032 $cm^{-1}$ can be assigned to linearly bonded CO [56,67]. The bands at the lower frequencies are of more complex attribution, and are usually assigned to bridged carbonyls, di-carbonyls, or three-fold carbonyl species on Ru sites in different oxidation states [67,69,72–74]. CO adsorption at room temperature was performed on a "conditioned" sample (yellow spectra) which was exposed in the to three cycles of capture/methanation at 350°C (capture conditions: $CO_2$ 5 mbar, $O_2$ 30 mbar, 10 min; reduction conditions: $H_2$ 40 mbar, 10 min). This

sample shows the same Ru-carbonyl bands observed on the fresh sample but with lower intensity, possibly indicating a decrease in the available Ru sites. CO adsorption at room temperature on the spent sample after the aging test reported in **Figure 5.2** (red spectra) resulted in a much lower and broader band, corresponding to the lowest absorbance in agreement with the CO chemisorption results reported in **Figure 5.5**. In addition to the lower intensity, the band corresponding to linearly bonded CO disappears, leaving only the broad band at ~1970 $cm^{-1}$.

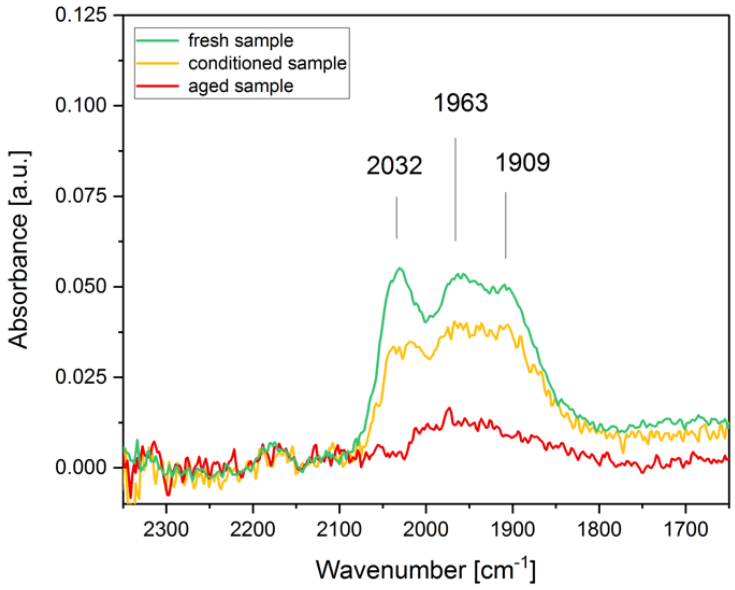


**Figure 5.6:** FT-IR spectra recorded after 20 min of 5 mbar of CO exposure on the fresh (red), conditioned (yellow) and aged (red) 0.5%Ru, 6.1% "$Na_2O$"/$Al_2O_3$ DFM granules. Experimental details can be found in Section 3.2.3.1.

## 5.4 Fixed bed microreactor transient study of low Ru loading DFM

Three sets of cycles were performed on fresh 0.5% Ru/DFM granules, as detailed in the experimental section, to investigate the dynamics of the $CO_2$ adsorption/reduction steps and the effect of the $O_2$ and steam presence during the adsorption feed on the catalyst transient behavior. The last cycle of each set is reported in **Figure 5.7**.

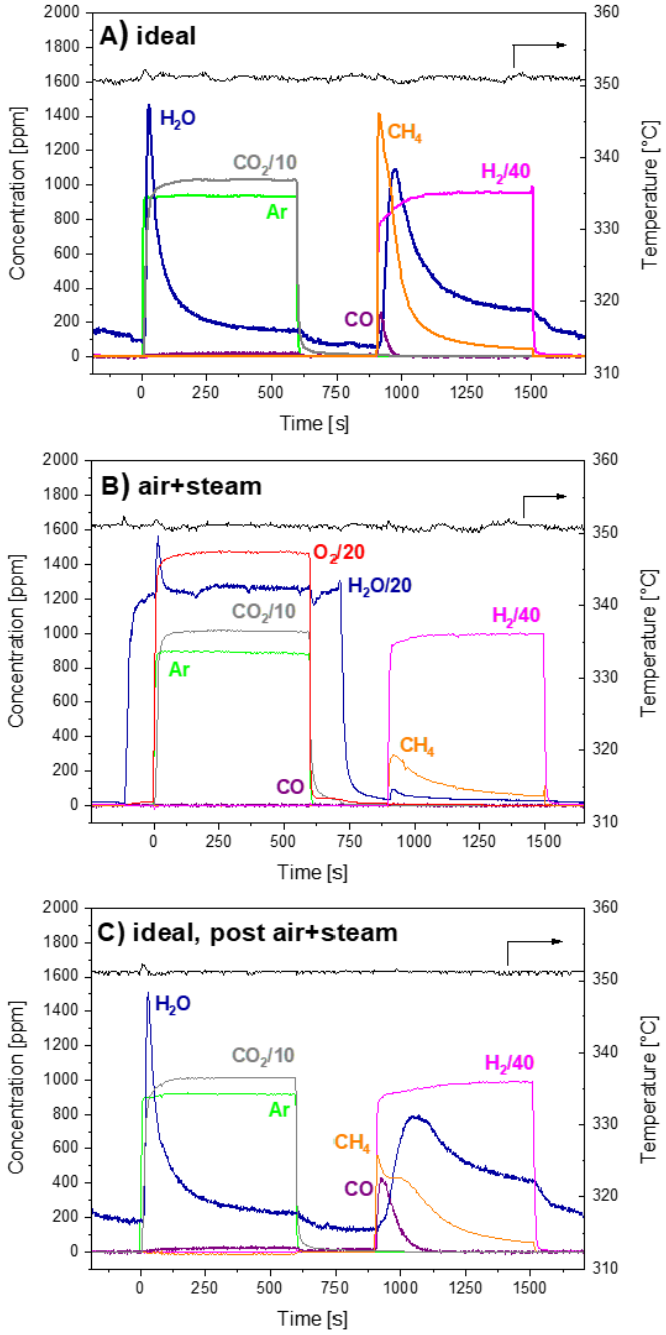


**Figure 5.7:** Cycles of sequential $CO_2$ capture and methanation on 0.5% DFM with different adsorption conditions: (**a**) 1% $CO_2$/He over a fresh catalyst sample (ideal, 3rd cycle), (**b**) 1% $CO_2$/ 3% $O_2$/ 2.5% $H_2O$ /He (air+steam, 6th cycle), (**c**) 1% $CO_2$/He (ideal, 9th cycle). Reduction conditions: 4% $H_2$/He. Experimental details can be found in Section 3.2.2.2.

**Figure 5.7**a refers to the "ideal" condition (i.e., cycles carried out in the absence of water and oxygen in the feed during the $CO_2$ capture step). Upon $CO_2$ admission, a sharp $H_2O$ peak is observed. This likely arises from the $CO_2$ adsorption on a hydrated sodium species, which forms a carbonated sodium carbonate species and water [68]. The concentration of $CO_2$ in the gas phase reaches the inlet value of 1% after 2 minutes of adsorption, indicating the quick saturation of the sample with $CO_2$ ad-species. These results are in good agreement with FT-IR results shown in **Figure 5.6**a.

When $H_2$ is admitted, a sharp $CH_4$ peak is produced along with water, that is tailing due to its adsorption on the surface. A lower peak of CO is also detected, likely as the result of incomplete $CO_2$ reduction occurring via reverse water gas shift reaction. The integrated amounts of $CH_4$ and CO produced during the cycles are shown in **Figure 5.8**a.

**Figure 5.7**b shows a cycle carried out in the presence of 3% $O_2$ and 2.5% $H_2O$ during the $CO_2$ capture step. Focusing on the reduction step, it appears that the presence of water and oxygen during the adsorption step results in a lower methane production once the carbonated DFM is exposed to $H_2$ (see also **Figure 5.8**a). Interestingly, the CO formation observed under the "ideal" conditions is completely suppressed.

Finally, ideal cycles were run on the same DFM after $O_2$/$H_2O$ cycles (**Figure 5.7**c). By comparing **Figure 5.7**a and c, it can be observed that the adsorption step is very similar, with comparable amounts of $CO_2$ adsorbed (and $H_2O$ released). On the other hand, the evolution of $CH_4$ and CO during the reduction step appears quite different. Indeed, the $CH_4$ (and $H_2O$) peak is broader upon hydrogenation after cycles in the presence of $O_2$/$H_2O$ (c), indicating a lower rate of $CH_4$ formation. Also, the production of CO (seen at the beginning of the hydrogenation phase)

appears enhanced. Yet, the overall amounts of $CH_4$ + CO evolved is similar to the ideal case on the fresh sample (**Figure 5.8**a).

The normalized cumulative integral of $CH_4$ formation as a function of time for the three cases shown in **Figure 5.7** are reported in **Figure 5.8**b. In this graph, the slope of each curve is proportional to the rate of $CH_4$ formation, regardless of the total amount of methane produced.

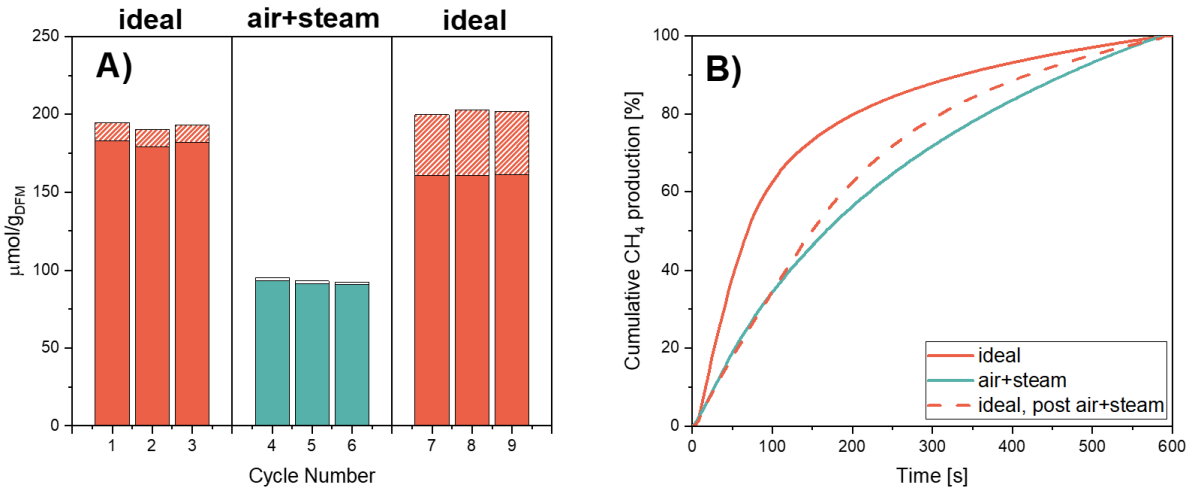


**Figure 5.8:** (**a**) Quantitative results in terms of amount of $CH_4$ (solid) and CO (dashed) formed during the reduction step during sequential cycles in the conditions reported in **Figure 5.7**; (**b**) Cumulative integral $CH_4$ formation during the three cycles shown in **Figure 5.7**.

In the presence of $O_2/H_2O$ during the capture step, the amount of methane produced is nearly half that of the fresh sample during ideal cycles (compare red and blue bars in **Figure 5.8**a). Furthermore, the rate of methane formation is slower after capture in the presence of $O_2/H_2O$ (**Figure 5.8**b), as indicated by the slightly lower slope of the cumulative methane formation at the beginning of the reduction step (compare solid red and blue lines).

When ideal cycles are performed again after $O_2/H_2O$ cycles, the amount of $CH_4$ formed during the reduction step is 12% lower than that formed in the same conditions on the fresh DFM. An opposite trend is observed in the case of CO, as higher amounts are detected after $O_2$ and $H_2O$

exposure. Additionally, the rate of $CH_4$ production appears compromised after cycles in the presence of $O_2$ and $H_2O$ as the cumulative $CH_4$ production retains the same initial lower slope observed during $O_2/H_2O$ cycles. However, as already pointed out, it is noteworthy that the total amount of C product ($CO+CH_4$) is comparable in both cases (before and after $O_2/H_2O$ exposure).

These results indicate that $O_2/H_2O$ exposure irreversibly affect the performance of the DFM. In fact, while the amount of captured $CO_2$ as well as the amount of C-containing reduction products remains comparable before and after $O_2/H_2O$ cycles, the conversion of the adsorbed $CO_2$ into $CH_4$ occurs with a lower rate and selectivity. This is consistent with a reduction in the activity of the catalyst induced by a decrease of the Ru active area of the DFM due to sintering.

# Chapter 6 : Investigating the role of $RuO_x$ in enhancing $CO_2$ adsorption capacity of $\gamma$-$Al_2O_3$ supported alkali and alkaline earth metals

*The results presented in this chapter are the subject of a provisional patent application (inventors: C. Jeong-Potter, M. Arellano-Trevino, R.J. Farrauto) and will be submitted for publication in C. Jeong-Potter, M. Abdallah, Mark Goldman, Shruti Kota, R.J. Farrauto, Investigating the role of $RuO_x$ in enhancing $CO_2$ adsorption capacity of $\gamma$-$Al_2O_3$ supported alkali and alkaline earth metals.*

In this chapter, we investigate an additional, unexpected function of the DFM. We observe that combining Ru with specific adsorbents and carriers substantially enhances $CO_2$ capture capacity. Investigation of several Ru + sorbent/carrier formulations shows that the enhancement effect is not inherent with Ru but requires specific combination of DFM components. Most surprisingly, significant enhancement of $CO_2$ adsorption occurs in $O_2$-containing environments where $RuO_x$ species are present. $Ru^0$ (and not $RuO_x$) is known to adsorb $CO_2$, as required for methanation, but the significant enhancement in the presence of $RuO_x$ is very interesting and opens up new pathways for designing materials with higher capture capacity than conventionally thought. Such materials can play a key role in mitigating the negative effects of climate change.

## 6.1 Literature review of $CO_2$ adsorption enhancement in the presence of catalytic metals

The effect of catalytic metals on $CO_2$ adsorption capacity of sorbents has, thus far, only been studied in the case of bulk sorbents and have exhibited mixed results. Al-Mamoori et al. previously investigated the effect of doping bulk CaO sorbent with Fe and Ga, which yielded increased adsorption compared to CaO alone [75,76]. On the other hand, Felice et al. noticed that doping calcined dolomite (a bulk (CaMg)O sorbent) with Fe and Ni showed substantially lower adsorption

capacity than bare (CaMg)O [76]. It should be noted that it is unclear if the results of these studies would differ in the presence of $O_2$, where the catalytic metals are expected to oxidize. The effect of $O_2$ should not be ignored as most $CO_2$-containing flue gas streams will also contain $O_2$.

Though not explicitly discussed or acknowledged, the earliest evidence of additional $CO_2$ capture capacity in the presence of catalytic metal can be found in work by Arellano-Treviño et al. [6]. Samples of $Na_2O/Al_2O_3$ with Rh, Ru, or Ni all exhibited capture capacities that were greater than of $Na_2O/Al_2O_3$ alone. These studies were all performed in the absence of $O_2$, where the fully reduced metals are expected to adsorb $CO_2$, as observed by Proaño et al. [56]. It is also discussed that the presence of such metals may increase the basicity of sorbents and carriers [77,78]. However, we have noticed that $CO_2$ capture in the presence of $O_2$ was significantly greater on 0.5% Ru, 6.1% $Na_2O/Al_2O_3$ than on $Na_2O/Al_2O_3$ alone [79]. This is surprising as the Ru loading was ten times lower than that used in previous DFMs (0.5% vs. 5%). In addition, these studies were performed in the presence of $O_2$ where there is no evidence that oxides of Ru, Ni, and Rh would adsorb significant amounts of $CO_2$ and, therefore, would not contribute to an increase in $CO_2$ capture capacity. This current paper will show, however, that even in the presence of oxidized Ru, the capture capacity is significantly increased.

In this chapter, we investigate the conditions and a number of combinations in which this enhancement effect can be observed. Several Ru, alkaline metal oxide sorbent, and carrier combinations are studied to show that though there are an array of combinations in which this effect is observable, the effect is not inherent with Ru since some combinations show little or no $CO_2$ enhancement. In addition, it is shown that this effect is evident in varying oxidizing environments. These results indicate the wide variety of ways to improve capture capacity and can be used to identify an optimized combination of catalytic metal, sorbent, and carrier in the future.

## 6.2 $CO_2$ capture capacity of combinations of 1% Ru, 10% alkali and alkaline earth metal sorbents supported on $\gamma$-$Al_2O_3$ in the presence of $O_2$-containing feed gas

Sorbents supported on $\gamma$-$Al_2O_3$ (10% $Na_2O/Al_2O_3$, 10% $CaO/Al_2O_3$, 10% $MgO/Al_2O_3$, and 10% $BaO/Al_2O_3$) and their 1% Ru-containing counterparts were exposed to a stream of 375 ppm $CO_2$, 19% $O_2$ and balance $N_2$ at room temperature (25°C) to simulate direct air capture of $CO_2$ at ambient conditions. Preliminary experiments were carried out in the TGA. In the case for the Ru-containing samples, it is expected that there will be some mass gain during adsorption associated with oxidation of Ru. The extent of oxidation was measured for all Ru-containing samples upon exposure to 19% $O_2/N_2$ (no $CO_2$). To better account for $CO_2$ adsorption, the mass gain profile attributable to Ru oxidation was subtracted from the total mass gain profile of the 1%Ru, 10% sorbent/$Al_2O_3$. The resulting thermal gravimetric (TG) profiles associated with $CO_2$ adsorption are shown in **Figure 6.1**.

Of the sorbent-only samples, 10% $Na_2O/Al_2O_3$ (dotted line in **Figure 6.1**a) exhibits the highest $CO_2$ capture capacity (in the presence of $O_2$) as indicated by the total mass gain. 10% $CaO/Al_2O_3$ and 10% $MgO/Al_2O_3$ (dotted lines in **Figure 6.1**b and **Figure 6.1**c, respectively) exhibit similar adsorption capacities, but lower than that of 10% $Na_2O/Al_2O_3$. The lowest adsorption capacity was noted for 10% $BaO/Al_2O_3$ (dotted line in **Figure 6.1**d).

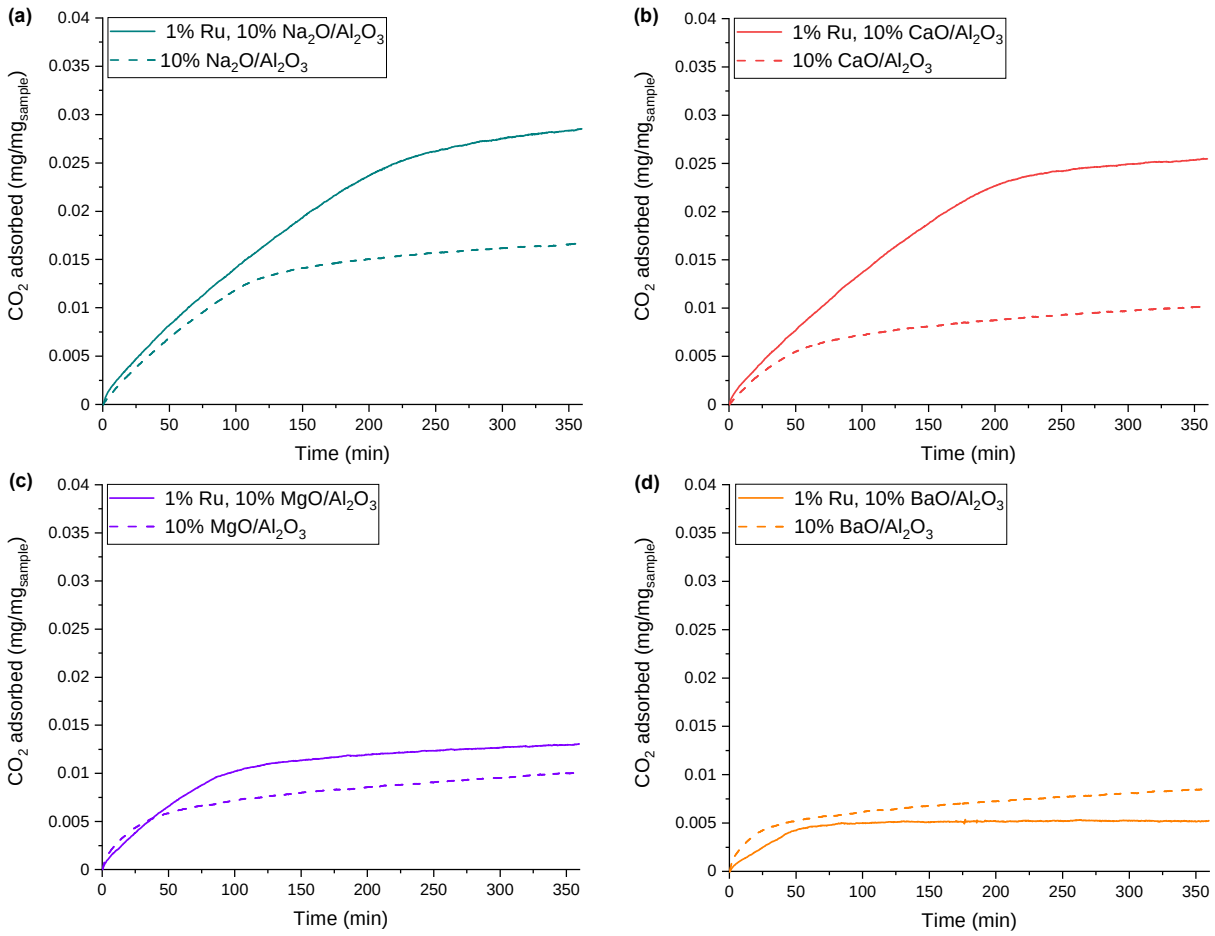


**Figure 6.1:** TG mass gain profiles of 10% sorbent/$Al_2O_3$ (dashed lines) and 1% Ru, 10% sorbent/$Al_2O_3$ (solid lines) upon exposure to 375 ppm $CO_2$, 19% $O_2$, and balance $N_2$ at 25°C. (**a**) Na-containing samples, (**b**) CaO-containing samples, (**c**) MgO-containing samples, and (**d**) BaO-containing samples. For Ru-containing samples, the mass gain profile associated with Ru oxidation has been subtracted from the total mass gain profile, yielding mass gain profiles attributable to just $CO_2$ adsorption. Experimental conditions can be found in Sections 3.3.2.1, 3.3.2.2, and 3.3.2.4.

The fact that the enhancement effect is observable to varying degrees between combinations indicate that the effect is not inherent with Ru; in other words, not all combinations of Ru + sorbent/$\gamma$-$Al_2O_3$ will exhibit enhanced adsorption capacities. Instead, it is expected that there are some synergistic interactions between Ru as an oxidized species and certain alkaline sorbents. To further prove this point, it should be noted that the additional $CO_2$ capture capacity seen with the Ru + sorbent/$\gamma$-$Al_2O_3$ samples are even greater than just $CO_2$ adsorption on Ru (or

$RuO_x$)/$Al_2O_3$. With no sorbent present, 1% Ru/$Al_2O_3$ exhibits 0.006 mg/$mg_{sample}$ of mass gain in the presence of the $O_2$-containing adsorption feed stream (see Section 3.3.2.5 for experimental details). After correcting for mass gain associated with Ru oxidation, $CO_2$ adsorption equates to just 0.0025 mg/$mg_{sample}$.. In addition, previous in-situ DRIFTS tests performed with oxidized Ru DFM showed that $CO_2$ adsorption over the Ru/$RuO_x$ species was undetectable [57]. Proaño et al. studied $CO_2$ adsorption behavior of 1% Ru, 10% Ni, 6.1% $Na_2O$/$Al_2O_3$ after a pre-oxidation step with 25% $O_2$/$N_2$, after which $RuO_x$ and NiO species were formed. The authors were unable to detect bands associated with Ru-CO species or any other bands associated with $CO_2$ adsorption on $RuO_x$. Thus, $CO_2$ adsorption on the Ru component is nominal and does not fully account for the observed increase in $CO_2$ adsorption on the Ru + sorbent/γ-$Al_2O_3$, particularly with the $Na_2O$ and CaO samples.

This enhancement effect can be verified with results from packed bed studies on 10% $Na_2O$/$Al_2O_3$, 0.1% Ru, 10% $Na_2O$/$Al_2O_3$, and 1% Ru, 10% $Na_2O$/$Al_2O_3$. In all cases the carrier is γ-$Al_2O_3$. The adsorption capacity of these materials for three cycles of $O_2$-containing $CO_2$ adsorption and desorption/methanation can be found in **Figure 6.2**. Over three cycles, 10% $Na_2O$/$Al_2O_3$ **(Figure 6.2**a) exhibited an average adsorption capacity of 0.019 g/$g_{sample}$. The adsorption enhancement is once again evident with the addition of Ru as the 0.1% Ru, 10% $Na_2O$/$Al_2O_3$ (**Figure 6.2**b) and 1% Ru, 10% $Na_2O$/$Al_2O_3$ samples (**Figure 6.2**c) display three-cycle adsorption averages of 0.025g/$g_{sample}$ and 0.027 g/$g_{sample}$, respectively. It can be observed that the sample with a higher Ru loading has a greater adsorption capacity (black dots). The effect of Ru loading on the enhancement effect is studied in detail in the next section. In addition to the greater $CO_2$ adsorption capacity, the higher Ru loading sample shows less $CO_2$ desorbed during heat up (green bars) and more methane production (purple bars).

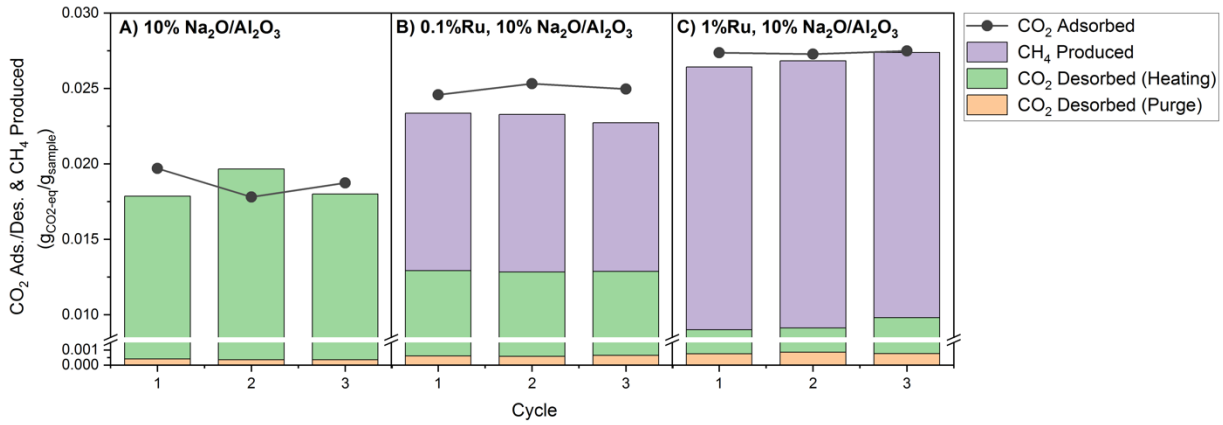


**Figure 6.2:** $CO_2$ adsorption measured for (**a**) 10% $Na_2O/Al_2O_3$, (**b**) 0.1% Ru, 10% $Na_2O/Al_2O_3$, and (**c**) 1% Ru, 10% $Na_2O/Al_2O_3$ three cycles of: i) adsorption at 25°C with in the presence of 400 ppm $CO_2$, 21% $O_2$, balance $N_2$ (black dots) and ii) desorption in $N_2$ (green bars) or methanation with 15% $H_2/N_2$ (purple bars) in packed bed configuration. Desorption of $CO_2$ on 10% $Na_2O/Al_2O_3$ was carried out at 400°C and methanation of $CO_2$ on Ru-containing samples was carried out at 300°C. Orange bars represent $CO_2$ that is desorbed during purge of the reactor between the adsorption and heat up steps. Experimental details can be found in Section 3.3.3.

## 6.3 Effect of %Ru loading on $O_2$-containing $CO_2$ adsorption enhancement

To determine the extent at which %Ru loading affects the observed enhancement, x% Ru, 10% $Na_2O/Al_2O_3$ (where x = 0, 0.1, 0.5, 1, 3, 5) samples were exposed to a stream of 375 ppm $CO_2$, 7.5% $O_2$, and balance $N_2$ at 25°C in the TGA. It should be noted that the $O_2$ concentration was 7.5% due to limitations of gas availability during the time of study. Once again, to better account for $CO_2$ adsorption, the mass gain profile attributable to Ru oxidation was subtracted from the total mass gain profile of the x% Ru, 10% $Na_2O/Al_2O_3$ samples. The resulting $CO_2$ adsorption profiles can be found in **Figure 6.3**.

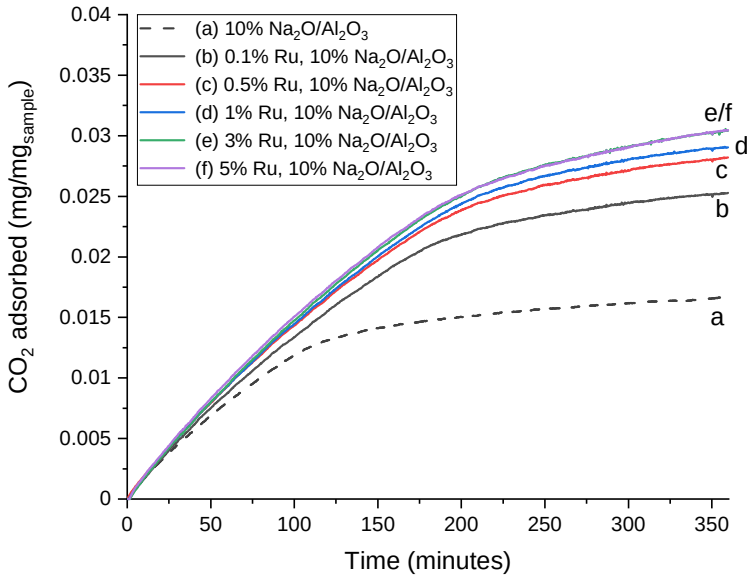


**Figure 6.3:** TG mass gain profiles of x% Ru, 10% $Na_2O/Al_2O_3$ samples where x = 0, 0.1, 0.5, 1, 3, and 5 (**a-f**, respectively) upon exposure to 375 ppm $CO_2$, 7.5% $O_2$, and balance $N_2$ at 25°C. For Ru-containing samples, the mass gain profile associated with Ru oxidation has been subtracted from the total mass gain profile, yielding mass gain profiles attributable to just $CO_2$ adsorption. Experimental conditions can be found in Sections 3.3.2.1, 3.3.2.3, and 3.3.2.4.

All of the Ru-containing samples (solid lines, **Figure 6.3**b-f) show $CO_2$ capture capacities greater than that of $Na_2O/\gamma\text{-}Al_2O_3$ alone (dotted line, **Figure 6.3**a). Even with a loading as low as 0.1% Ru, the $CO_2$ adsorption of the DFM increases by more than 50% relative to that of the $Na_2O$-only sample. The $CO_2$ capture capacity continues to increase with higher Ru loading. This can be more clearly seen in **Figure 6.4** where the increase of $CO_2$ adsorption relative to $Na_2O/Al_2O_3$ alone is shown. The extent of enhancement is most pronounced between 0.1% and 1% Ru with the effect dampening thereafter. The observed $CO_2$ capture capacity levels off after 3% Ru such that the adsorption profiles are superimposed for samples of 3% Ru and 5% Ru (**Figure 6.3**e, f). The total $CO_2$ adsorbed plateaus at 0.0304 $mg/mg_{sample}$, equating to an overall 83% increase in capture capacity compared to $Na_2O/Al_2O_3$ only. These results indicate that it may be more efficient to dope

the sorbents with a smaller amount of Ru, as higher Ru loadings do not necessarily equate with a proportional increase in $CO_2$ adsorption.

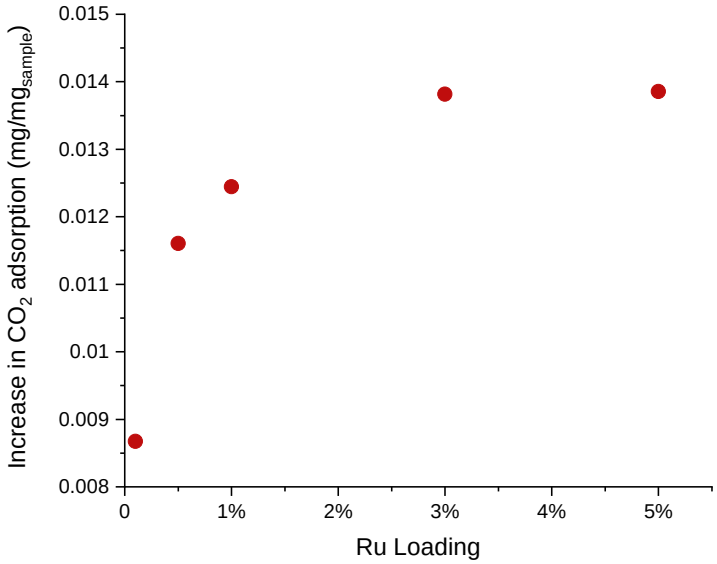


**Figure 6.4:** Increase in $CO_2$ adsorption exhibited by x% Ru, 10% $Na_2O/Al_2O_3$ samples, relative to $Na_2O/Al_2O_3$ alone. Adsorption was performed in the presence of $O_2$.

This is further verified by the trend in $H_2$ chemisorption as found in **Table 6.1**. These results show that increasing the Ru loading from 0.1% to 1% resulted in a 3.9-fold increase of $H_2$ adsorbed consistent with the equally dramatic increase in $CO_2$ adsorption shown previously. While the 0.1% Ru DFM sample adsorbed 24.5 µL/g, the 1% Ru DFM sample adsorbed 120.7 µL/g. The increase in $H_2$ is not as pronounced between the 1% Ru DFM and 3% Ru DFM, which is also consistent with the dampening of the $CO_2$ adsorption enhancement as Ru loadings increased above 1%. It can also be seen that the dispersion decreases (larger Ru crystallites) as the Ru loading increases, which could explain the observed dampening effect with higher Ru loadings.

A turn over number-like (TON) quantity can be calculated using the dispersion values obtained from $H_2$ chemisorption to further emphasize that the enhancement effect is more efficient

at lower levels of $RuO_x$. By dividing the amount of enhanced $CO_2$ adsorption by the amount of available Ru sites as indicated by the dispersion ($mol_{CO2\text{-}enhanced}/mol_{Ru\text{-}avail}$), we see that the "TON" of 0.1% Ru DFM is 90.3 while it is much lower for 3% Ru DFM at 27.6. We would like to note, however, that this TON-like quantity does not have much physical significance as the $CO_2$ is not adsorbed on only the $Ru/RuO_x$ species but rather in some combination of the various components of the DFM.

**Table 6.1:** Results of $H_2$ chemisorption – specific volume of $H_2$ adsorbed, average crystalline size, dispersion, and a turn over number-like quantity. Experimental details can be found in Section 3.3.4.

| Sample | $H_2$ adsorbed [$\mu L/g_{sample}$] | Average crystalline size [nm] | Dispersion | "TON" [$mol_{CO2\text{-}enhanced}/mol_{Ru\text{-}avail}$] |
|---|---|---|---|---|
| 0.1% Ru, 10% $Na_2O/Al_2O_3$ | 24.5 | 2.02 | 22.1% | 90.3 |
| 1% Ru, 10% $Na_2O/Al_2O_3$ | 120.7 | 4.09 | 10.9% | 26.3 |
| 3% Ru, 10% $Na_2O/Al_2O_3$ | 127.8 | 11.6 | 3.84% | 27.6 |

Sun et al., whose work involved measuring $CO_2$ adsorption on $Ru/CeO_2$ in the presence of 70% $CO_2/N_2$ (no oxygen), observed that samples with a higher Ru metal loading adsorbed more $CO_2$ [78]. This is expected since the Ru metal adsorbs $CO_2$. Sun et al. attributed this to increased basicity of the $CeO_2$ support in the presence of Ru. The authors also examined adsorption capacities of mechanical mixtures of $Ru/CeO_2$ and bulk MgO. Though not discussed, it was apparent that mixtures with lower Ru loadings show higher initial $CO_2$ capture capacity (though it eventually decreases due to a lower methanation activity), which is the opposite effect of that shown in our work reported here. It is evident that mechanical mixtures of Ru and sorbent do not show the same enhancement effect, indicating that it may be crucial that the sorbent and catalyst

be dispersed on the same carrier to promote intimate contact in order to observe the enhancement effect.

### 6.4 Effect of carrier on observed $O_2$-containing $CO_2$ adsorption enhancement

It was necessary to understand if the $\gamma$-$Al_2O_3$, in combination with $RuO_x$ and specific alkaline sorbents, is contributing to $CO_2$ adsorption enhancements. A sample of 6.1% $Na_2O/ZrO_2$-Y and its 5% Ru-containing counterparts were exposed to 375 ppm $CO_2$, 19% $O_2$, and balance $N_2$ at 25°C. The resulting $CO_2$ adsorption profiles are shown in **Figure 6.5**. Once again, the mass gain profile associated with Ru oxidation has been subtracted.

The oxidized Ru-containing samples demonstrate a greater mass gain in the presence of $CO_2$ compared to the $Na_2O$/ZrO2-Y-only sample. Unlike $\gamma$-$Al_2O_3$-supported $Na_2O$, $ZrO_2$-Y-supported $Na_2O$ shows very insignificant $CO_2$ adsorption of 0.0011 $mg/mg_{sample}$. This low $CO_2$ adsorption capacity is enhanced with the addition of 5% Ru. The total $O_2$-containing $CO_2$ adsorption on 5% Ru, 6.1% $Na_2O/ZrO_2$-Y is 0.00531$mg/mg_{sample}$, equating to a capture capacity that is almost 4 times greater than $Na_2O/ZrO_2$-Y alone. It should be noted, however, that 5% Ru, 6.1% $Na_2O/ZrO_2$-Y is not an efficient combination for $CO_2$ capture, given its low overall capture capacity. In fact, its $CO_2$ capture capacity is lower than all of the $\gamma$-$Al_2O_3$-supported sorbents studied in Section 6.2, even in the absence of Ru. Nevertheless, the effect of $RuO_x$ addition is significant in this case and the ability of Ru to enhance $CO_2$ adsorption, in the presence of $O_2$, even on carriers with low internal surface area cannot be denied. More supports should be further studied to better understand this effect.

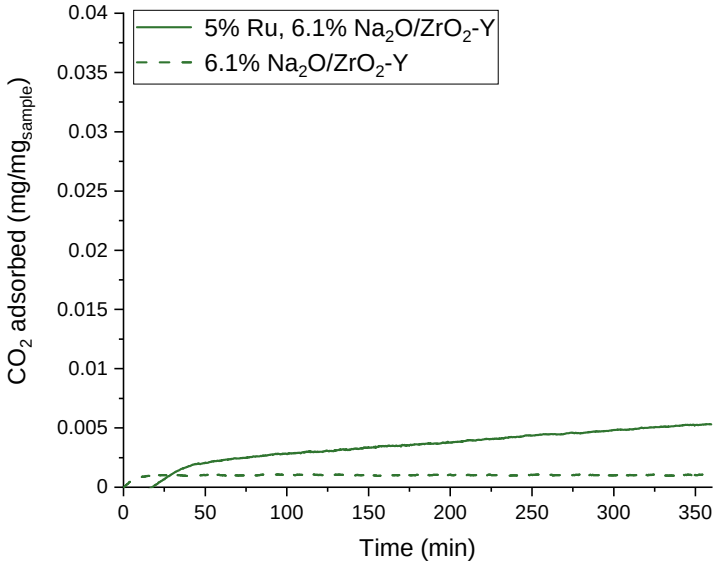


**Figure 6.5:** TG mass gain profiles of 5% Ru, 6.1% $Na_2O$ (solid line) and 6.1% $Na_2O$ (dashed line) supported on $ZrO_2$-Y upon exposure to 375 ppm $CO_2$, 19% $O_2$, and balance $N_2$ at 25°C. For Ru-containing samples, the mass gain profile associated with Ru oxidation has been subtracted from the total mass gain profile, yielding mass gain profiles attributable to just $CO_2$ adsorption. Experimental conditions can be found in Sections 3.3.2.1, 3.3.2.2, and 3.3.2.4.

# Chapter 7 : Conclusions and Future Work

## 7.1 Thesis Conclusions

In this thesis, the novel dual function material (DFM) process, originally demonstrated for $CO_2$ capture and conversion from power plant effluents (320°C), has been adapted to direct air capture of low levels of $CO_2$ under ambient adsorption conditions (DAC), providing a unique path forward towards mitigating climate change. The feasibility of using DFMs for combined DAC and catalytic methanation (DAC-M) was investigated. A direct translation of the DFM technology (i.e., isothermal adsorption and methanation cycles at 320°C) is possible, with the DFM successfully adsorbing $CO_2$ from a very dilute feed stream (400 ppm) in DAC and subsequently methanating it with the introduction of $H_2$. It was recognized, however, that isothermal cyclic operation would be too energy intensive in the case of DAC-M and temperature-swing operation was adopted. In this new process, the DFM adsorbs $CO_2$ from air at ambient temperature and humidity conditions and then catalytically produces methane upon heating with the introduction of $H_2$. At the new inlet adsorption temperature (25°C), the $CO_2$ adsorption capacity was greatly increased. The DFM was also shown to have excellent adsorption performance in humid ambient environments; in fact, the adsorption capacity was further enhanced in these conditions. This is a unique feature as alternative DAC technologies are subject to negative impact of moisture in ambient air. Further engineering is required to advance implementation of DFM for DAC. An important engineering issue is efficient and environmentally green energy sources for heating to initiate catalytic methanation. This and a complete process design will be addressed during current DOE-sponsored scale-up studies. The final design will include use of existing automobile-type monolith structures for

washcoating the DFM, providing low pressure drop and excellent heat transfer capabilities and structural integrity while selectively heating of the washcoat to methanation temperatures.

Due to economic concerns, low Ru loadings were used for these DAC-M studies. Subsequently, the stability of these reduced Ru loadings is a necessity. Thus, low Ru loading DFMs (0.5% Ru, 6.1% "$Na_2O$"/$Al_2O_3$ and 1% Ru, 6.1% "$Na_2O$"/$Al_2O_3$) were aged in simulated natural gas power plant effluent conditions (7.5% $CO_2$, 4.5% $O_2$, 15% $H_2O$, balance $N_2$; 320°C). This study can serve as a baseline assessment of these materials as the operating conditions are more severe; the material is constantly exposed to higher temperature (320°C) during both adsorption and methanation whereas for DAC, the adsorption temperature is ambient and the DFM is exposed to methanation temperatures for a relatively short period of time.

Low %Ru loaded DFMs showed evidence of deactivation, which is more severe as the Ru level decreases. When the 0.5% Ru DFM was cyclically aged in the absence of $O_2$ and $H_2O$, deactivation was not detected, indicating that these gaseous components and the higher temperatures contributed to the deactivation of the materials. Characterization with CO chemisorption and in-situ FT-IR showed that the aged samples all had less active Ru, due to sintering, which then leads to, formation of stable, unmethanated residual carbonates on the DFM surface. As a result, higher Ru loadings may still be required to ensure a long material lifetime. Fortunately, Ru can be leased and recycled, which is one way the cost of DFM can be mitigated. Additionally, with lower operating temperatures for DAC, sintering is expected to be minimized.

Lastly, it was discovered that the unique combination of Ru, $Na_2O$ and $\gamma$-$Al_2O_3$ exhibits an adsorption capacity that is significantly superior to other combinations of Ru + sorbents/carriers. The addition of Ru to $Na_2O/Al_2O_3$ shows a great enhancement in $CO_2$ capture capacity compared to bare $Na_2O/Al_2O_3$, surprisingly in the presence of oxidized Ru ($RuO_x$), which is not active for

$CO_2$ adsorption. The increased $CO_2$ capacity was greater than the capture capacity exhibited by Ru (or $RuO_x$) on $\gamma$-$Al_2O_3$ indicating a greater synergistic effect between the sorbents and Ru (and its oxides) and $\gamma$-$Al_2O_3$ to enable the enhancement effect. In addition, the enhancement effect was shown to increase with Ru loading; however, the effect is greatest at low levels of $RuO_x$ and becomes less pronounced at higher Ru loadings, plateauing at 83% increase in capture capacity.

## 7.2 Future Work

This thesis has demonstrated that the DFM has great potential to be used not only for capture and conversion of $CO_2$ from power plant effluents but also for capture and conversion of $CO_2$ from humid ambient air, further proving that DFM is a robust and flexible technology. However, there are still many rich research areas to demonstrate the DFM can be sustainably scaled-up for real-world applications.

### 7.2.1 Scale-up of DFM for DAC-M: Monolithic substrates

In Chapter 4, we showed that the rate of adsorption using DFM for DAC was mass transfer limited and that the rate can be optimized by increasing the flowrate of air. This is a critical realization as increasing flowrate results in pressure drop increases which contributes to energy penalties. These penalties can be minimized by optimizing the configuration of the DFM.

Monoliths are well-known structured substrates that are designed to minimize pressure drop via high open frontal areas and thin walls upon which DFM will be washcoated. They are the only structured supports used in the catalytic converters. They were first used in 1980 in the US and are now utilized worldwide for applications where high geometric surface areas are required for enhanced mass transfer while minimizing pressure drop.

Methods for transferring the DFM technology onto monolithic substrates will need to be developed. DFM washcoating methods should be optimized to consider the impregnation of the multiple active components of the material, the adhesion of the washcoat, suitable materials for monolithic support, and overall scalability of the DFM-monolith washcoating process.

### 7.2.2 Parametric studies for process optimization of DFM for DAC-M

The feasibility of using DFM for DAC-M was shown; however, the engineering and aging parameters of the cyclic process are yet to be investigated in detail. The issue of $CO_2$ desorption during heat-up is of particular interest – one that can be minimized with fine tuning several process parameters such as selectively heating the active DFM washcoat. It would be worthwhile to test multiple parameters to observe trends in $CO_2$ desorption, methanation production and rate, and the subsequent adsorption of $CO_2$. Some of those parameters may include (but are not limited to) $H_2$ flowrate, $H_2$ concentration, methanation temperature and heating rate.

### 7.2.3 Study of various ambient conditions simulating different geographic locations and seasons

It is critical to further investigate additional parameters during adsorption. To further establish the robustness of the DFM technology for DAC, various ambient environments should be simulated and tested. A range of adsorption temperatures and relative humidities (i.e., concentration of $H_2O$) to model different geographic climates and their seasons need to be investigated.

### 7.2.4 Recyclability of Ru

Chapter 5 showed that stability of the DFM improves with increased Ru content. DFM with high Ru loading (>1%) may be required to achieve a suitable material lifetime. One way to mitigate the cost of high Ru loading DFMs is to investigate the efficiency of recycling the Ru. This is also a matter of importance for sustainability as recycling Ru can reduce the need for mining. The sustainability of the recycle process must also be investigated, in addition to its efficiency.

### 7.2.5 Investigating the use of other methanation catalysts for DAC-M

The cost and availability of Ru will most likely be a challenge in moving the DFM to commercialization. To this regard, it is worth investigating the use of other methanation catalysts, especially for DAC-M, where cyclic conditions are less severe. It has already been established by previous work that Ni, a common methanation catalyst, alone is not a viable candidate for our DFM applications due to its inevitable oxidation in the presence of oxygen and the subsequent temperatures required for re-activation (>600°C) [6]. However, other non-noble metal catalysts, such as Co or Fe [47,80], have not yet been investigated for the DFM.

Additionally, we have seen that by combining Ru and Ni in the DFM (as opposed to Ni alone), the temperature required for reduction of $NiO_x$ is greatly reduced [12]. With the Ru present, Ni can therefore be reactivated for methanation at 320°C. This may allow a path for the reduction of Ru content in the DFM. This combination has been tested only for power plant flue gas applications and would be worthwhile to be tested for the DAC-M application. Furthermore, it would also be worthwhile to see if a combination of other methanation catalysts would yield similar results (for example, Ru+Fe).

For applications such biogas upgrading, where $O_2$ is not present in the capture step, Ni or other transition metals may be feasible catalyst candidates for $CO_2$ methanation. Furthermore, there are other point sources of $CO_2$ like enhanced steam reforming/water gas shift where there is also no $O_2$ present and other catalysts can be used to upgrade $CO_2$ to other valuable C1 or C2 products.

### 7.2.6 Investigating use of other catalytic metal oxides for $CO_2$ enhancement for DAC adsorption and desorption

Chapter 6 investigated combinations of Ru, alkaline sorbents, and carriers for enhancement of $CO_2$ adsorption. A range of sorbents and carriers were investigated but other catalytic metals were not included in this investigation. There can be large implications for DAC adsorption and desorption if indeed other, less expensive, catalytic metals exhibit a similar phenomenon. Without the production of methane, the use of Ru in the sorbent is not economically justifiable. Less expensive metal oxides may have the potential to increase $CO_2$ adsorption capacity in these sorbents and would be more economically feasible. The $CO_2$ desorbed in a DAC adsorption/desorption process can be utilized in a variety of ways, given the geographic freedom of DAC. Such DAC units can be strategically placed at the site of utilization to prevent the logistics of transporting $CO_2$.

### 7.2.7 Applications of DFM for production of other chemicals beside $CH_4$

The end product of the processes proposed in this thesis is methane. While renewable methane (or RNG) is an excellent transition fuel and precursor for synthesis gas production, taking advantage of the already established vast natural gas infrastructure, fossil methane is inexpensive. This makes the economics of renewable methane utilization (such as for $H_2$ production)

noncompetitive. Other C1 products – such as CO and methanol – have the potential to be more economically competitive. These products can be upgraded to high energy density synthetic fuels, and related carbonaceous products, for more sustainable alternatives in industries that are difficult to decarbonize, specifically heavy-duty vehicles and aviation.

## 7.3 Major Challenges towards commercialization of DFM

There are some foreseeable challenges in moving this technology to commercial scale. The first is the reliance of the DFM on Ru. This metal is a unique catalyst that can be easily reduced at moderate temperatures (< 200°C) for methanation upon $H_2$ addition once oxidized after exposure to air ($O_2$) during the $CO_2$ capture step [6,12]. The challenge is that Ru is a rare resource. Though it is an inexpensive precious metal ($18.01/g compared to $29.84/g-Pt or $450.11/g-Rh as of December 2021), it is scarce. Since it is a by-product of Pt mining, the continued supply of Ru would be a great challenge, especially for large scale deployment and regular maintenance of the DFM. Precious metal mining is also subject to geopolitical issues, making it an even more rare resource. Additionally, the price of Ru has risen drastically over the last decade (peaking at ~$25/g in 2021 from $5/g in 2012), and it is difficult to project future costs (**Figure 7.1**). Yet, the current practice of Ru reclaiming for reuse is one promising aspect of its usage [82].

A volatilization process, where Ru is converted to $RuO_4$ and off gassed, is commercially used. If this can be done with efficiencies higher than 90%, the reliance and burden on the Ru supply chain may be lessened.

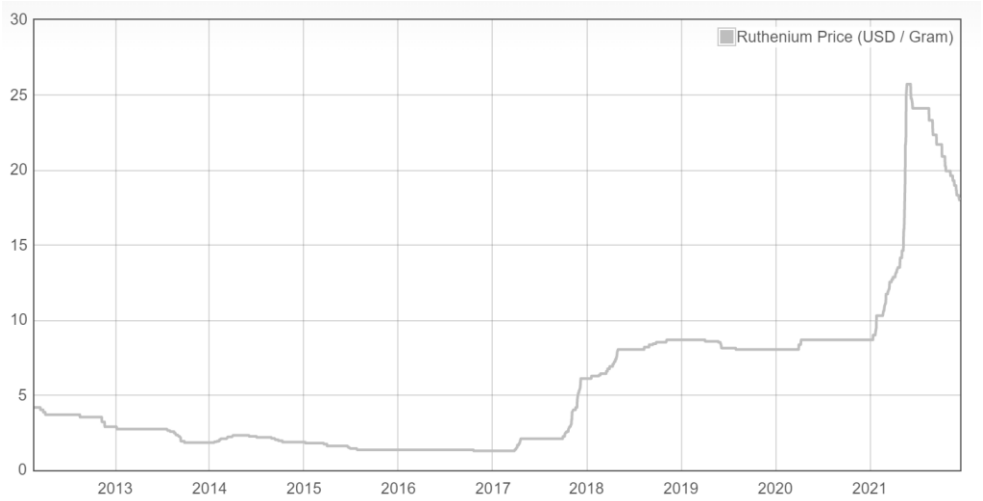


**Figure 7.1:** Price of Ru (USD/gram) over 10 years (2012 to 2022) [83].

Additionally, the supply of $H_2$ is a foreseeable issue. Currently, 95% of $H_2$ in the United States is supplied through steam-reforming of natural gas (or fossil methane) [84]. Not only is this process energy intensive, requiring temperatures as high as 800°C and pressures as high as 25 bar, $CO_2$ is also produced as a byproduct. Methane is catalytically reformed with steam to produce CO and $H_2$ (7). The product stream is then further processed via the water-gas shift reaction to convert the CO byproduct to $CO_2$ and $H_2$ (8), thereby producing more $H_2$. The product is referred to as "grey $H_2$", which is currently much less expensive than $H_2$ generated by alternative methods.

| | | |
|---|---|---|
| **Steam reforming** | $CH_4 + H_2O \rightarrow CO + 3H_2$ | (7) |
| **Water-gas shift** | $CO + H_2O \rightarrow CO_2 + H_2$ | (8) |

The least carbon-intensive $H_2$ (i.e., $H_2$ that is associated with the least $CO_2$ emissions) is achieved through electrolysis of water using renewable energy – this is called "green $H_2$". This hydrogen is currently not cost competitive to fossil derived $H_2$ (see bars for natural gas and renewable derived $H_2$ in **Figure 7.2**). Although there is great push to reduce its cost, it is forecasted

to take at least a decade for a competitive price (<$2/kg) [85]. Additionally, green $H_2$ is reliant on the availability of renewable energy sources (such as solar and wind), which will also need to supply the existing electricity demands. Furthermore, the impact that widespread water electrolysis can have on water supply needs to be considered. Some immediate relief can come from waste or by-product $H_2$, generated during dehydrogenation reactions and often simply flared or burned for its heat value [86]. One issue with waste $H_2$ would be the quality of the stream and the co-present impurities. Some reactive species, like olefins, could be detrimental to the catalyst methanation performance (i.e., coke formation).

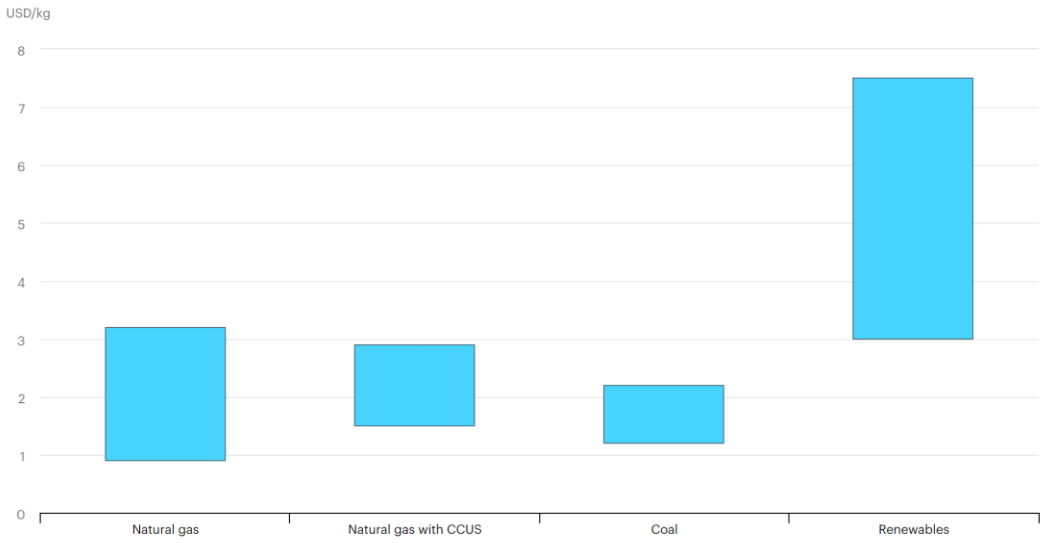


**Figure 7.2:** Cost of $H_2$ (USD/kg) based on source [87].

Particularly related to the $H_2$ issue are the progress optimizations that are required to bring the DFM technology to market. In particular, the heat up progress for DAC-M should be done quickly and efficiently, not just for energy reasons but also for efficient use of $H_2$. Longer heating

times will result in more desorption of unreacted $CO_2$ and prolonged flow of unutilized $H_2$. The flowrate of $H_2$ should be investigated and optimized (perhaps to be as low as possible) – this is also beneficial not just to lower the $H_2$ requirement of the process but also to prevent the additional step to separate $CH_4$ and $H_2$ to meet pipeline guidelines.

# References


[1] E. Dlugokencky, P. Tans, Trends in Atmospheric Carbon Dioxide, Www.Esrl.Noaa.Gov/Gmd/Ccgg/Trends/. (2020).

[2] IEA, World Energy Outlook 2017, OECD Publishing, Paris, 2017. https://doi.org/10.1787/weo-2017-en.

[3] P. Melo Bravo, D.P. Debecker, Combining $CO_2$ capture and catalytic conversion to methane, Waste Disposal & Sustainable Energy. 1 (2019) 53–65. https://doi.org/10.1007/s42768-019-00004-0.

[4] R.J. Farrauto, M.S. Duyar, A.A. Park, Methods, systems and materials for capturing carbon dioxide and converting it to a chemical product, WO 2016/007825 A1, 2016.

[5] M.S. Duyar, S. Wang, M.A. Arellano-treviño, R.J. Farrauto, $CO_2$ utilization with a novel dual function material (DFM) for capture and catalytic conversion to synthetic natural gas: An update, Journal of $CO_2$ Utilization. 15 (2016) 65–71. https://doi.org/10.1016/j.jcou.2016.05.003.

[6] M.A. Arellano-Treviño, Z. He, M.C. Libby, R.J. Farrauto, Catalysts and adsorbents for $CO_2$ capture and conversion with dual function materials: Limitations of Ni-containing DFMs for flue gas applications, Journal of $CO_2$ Utilization. 31 (2019) 143–151. https://doi.org/10.1016/j.jcou.2019.03.009.

[7] M.S. Duyar, M.A. Arellano, R.J. Farrauto, Dual function materials for $CO_2$ capture and conversion using renewable $H_2$, Applied Catalysis B: Environmental. 168 (2015) 370–376. https://doi.org/10.1016/j.apcatb.2014.12.025.

[8] C. Janke, M.S. Duyar, M. Hoskins, R. Farrauto, Catalytic and adsorption studies for the hydrogenation of $CO_2$ to methane, Applied Catalysis B: Environmental. 152–153 (2014) 184–191. https://doi.org/10.1016/j.apcatb.2014.01.016.

[9] Q. Zheng, R.J. Farrauto, A. Chau Nguyen, Adsorption and methanation of flue gas $CO_2$ with dual functional catalytic materials: a parametric study, Industrial and Engineering Chemistry Research. (2016). https://doi.org/10.1021/acs.iecr.6b01275.

[10] S. Wang, E.T. Schrunk, H. Mahajan, and R.J. Farrauto, The Role of Ruthenium in $CO_2$ Capture and Catalytic Conversion to Fuel by Dual Function Materials (DFM), Catalysts. 7 (2017) 88. https://doi.org/10.3390/catal7030088.

[11] S. Wang, R.J. Farrauto, S. Karp, J.H. Jeon, E.T. Schrunk, Parametric, cyclic aging and characterization studies for $CO_2$ capture from flue gas and catalytic conversion to synthetic natural gas using a dual functional material (DFM), Journal of $CO_2$ Utilization. 27 (2018) 390–397. https://doi.org/10.1016/j.jcou.2018.08.012.

[12] M.A. Arellano-treviño, N. Kanani, C.W. Jeong-potter, R.J. Farrauto, Bimetallic catalysts for $CO_2$ capture and hydrogenation at simulated flue gas conditions, Chemical Engineering Journal. 375 (2019) 121953. https://doi.org/10.1016/j.cej.2019.121953.

[13] K. Lackner, H.-J. Ziock, P. Grimes, Carbon capture from air, is it an option?, in: 24th Annual Technical Conference on Coal Utilization & Fuel Systems, Clearwater, FL, 1999.

[14] D. Keith, M. Ha-duong, J. Stolaroff, Climate strategy with $CO_2$ capture from the air, Climatic Change. 74 (2006) 17–45.

[15] D.W. Keith, Why capture $CO_2$ from the atmosphere?, Science. 325 (2009) 1654–1655. https://doi.org/10.1126/science.1175680.

[16] C.W. Jones, $CO_2$ Capture from Dilute Gases as a Component of Modern Global Carbon Management, Annual Review of Chemical and Biomolecular Engineering. 2 (2011) 31–52. https://doi.org/10.1146/annurev-chembioeng-061010-114252.

[17] IEA, Global Energy & $CO_2$ Status Report 2019, (2019). https://www.iea.org/reports/global-energy-co2-status-report-2019 (accessed June 4, 2020).

[18] IEA, Global Energy Review 2019, (2020). https://www.iea.org/reports/global-energy-review-2019 (accessed June 5, 2020).

[19] NOAA, Annual Greenhouse Gas Index (AGGI), (2020). https://www.esrl.noaa.gov/gmd/aggi/aggi.html (accessed June 5, 2020).

[20] Scripps Institution of Oceanography, Carbon Dioxide Levels Hit Record Peak in May, (2019). https://scripps.ucsd.edu/programs/keelingcurve/2019/06/04/carbon-dioxide-levels-hit-record-peak-in-may/ (accessed June 5, 2020).

[21] J. Blunden, D.S. Arndt, eds., State of the Climate in 2018, Bulletin of the American Meterological Society. 100 (2019).

[22] M. Allen, O.P. Dube, W. Solecki, F. Aragon-Durand, W. Cramer, S. Humphreys, M. Kainuma, J. Kala, N. Mahowalf, Y. Mulugetta, R. Perez, M. Wairiu, K. Zickfeld, Framing and Context (Global Warming of 1.5C, An IPCC Special Report), 2018.

[23] The Paris Agreement, United Nations Framework Convention on Climate Change. (n.d.). https://unfccc.int/process-and-meetings/the-paris-agreement/the-paris-agreement (accessed November 19, 2021).

[24] United Nations, Adoption of the Paris Agreement, (2015). https://doi.org/10.1007/BF02327128.

[25] T. Stocker, D. Qin, G. Plattner, M. Tignor, S. Allen, J. Boschung, A. Nauels, Y. Xia, V. Bex, P. Midgley, eds., Summary for Policy Makers, In: Climate Change 2013: The Physical Science Basis. Contribution of Working Group I to the Fifth Assessment Report of the Intergovernmental Panel on Climate Change, in: Cambridge University Press, Cambridge, United Kingdom and New York, NY, USA, 2013. www.climatechange2013.org.

[26] COP26: More than 40 countries pledge to quit coal, BBC News - Science. (2021). https://www.bbc.com/news/science-environment-59159018 (accessed November 19, 2021).

[27] Carbon Dioxide Emissions Coefficients, EIA. (2021). https://www.eia.gov/environment/emissions/co2_vol_mass.php (accessed November 19, 2021).

[28] IPCC, CH02: Mitigation pathways compatible with 1.5°C in the context of sustainable development, in: Special Report: Global Warming of 1.5°C, 2018. https://www.ipcc.ch/sr15/chapter/chapter-2/.

[29] IEA, World electricity generation mix by fuel, 1971-2019, Paris, 2021. https://www.iea.org/data-and-statistics/charts/world-electricity-generation-mix-by-fuel-1971-2019 (accessed December 19, 2021).

[30] P. Markewitz, W. Kuckshinrichs, W. Leitner, J. Linssen, P. Zapp, R. Bongartz, A. Schreiber, T.E. Müller, Worldwide innovations in the development of carbon capture technologies and the utilization of $CO_2$, Energy and Environmental Science. 5 (2012) 7281–7305. https://doi.org/10.1039/c2ee03403d.

[31] IECM Technical Documentation: Amine-based Post-Combustion $CO_2$ Capture, Pittsburgh, PA, 2019. www.iecm-online.com.

[32] M. Ge, K. Lebling, K. Levin, J. Friedrich, Tracking Progress of the 2020 Climate Turning Point, Washington, DC, 2019.

[33] D. Leeson, N. Mac Dowell, N. Shah, C. Petit, P.S. Fennell, A Techno-economic analysis and systematic review of carbon capture and storage (CCS) applied to the iron and steel, cement, oil refining and pulp and paper industries, as well as other high purity sources, International Journal of Greenhouse Gas Control. 61 (2017) 71–84. https://doi.org/10.1016/j.ijggc.2017.03.020.

[34] M. Fasihi, O. Efimova, C. Breyer, Techno-economic assessment of $CO_2$ direct air capture plants, Journal of Cleaner Production. 224 (2019). https://doi.org/10.1016/j.jclepro.2019.03.086.

[35] C. Beuttler, L. Charles, J. Wurzbacher, The Role of Direct Air Capture in Mitigation of Anthropogenic Greenhouse Gas Emissions, Frontiers in Climate. 1 (2019). https://doi.org/10.3389/fclim.2019.00010.

[36] E.S. Sanz-Pérez, C.R. Murdock, S.A. Didas, C.W. Jones, Direct Capture of $CO_2$ from Ambient Air, Chemical Reviews. 116 (2016) 11840–11876. https://doi.org/10.1021/acs.chemrev.6b00173.

[37] V. Nikulshina, C. Gebald, A. Steinfeld, $CO_2$ capture from atmospheric air via consecutive CaO-carbonation and $CaCO_3$-calcination cycles in a fluidized-bed solar reactor, Chemical Engineering Journal. 146 (2009) 244–248. https://doi.org/10.1016/j.cej.2008.06.005.

[38] A. Kumar, D.G. Madden, M. Lusi, K.J. Chen, E.A. Daniels, T. Curtin, J.J. Perry, M.J. Zaworotko, Direct Air Capture of $CO_2$ by Physisorbent Materials, Angewandte Chemie - International Edition. 54 (2015) 14372–14377. https://doi.org/10.1002/anie.201506952.

[39] V.S. Derevschikov, J. V. Veselovskaya, T.Y. Kardash, D.A. Trubitsyn, A.G. Okunev, Direct CO2 capture from ambient air using K2CO 3/Y2O3 composite sorbent, Fuel. 127 (2014) 212–218. https://doi.org/10.1016/j.fuel.2013.09.060.

[40] S. Stucki, A. Schuler, M. Constantinescu, Coupled $CO_2$ recovery from the atmosphere and water electrolysis: Feasibility of a new process for hydrogen storage, International Journal of Hydrogen Energy. 20 (1995) 653–663. https://doi.org/10.1016/0360-3199(95)00007-Z.

[41] C. Graves, S.D. Ebbesen, M. Mogensen, K.S. Lackner, Sustainable hydrocarbon fuels by recycling $CO_2$ and $H_2O$ with renewable or nuclear energy, Renewable and Sustainable Energy Reviews. 15 (2011) 1–23. https://doi.org/10.1016/j.rser.2010.07.014.

[42] F.V. Vázquez, J. Koponen, V. Ruuskanen, C. Bajamundi, A. Kosonen, P. Simell, J. Ahola, C. Frilund, J. Elfving, M. Reinikainen, N. Heikkinen, J. Kauppinen, P. Piermartini, Power-to-X technology using renewable electricity and carbon dioxide from ambient air: SOLETAIR proof-of-concept and improved process concept, Journal of $CO_2$ Utilization. 28 (2018) 235–246. https://doi.org/10.1016/j.jcou.2018.09.026.

[43] Climeworks, Direct Air Capture, (n.d.). https://www.climeworks.com/page/co2-removal (accessed June 5, 2020).

[44] Carbon Engineering, Our Technology, (n.d.). https://carbonengineering.com/our-technology/ (accessed June 5, 2020).

[45] Carbon Engineering, History & Trajectory, (n.d.). https://carbonengineering.com/history-trajectory/ (accessed June 5, 2020).

[46] G. Garbarino, D. Bellotti, P. Riani, L. Magistri, G. Busca, I. Civile, A. Dicca, Methanation of carbon dioxide on $Ru/Al_2O_3$ and $Ni/Al_2O_3$ catalysts at atmospheric pressure: Catalysts activation, behaviour and stability, International Journal of Hydrogen Energy. 40 (2015) 9171–9182. https://doi.org/10.1016/j.ijhydene.2015.05.059.

[47] P. Frontera, A. Macario, M. Ferraro, P. Antonucci, Supported Catalysts for $CO_2$ Methanation: A Review, Cataysts. 59 (2017) 1–28. https://doi.org/10.3390/catal7020059.

[48] A.I. Tsiotsias, N.D. Charisiou, I. v. Yentekakis, M.A. Goula, Capture and Methanation of $CO_2$, Catalysts. 10 (2020) 36.

[49] J. v Veselovskaya, P.D. Parunin, O. v Netskina, A.G. Okunev, A Novel Process for Renewable Methane Production: Combining Direct Air Capture by $K_2CO_3$/Alumina Sorbent with $CO_2$ Methanation over Ru/Alumina Catalyst, Topics in Catalysis. 61 (2018) 1528–1536. https://doi.org/10.1007/s11244-018-0997-z.

[50] J. v. Veselovskaya, P.D. Parunin, O. v. Netskina, L.S. Kibis, A.I. Lysikov, A.G. Okunev, Catalytic methanation of carbon dioxide captured from ambient air, Energy. 159 (2018) 766–773. https://doi.org/10.1016/j.energy.2018.06.180.

[51] J. v. Veselovskaya, A.I. Lysikov, O. v. Netskina, D. v. Kuleshov, A.G. Okunev, $K_2CO_3$-Containing Composite Sorbents Based on Thermally Modified Alumina: Synthesis, Properties, and Potential Application in a Direct Air Capture/Methanation Process, Industrial and Engineering Chemistry Research. 59 (2020) 7130–7139. https://doi.org/10.1021/acs.iecr.9b05457.

[52] I.S. Omodolor, H.O. Otor, J.A. Andonegui, B.J. Allen, A.C. Alba-Rubio, Dual-Function Materials for $CO_2$ Capture and Conversion: A Review, Industrial and Engineering Chemistry Research. 59 (2020) 17612–17631. https://doi.org/10.1021/acs.iecr.0c02218.

[53] A. Porta, C.G. Visconti, L. Castoldi, R. Matarrese, C. Jeong-Potter, R. Farrauto, L. Lietti, Ru-Ba synergistic effect in dual functioning materials for cyclic $CO_2$ capture and methanation, Applied Catalysis B: Environmental. 283 (2021) 119654. https://doi.org/10.1016/j.apcatb.2020.119654.

[54] A. Porta, R. Matarrese, C.G. Visconti, L. Castoldi, L. Lietti, Storage Material Effects on the Performance of Ru-Based $CO_2$ Capture and Methanation Dual Functioning Materials, Industrial & Engineering Chemistry Research. 60 (2021) 6706–6718. https://doi.org/10.1021/acs.iecr.0c05898.

[55] C.J. Keturakis, F. Ni, M. Spicer, M.G. Beaver, H.S. Caram, I.E. Wachs, Monitoring solid oxide $CO_2$ capture sorbents in action, ChemSusChem. 7 (2014) 3459–3466. https://doi.org/10.1002/cssc.201402474.

[56] L. Proaño, E. Tello, M.A. Arellano-Trevino, S. Wang, M. Cobo, R.J. Farrauto, In-situ DRIFTS study of two-step $CO_2$ capture and catalytic methanation over Ru,"$Na_2O$"/$Al_2O_3$ Dual Functional Material, Applied Surface Science. 479 (2019) 25–30. https://doi.org/10.1016/j.apsusc.2019.01.281.

[57] L. Proaño, M.A. Arellano-Treviño, R.J. Farrauto, M. Figueredo, C. Jeong-Potter, M. Cobo, Mechanistic assessment of dual function materials, composed of Ru-Ni, $Na_2O/Al_2O_3$ and Pt-Ni, $Na_2O/Al_2O_3$, for $CO_2$ capture and methanation by in-situ DRIFTS, Applied Surface Science. 533 (2020) 147469. https://doi.org/10.1016/j.apsusc.2020.147469.

[58] F. Garisto, Thermodynamic Behaviour of Ruthenium At High Temperatures, AECL-9552, Whiteshell Nuclear Research Establishment. (1988).

[59] E. Guglielminotti, F. Boccuzzi, M. Manzoli, F. Pinna, M. Scarpa, Ru/$ZrO_2$ Catalysts: I. $O_2$, CO, and NO Adsorption and Reactivity, Journal of Catalysis. 192 (2000) 149–157. https://doi.org/10.1006/jcat.2000.2835.

[60] A. Porta, L. Falbo, C.G. Visconti, L. Lietti, C. Bassano, P. Deiana, Synthesis of Ru-based catalysts for $CO_2$ methanation and experimental assessment of intraporous transport limitations, Catalysis Today. (2019) 0–1. https://doi.org/10.1016/j.cattod.2019.01.042.

[61] A. Comas-Vives, K. Furman, D. Gajan, M.C. Akatay, A. Lesage, F.H. Ribeiro, C. Copéret, Predictive morphology, stoichiometry and structure of surface species in supported Ru nanoparticles under $H_2$ and CO atmospheres from combined experimental and DFT studies, Physical Chemistry Chemical Physics. (2016). https://doi.org/10.1039/c5cp06710c.

[62] C. Li, H. Shi, Y. Cao, Y. Kuang, Y. Zhang, D. Gao, L. Sun, Modeling and optimal operation of carbon capture from the air driven by intermittent and volatile wind power, Energy. 87 (2015) 201–211. https://doi.org/10.1016/j.energy.2015.04.098.

[63] F. Kosaka, Y. Liu, S.Y. Chen, T. Mochizuki, H. Takagi, A. Urakawa, K. Kuramoto, Enhanced Activity of Integrated $CO_2$ Capture and Reduction to $CH_4$ under Pressurized Conditions toward Atmospheric $CO_2$ Utilization, ACS Sustainable Chemistry and Engineering. 9 (2021) 3452–3463. https://doi.org/10.1021/acssuschemeng.0c07162.

[64] A. Samanta, A. Zhao, G.K.H. Shimizu, P. Sarkar, R. Gupta, Post-combustion $CO_2$ capture using solid sorbents: A review, Industrial and Engineering Chemistry Research. 51 (2012) 1438–1463. https://doi.org/10.1021/ie200686q.

[65] Y. Qiao, J. Wang, Y. Zhang, W. Gao, T. Harada, L. Huang, T.A. Hatton, Q. Wang, Alkali Nitrates Molten Salt Modified Commercial MgO for Intermediate-Temperature $CO_2$

Capture: Optimization of the Li/Na/K Ratio, Industrial & Engineering Chemistry Research. 56 (2017) 1509–1517. https://doi.org/10.1021/acs.iecr.6b04793.

[66] J. Zheng, C. Wang, W. Chu, Y. Zhou, K. Köhler, $CO_2$ Methanation over Supported $Ru/Al_2O_3$ Catalysts: Mechanistic Studies by In situ Infrared Spectroscopy, ChemistrySelect. 1 (2016) 3197–3203. https://doi.org/10.1002/slct.201600651.

[67] S.Y. Chin, C.T. Williams, M.D. Amiridis, FTIR studies of CO adsorption on $Al_2O_3$- and $SiO_2$-supported Ru catalysts, Journal of Physical Chemistry B. 110 (2006) 871–882. https://doi.org/10.1021/jp053908q.

[68] A. Bermejo-López, B. Pereda-Ayo, J.A. González-Marcos, J.R. González-Velasco, Mechanism of the $CO_2$ storage and in situ hydrogenation to $CH_2$. Temperature and adsorbent loading effects over $Ru\text{-}CaO/Al_2O_3$ and $Ru\text{-}Na_2CO3/Al_2O_3$ catalysts, Applied Catalysis B: Environmental. 256 (2019). https://doi.org/10.1016/j.apcatb.2019.117845.

[69] L. Falbo, C.G. Visconti, L. Lietti, J. Szanyi, The effect of CO on $CO_2$ methanation over $Ru/Al_2O_3$ catalysts: a combined steady-state reactivity and transient DRIFT spectroscopy study, Applied Catalysis B: Environmental. 256 (2019). https://doi.org/10.1016/j.apcatb.2019.117791.

[70] Md.I. Alam, R. Cheula, G. Moroni, L. Nardi, M. Maestri, Mechanistic and multiscale aspects of thermo-catalytic $CO_2$ conversion to C1 products, Catalysis Science & Technology. 11 (2021) 6601–6629. https://doi.org/10.1039/d1cy00922b.

[71] K. Villani, C.E.A. Kirschhock, D. Liang, G. Van Tendeloo, J.A. Martens, Catalytic carbon oxidation over ruthenium-based catalysts, Angewandte Chemie - International Edition. 45 (2006) 3106–3109. https://doi.org/10.1002/anie.200503799.

[72] M. Nawdali, H. Ahlafi, G.M. Pajonk, D. Bianchi, Elementary steps involved in the hydrogenation of the linear CO species adsorbed on a $Ru/Al_2O_3$ catalyst, Journal of Molecular Catalysis A: Chemical. 162 (2000) 247–256. https://doi.org/10.1016/S1381-1169(00)00293-4.

[73] P. Dongapure, S. Bagchi, S. Mayadevi, R.N. Devi, Variations in activity of $Ru/TiO_2$ and $Ru/Al_2O_3$ catalysts for $CO_2$ hydrogenation: An investigation by in-situ infrared spectroscopy studies, Molecular Catalysis. 482 (2020) 110700. https://doi.org/10.1016/j.mcat.2019.110700.

[74] S. Chen, A.M. Abdel-Mageed, M. Dyballa, M. Parlinska-Wojtan, J. Bansmann, S. Pollastri, L. Olivi, G. Aquilanti, R.J. Behm, Raising the COx Methanation Activity of a $Ru/\gamma$-$Al_2O_3$Catalyst by Activated Modification of Metal–Support Interactions, Angewandte Chemie International Edition. 59 (2020) 22763–22770. https://doi.org/10.1002/anie.202007228.

[75] A. Al-Mamoori, S. Lawson, A.A. Rownaghi, F. Rezaei, Improving Adsorptive Performance of CaO for High-Temperature $CO_2$ Capture through Fe and Ga Doping, Energy and Fuels. 33 (2019) 1404–1413. https://doi.org/10.1021/acs.energyfuels.8b03996.

[76] L. di Felice, C. Courson, P.U. Foscolo, A. Kiennemann, Iron and nickel doped alkaline-earth catalysts for biomass gasification with simultaneous tar reformation and $CO_2$ capture, International Journal of Hydrogen Energy. 36 (2011) 5296–5310. https://doi.org/10.1016/j.ijhydene.2011.02.008.

[77] L. He, Q. Lin, Y. Liu, Y. Huang, Unique catalysis of Ni-Al hydrotalcite derived catalyst in $CO_2$ methanation: Cooperative effect between Ni nanoparticles and a basic support,

Journal of Energy Chemistry. 23 (2014) 587–592. https://doi.org/10.1016/S2095-4956(14)60144-3.

[78] H. Sun, Y. Zhang, S. Guan, J. Huang, C. Wu, Direct and highly selective conversion of captured $CO_2$ into methane through integrated carbon capture and utilization over dual functional materials, Journal of $CO_2$ Utilization. 38 (2020) 262–272. https://doi.org/10.1016/j.jcou.2020.02.001.

[79] C. Jeong-Potter, R. Farrauto, Feasibility Study of Combining Direct Air Capture of $CO_2$ and Methanation at Isothermal Conditions with Dual Function Materials, Applied Catalysis B: Environmental. 282 (2021) 119416. https://doi.org/10.1016/j.apcatb.2020.119416.

[80] J. Ashok, S. Pati, P. Hongmanorom, Z. Tianxi, C. Junmei, S. Kawi, A review of recent catalyst advances in $CO_2$ methanation processes, Catalysis Today. 356 (2020) 471–489. https://doi.org/10.1016/j.cattod.2020.07.023.

[81] B. Gautam, P. Hobson, Platinum and palladium forecasts slashed after chip shortage hits auto sector, Reuters, Business. (2021). https://www.reuters.com/business/platinum-palladium-forecasts-slashed-after-chip-shortage-hits-auto-sector-2021-10-28/ (accessed December 15, 2021).

[82] L. Xu, B. Lai, D. Song, Q. Liu, Y. Han, METHOD FOR PREPARING SOLID NITROSYL RUTHENIUM NITRATE BY USING WASTE CATALYST CONTAINING RUTHENIUM, WO 2013/131451, 2015.

[83] Metal Spot Price Charts, Daily Metal Prices. (n.d.). http://www.dailymetalprice.com/metalpricecharts.php?c=ru&u=g&d=2400 (accessed December 15, 2021).

[84] Hydrogen and Fuel Cell Technologies Office, Hydrogen Production: Natural Gas Reforming, U.S. Department of Energy. (2021). Hydrogen Production: Natural Gas Reforming (accessed December 15, 2021).

[85] Hydrogen and Fuel Cell Technologies Office, Hydrogen Shot, U.S. Department of Energy. (2021). https://www.energy.gov/eere/fuelcells/hydrogen-shot (accessed December 15, 2021).

[86] P. Bernardo, Ethylene Off-gas, in: Encyclopedia of Membranes, Springer Berlin Heidelberg, 2016. https://doi.org/10.1007/978-3-662-44324-8.

[87] IEA, The Future of Hydrogen, Paris, 2019. https://www.iea.org/reports/the-future-of-hydrogen/data-and-assumptions (accessed December 15, 2021).